NTNU
Norwegian University of
Science and Technology

Error and Ellipses of Uncertainty Analysis in Far North

Shaine Muhammadali

Petroleum Engineering
Submission date: June 2017
Supervisor: Sigbjørn Sangesland, IGP
Co-supervisor: Bjorn Berchan, IGP

Norwegian University of Science and Technology
Department of Geoscience and Petroleum

Department of Petroleum Engineering and Applied Geophysics

MASTER OF SCIENCE THESIS

The candidate name: ***Shaine Muhammadali Lalji***

Title of Thesis: ***Error and Ellipses of Uncertainty Analysis in Far North***

Objective:

The main objective is to analyze different error sources associated with directional survey in far north, in order to calculate the ellipses of uncertainty. Analyzing and rectifying the error sources may decrease the uncertainty and will lead the well path at the desire location, which is the main concern of this thesis. The work also focuses on the probability of intersection between the two wells, in order to stop the unwanted flow of oil and gas up to the surface.

Task:

1) Analyzing the error sources in positional uncertainty
2) Development of Model and compare with industry standards
3) Analyzing contribution from different error sources in operations in far north
4) Comparison study related to different Anti-collision and EOU parameters between Industry model and self-made model.
5) Analyzing the impact to positional uncertainty from change of Kickoff Point (KOP) and number of survey stations

Supervisor: ***Sigbjørn Sangesland***

Co-supervisor: ***Bjørn Brechan***

Specialization Field: ***Drilling Engineering***

Date: ***11th June 2017***

SUMMARY

Drilling in Barents Sea and North Sea proves to be an extremely difficult task, as these regions are situated in auroral zones having higher latitude, where, magnetic interferences develop from magnetic field, magnetic storms and magnetic materials inside subsurface are quite common. For these regions, monitoring of magnetic field is utterly significant as any fluctuations can distort the tool sensor performance. This information is obtained through the space weather forecast, which provides data related to Sun and interplanetary space and is recorded from any onshore variometer station. However, for the Barents Sea the major drawback is this onshore variometer stations as they are situated approximately 400 km away from the rig-site, therefore, the error analysis for this zone needs some special consideration.

The study revolves around the Relief Well that is created to protect the unwanted flow of oil and gas up to the surface from the Targeted Well. The well is planned to be 700 km away from the Targeted Well and is oriented in the North direction, with very small changes in azimuth. The main aim on the other hand, is to create a model along with the specific tool, and then try to estimate the Ellipses of Uncertainty (EOU) for both wells. Finally, a comparison study is also performed between the industry standard model and the self-made model.

The total Measured Depth for the Relief Well is 1400 mMD, while for the Targeted Well it is 2354 mMD. However, the depth of interest for the Targeted Well is 690 mMD which is assumed to be the intersection location.

The struggle begins by importing the new tool developed in COMPASS^{TM} to try and observe the EOU dimension for both wells. For the Relief Well, the Semi Major Axis length at the final depth of 1400 mMD is 19.69 m, while for the Targeted Well it is 2.34 m. The next step is to individually assess and determine each error term contribution in the total length. This is done by removing all the error terms from the IPM file except the one that needs to be assessed. It is observed that Declination contributes 90.7% in total in Semi Major Axis length, while remaining 9.3% are from other errors.

This same idea is also implemented to the self-made model. However, for the model an extensive study was performed for each error term to determine the individual contribution. Before the start of ellipse analysis, two separate studies are performed that relates to Temperature and Drill String Interferences (DSI). Temperature analysis is perform as a

Quality Control (QC) check, ensuring that the MWD tool is reliable at that depth. Since the study is based on shallow formation, it is discovered that the BHA will not suffer any changes in length and MWD tool will operate in the designated range. However, this analysis is important for the HTHP wells, which might suffer an alteration in BHA length and will distort MWD sensor measurements.

A second analysis is done relating to DSI. The BHA is divided into three regions, and the higher interference region is determined. Out of all, Region 1 that comprises of Bit is considered to be the highest Interference region, which is responsible for a severe distortion in MWD sensor. To combat this effect, the physical distance between the Bit and MWD sensor is increase by using the appropriate NMDC

After the entire QC's check, the total Semi Major Axis size is evaluated from the model which is approximately 19.02 m. However, in the model, error terms such as Declination, DIP Angle and Total Magnetic Field (TMF) which are the strong functions of Geomagnetic Field of the area of interest contribute heavily in uncertainty. It is also perceived that a major of 30% error deviation exists between the two models; on the contrary, at the depth of interest, there is less than 5% deviation in ellipse dimension.

Apart from ellipse dimension calculations, a comparison analysis is also executed related to probability of intersection at the plan location. It is observed that, from both models a probability of 0.039 which indicates one strike in every 25 attempts is obtained. For this analysis, the center to center distance and radii of the Targeted Well and Relief Well are necessary. From COMPASS^{TM} a 14.6 m center to center distance along with the Separation Factor of 0.33 is retrieve from Anti-Collision Report, while from the model they are 14.76 m and 0.35 calculated.

Furthermore, two distinguished studies are also performed in order to reduce the uncertainty ellipse dimension. In the first case, the numbers of survey stations are decrease from 38 to 26. It is figure out that, the ellipse size increases from 19.02 to 21 m after the reduction in survey stations. It is because of the decline in tool performance, while in the second study KOP is change from 505 m initially to 645 m, keeping the number of stations constant at 26. A drastic reduction is observed in ellipse dimension from 21 m to 15 m.

Overall, the model involves an extensive computation, which comprises of some deficiencies that needs to be assessed in future in order to make it more feasible and functional.

ACKNOWLEDGEMENT

The work done in this dissertation would not been possible without the assistance of my Supervisor and Co-Supervisor, Sigbjørn Sangesland and Bjørn Brechan. They both played the foundation role in supporting my career and worked intensely in guiding and providing me with utmost knowledge, so that I can pursue my goals.

I am also grateful to both Norwegian University of Science and Technology (NTNU) and NED University of Engineering and Technology (NEDUET) for helping me in achieving my dream. I would also like to thank the Chairman of Petroleum Engineering Department Prof. Dr. Abid Murtaza, without his financial support I would not be able to achieve anything. He is not only a mentor, but is also a teacher who is always there with me in my highs and lows.

I would also like to thank my parents and my family members, whose love and affection helped me in changing my destiny. Finally, I would like to thank my wife, Shahzana Zulfiqar, who continuously provided me support and is a source of never ending inspiration.

Trondheim, 11th June 2017

Shaine Muhammadali Lalji

CONTENTS

LIST OF FIGURES XI

LIST OF TABLES XIII

ABBREVIATIONS XIV

1 Introduction of Directional Drilling in Auroral Zones 1

1.1 Directional Drilling 1

1.2 Directional Drilling Principles 1

1.3 Applications of Directional Drilling 2

1.4 Challenges Related to Shallow Reservoir 2

1.5 Earth Magnetosphere and Electrojet Phenomenon 3

1.6 Directional Drilling in Auroral Zones 3

1.7 Behavior of Earth's Magnetic Field in Auroral Zones 4

1.8 Barents Sea a Challenge for Industry 5

1.9 Solutions to Minimize the Auroral Effects 6

2 Models & Errors in Wellbore Position 7

2.1 Walstorm Model 7

2.2 Wolff de Wardt Error Model 7

2.3 Instrument Performance Model 7

2.4 ISCWSA 8

2.4.1 MWD Error Model 8

2.4.2 GYRO Error Model 8

2.5 Types of Errors 8

2.5.1 Random Error 9

2.5.2 Systematic Error 9

2.5.3 Gross Error 10

2.6 Directional Survey Errors 10

2.6.1 Magnetic Interferences from Drill String 11

2.6.2 BHA Sag 12
2.6.3 Measured Depth Error 12
2.6.4 Gyro Drift and Gimbal Effect 13
2.6.5 Magnetic Declination 14
2.6.6 Geomagnetic Field 14
2.6.7 Temperature and Stresses 15
2.6.8 Cross-Axial Magnetic Interferences 15
3 Error Analysis 17
3.1 Short Collar Method 17
3.2 Multi-Station Analysis Technique 17
3.3 Gravity Error Test 19
3.4 In-Run and Out-Run Misalignment Test 19
3.5 Demagnetizing Factor Method (Aklestad, 2015) 20
3.6 Inclination Difference Test 22
3.7 Azimuth Difference Test 22
3.8 Measured Depth 23
3.9 Noise Induced by Vibration 23
3.10 In-Field Referencing (IFR) 23
4 Positional Uncertainty Analysis and Probability 27
4.1 Introduction 27
4.2 Ellipses of Uncertainty 27
4.3 Steps Involved in Calculations of EOU 28
4.4 Probability of Hitting (J.Bang, 2017) 31
5 RESULTS & DISCUSSION 34
5.1 Introduction 34
5.2 Relief Well 34
5.3 Error Analysis from COMPASS^{TM} 35

5.4 Probability of Hitting from COMPASS™ 37
5.5 Model and Performance 38
5.5.1 BHA Interferences 38
5.5.2 Permanent Magnetism 41
5.5.3 Temperature Quality Control Check 42
5.5.4 Sensor Errors 44
5.5.5 Misalignment Error 48
5.5.6 Calculation Related to the Contribution of each Error Term in EOU 49
5.6 Comparison between MODEL and COMPASS™ Results 51
5.6.1 Center-Center Distance 51
5.6.2 Separation Factor Plot 53
5.6.3 Probability of Collision 54
5.6.4 Ellipse of Uncertainty Comparison 55
5.7 Effect of Changing KOP 56
5.8 Effect of Changing the Number of Survey Stations 59
CONCLUSION 64
FURTHER WORK 65
BIBLIOGRAPHY 66
APPENDIX A 69
APPENDIX B 73

LIST OF FIGURES

Figure 1 Directional Drilling (Design, 2009) 1
Figure 2 Directional Surveys and Magnetic Field Connection (Edvardsen, 2015) 5
Figure 3 Random Error (M.K.Trochim, 2006) 9
Figure 4 Systematic Error (M.K.Trochim, 2006) 10
Figure 5 SAG (Misalignment Error) (Bergstrom, 2010) 12
Figure 6 Gimbal effect in Gyro 13
Figure 7 Improvement in Azimuth after MSA (Lima, 2004) 18
Figure 8 Accelerometer in MWD and its Components (Roar Sognnes, 1996) 19
Figure 9 Effect of Magnetic field on Magnetic Material (Aklestad, 2015) 20
Figure 10 Closest Variometer Station to Barents Sea (I.Edvardsen E. B., 2013) 25
Figure 11 Ellipses of Uncertainty (B. Poedjono, 2007) 27
Figure 12 Relief Well Trajectory in North and East Coordinate System 35
Figure 13 Relief Well 1 Semi Major Axis Size for each Error Terms 36
Figure 14 Target Well Semi Major Axis Size from each Error Terms 37
Figure 15 Contribution of each Error Term in Total Probability for the Relief Well 38
Figure 16 NMDC Sensitivity Analyses 41
Figure 17 Formation Temperature and MWD Operating Range 43
Figure 18 BHA Components change in Length 44
Figure 19 Magnetometer Biased and Scale Factor Error 45
Figure 20 Accelerometer Biased and Scale Factor Error 47
Figure 21 Deflection in Azimuth and Inclination due to Misalignment Error 49
Figure 22 Model EOU for each Error Term 50
Figure 23 Target Well EOU from Model 51
Figure 24 Comparison of Center to Center Distance Between Two Models 52
Figure 25 Separation Factor Plot Comparison between Two Data Series 54
Figure 26 Probability of Collision Comparison between Two Data Series 55
Figure 27 EOU Comparison Analysis 56
Figure 28 COMPASS Semi Major Axis Data at the KOP of 645 mMD 57
Figure 29 Model Semi Major Axis Data at the KOP of 645 mMD 57
Figure 30 Error Analysis between two Data Series (COMPASS™ and Model) at 645 mMD 58
Figure 31 Change in EOU between two cases 58
Figure 32 COMPASS Data for Contribution from Each Error Term in EOU 60

Figure 33 Model Data for Contribution from Each Error Term in EOU at 505 mMD 60
Figure 34 Error Analysis for the Two Data Series 61
Figure 35 Comparison between Models with same KOP but Different Number of Stations..... 61
Figure 36 Increase in Error Percentage in EOU After Changing in Numbers of Stations 62
Figure 37 Exemplar BHA (A.Berchan, 2015) 75
Figure 38 Impact of NMDC on Z-Axis Component of Magnetometer..... 76
Figure 39 Center to Center Distance from COMPASS and MODEL 76
Figure 40 Separation Factor Plot from COMPASS and MODEL..... 77
Figure 41 Number of Collision from COMPASS and MODEL 77
Figure 42 Semi Major Axis from COMPASS and MODEL for 38 Number of Stations 78
Figure 43 Semi Major Axis from COMPASS and MODEL for 26 Number of Stations 78

LIST OF TABLES

Table 1 Relief Well Last Station Probability for each Error Term ----------37
Table 2 BHA Interferences ----------39
Table 3 Length of NMDC verses Interferences ----------40
Table 4 Relief Well Semi Major Axis Size From Compass For Each Error Source ----------69
Table 5 Targeted Well Semi Major Axis Size From Compass For Each Error Source ----------70
Table 6 Relief Well EOU For Each Error Source ----------71
Table 7 Targeted Well EOU For Each Error Source From Model ----------72
Table 8 Error Model Parameters For MWD (Jamieson, 2017) ----------73

ABBREVIATIONS

AB	Accelerometer Biased
ASF	Accelerometer Scale Factor
BHA	Bottom Hole Assembly
BHP	Bottom Hole Pressure
D	Declination
I	Dip Angle
DLS	Dogleg Severity
DSI	Drill String Interference
EOU	Ellipse of Uncertainty
ERD	Extended Reached Drilling
IFR	In-Field Referencing
KOP	Kickoff Point
LWD	Logging While Drilling
MB	Magnetic Biased
MSF	Magnetic Scale Factor
MWD	Measurement While Drilling
MSA	Multi-Station Analysis
NBI	Near-Bit Inclinometer
OWC	Oil-Water Contact
SF	Scale Factor
SWF	Shallow Water Flow
SGF	Shallow Gas Flow
F	Total Field Strength
TMF	Total Magnetic Field
WOB	Weight on Bit
λ	Eigen Value

Introduction of Directional Drilling in Auroral Zones

1.1 Directional Drilling

Directional Drilling is now an integral part for Well Planning Process. It is the technique used to deflect a wellbore along a predetermined course to a target whose lateral distance is known from vertical (Neal J.Adams, 1985). Earlier, the well path are planned to keep as vertical as possible. But, now with the advancement of sophisticated techniques the well can be guided in any direction to hit the specific zone of interest. There are three major applications of directional drilling which includes extended reached drilling (ERD), multilateral drilling and short radius drilling (Mantle, 2013/2014).

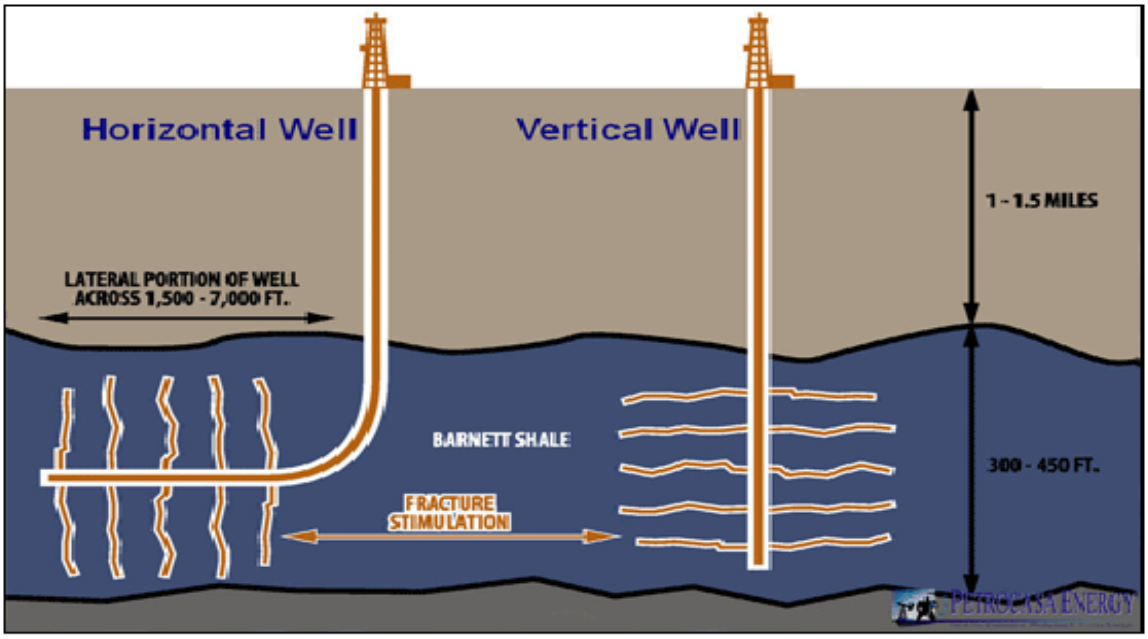

Figure 1 Directional Drilling (Design, 2009)

1.2 Directional Drilling Principles

Directional wells are also known as horizontal wells. Drilling of these wells begins the same as that of conventional vertical wells, with no inclination in vertical section i.e. the conductor casing zone. Then at a particular depth, known as Kickoff Point (KOP) the well start to get an inclination and it starts to deviate from the vertical. To keep the well path trajectory moving in the planned path, surveys are taken which provides information related to inclination, azimuth, toolface, direction of the bit and so on. The purpose of the directional driller is to

monitor these changes and accordingly adjust the well path so that the next preplanned target can be hit with utmost precision.

The major change that is brought in the bottom-hole assembly (BHA) as compared with drilling in the vertical section is the placement of the stabilizer in the Drill String (DS). By changing the placement of stabilizer the desire building holding or dropping angle can be achieve. (Mantle, 2013/2014). Another important factor that needs to be considered while drilling is to maintain the dogleg severity (DLS) as low as possible because that will create problem during casing run. DLS is depended on inclination and azimuth; any major changes in these two factors will cause a drastic change in dogleg severity and will ultimately cause problems during casing run, as it creates high friction forces.

Today, the course of directional drilling has completely changed, directional driller can even look ahead of the bit while drilling, this not only reduces the complications of drilling large complex geological structures but also increase the level of precision for hitting the predetermined target.

1.3 Applications of Directional Drilling

Vertical drilling is considered to be the primary drilling, but with an increase in demand, service companies now explore those areas that are difficult to drill through the use of conventional drilling. The major applications of directional drilling include inaccessible location, relief well, sidetracking and so on.

1.4 Challenges Related to Shallow Reservoir

Drilling into shallow formation is an immensely complicated task that needs to be addressed in order to avoid any kind of catastrophic event which results in loss of life and property. While drilling into these formations driller usually encounters high DLS as a result of immediate changes in inclination and azimuth which later creates problems while casing run. The unconsolidated formations at these depths could also results in loss of well integrity.

Sometimes, shallow water flow (SWF) or shallow gas flow (SGF) makes the drilling even more challenging, as they are difficult to stop because of narrow pressure margin between pore and fracture pressure. The horizontal section is the most challenging one, as it is crucial to maintain the optimum stability from the walls in these sections (G.Gutierrez Murillo, 2014). Also, geosteering through the pay zone is difficult to maintain, which could result in

poor quality borehole data. Sometimes, stuck pipe events are extremely common because of unconsolidated formations that could result in loss of wellbore integrity too.
.

1.5 Earth Magnetosphere and Electrojet Phenomenon

Magnetosphere is the part of Earth atmosphere where magnetic field of Earth is the most prominent factor. This region is formed between the interaction of solar wind and Earth's magnetic field. Solar wind comprises of negative and positive charges along with some magnetic field. This interaction between solar wind and Earth's magnetic field creates current inside magnetosphere, which alters the condition inside it and is responsible for the generation of space weather[1] that can affect the navigation system and creates ambiguity in directional survey ((OCIO)). Of the entire consequences, electrojet is the most dominant one and is responsible for uncertainty in auroral zone. Electric fields are generated in magnetosphere when there is an interaction between solar wind and Earth's magnetic field.

1.6 Directional Drilling in Auroral Zones

Directional surveying plays an integral role in order to make sure that the well path follows its predetermined plan. Tools that are used to make these surveys measurements include MWD and Gyro. MWD comprises of magnetometer and accelerometer (A.Berchan, 2015). These magnetometers are sensitive to the interferences from the steel components that are present in the drillstring assembly and also from the interferences from the nearby wells. The measurements taken from MWD are highly depended on magnetic north, whereas, for Gyros geographical north plays an important part (Edvardsen, 2015). For MWD the north reference is obtained through geomagnetic field while for Gyro it is obtained with the help of spin vector. In each case, as the latitude increases the magnitude of the horizontal component decreases, as a result the azimuth measurement becomes less pronounced (J.Bang T. , 2009).

The auroral zones are higher in latitude that cause the external magnetic field to be unidirectional because of auroral electrojet[2] and this is responsible for creating problem during drilling operation (I.Edvardsen T. M., 2012). In auroral zones due to magnetic storms there is further degradation in earth's magnetic field. Declination is the most sensitive component in the magnetic field and it suffers from a high degree of variation due to shifting

[1] Physical processes that starts on Sun and affect humans on Earth
[2] Exaggerated current flowing between east west directions in ionosphere

in external magnetic field. To remove these factor from the survey data, the driller can either resurveyed the either zone while pulling out of the hole or wait for the external field to calm down enough to get the proper survey (Edvardsen, 2015).

1.7 Behavior of Earth's Magnetic Field in Auroral Zones

Earth comprises of both the magnetic as well as electrical field. Its magnetic field is originates from three major components that include archeological data which is basically burnt clay, geological data that comprises of volcanic mountain matter and inner electric current that flows as a result of liquid element such as nickel and iron.

The field is not stable and has magnetic variations which are divided into two categories that include variation in the interior part of the earth which last longer and variation in the upper atmosphere as a result of electric current. Another important phenomenon that contributes to the change in the earth's magnetic field is magnetic storms. These are most common in auroral zones and are generated as a result of electric storms in proximity. Since, the magnetic field in auroral zones is perpendicular to the earth surface which creates more variation in these zones (Hansen, 2014).

During directional surveying all these parameters contribute to the total uncertainty of the wellbore position. Of the entire parameters azimuth suffers the most. It is extremely crucial that azimuth calculations should be improved, as it is necessary for the proper placement of wellbore, but this parameter is highly sensitive especially when MWD is used because of interference from steel in vicinity from nearby wells and BHA.

BHA needs magnetic measurement in order to navigate itself in the preplanned direction. However, these measurements are strongly affected by the charge particle that develops in the interior of the Sun. This gives rise to several current inside the earth's magnetosphere that brings changes in the directional survey as shown in **Figure 2**. The current that are generated creates variations that last for a longer period and hence, when MWD is run these variations are also detected as a part of the true measurement. Hence, the directional surveying measurements are not that reliable in auroral zones (Edvardsen, 2015).

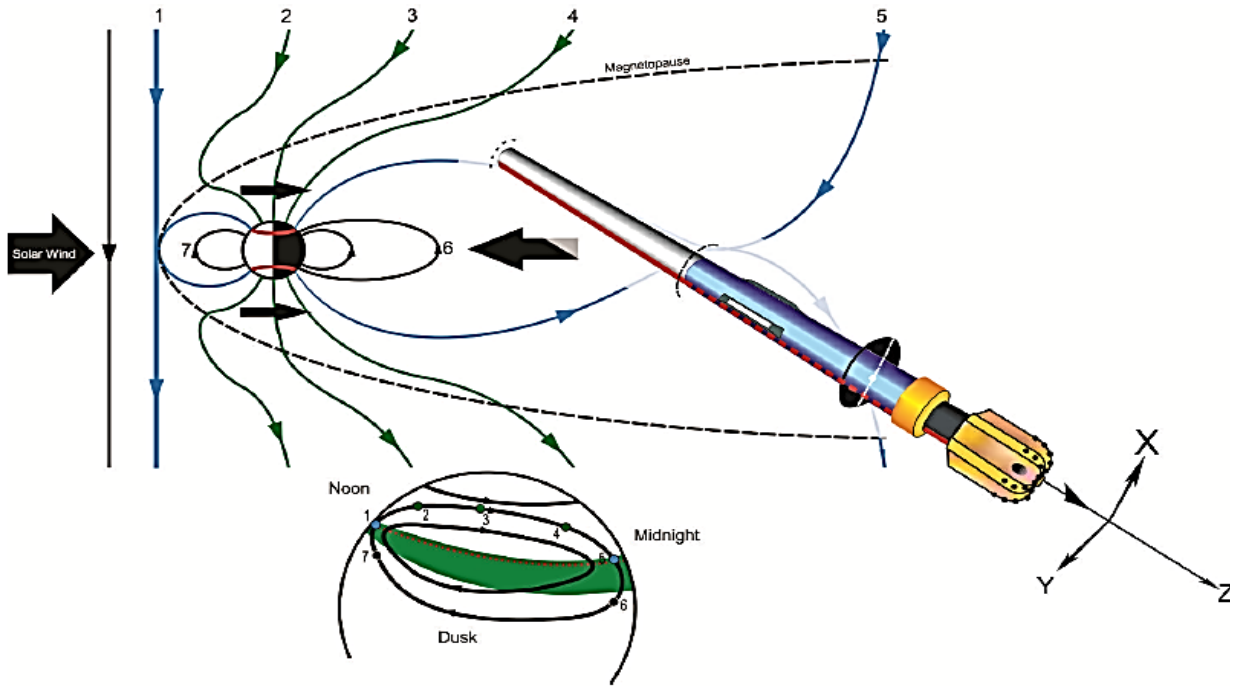

Figure 2 Directional Surveys and Magnetic Field Connection (Edvardsen, 2015)

1.8 Barents Sea a Challenge for Industry

Barents Sea is in region having high geomagnetic latitude in the auroral zone which is the reason that amplifies the azimuth uncertainty when MWD is used as compared with North and Norwegian Sea drilling operations. Two main factors that contribute to this uncertainty in Barents Sea are the electric currents that are generated in ionosphere and the magnetic interference from drill string (I.Edvardsen E. U., 2014). To counter the effect of these two factors it is extremely crucial to study the behavior of magnetic field before the start of any drilling activity. Data is gathered from the nearby onshore location to check the validation of external magnetic field. To apply the interpolation technique in order to reduce the uncertainty associated with azimuth the distance of the rig site should be within 200 km from the variometer station (I.Edvardsen T. M., 2012).

However, for Barents Sea this is not an ideal theory as the closest station on shore is approximately 400 km away. Variations in the middle of Barents Sea are extremely high, for this reason the data obtained from that part comprises of high level of uncertainty and does not fulfills the quality control requirements, that results in the delay of operational activity (Mcculloch).

New equipment must be tested to ensure the reliability of the directional survey. To reduce the effect of drill string interference (DSI), non-magnetic steel must be used. The most decisive part is to give high priority to the surveying technique in this area that ensures the proper placement of the well.

1.9 Solutions to Minimize the Auroral Effects

Directional survey measurements are reliable only if the auroral zone effects are eliminated. For this purpose, most of the drilling companies gather information from the space weather forecasts. This information comprises of the condition that is there on the Sun along with interplanetary space.

If a drilling company is working in low and mid high latitudes region then this information is not that useful since the disturbances are not affecting the survey measurements. However, for high latitudes regions this information plays a vital role (Edvardsen, 2015). The main problem correlated with such high latitudes is that the horizontal component of geomagnetic field decreases, this causes the error associated with the surveying to accumulate and creates more uncertainty (Benny Poedjone, 2013). Auroral zones are situated in the higher latitudes region, where changes in the current in the Earth's ionosphere cause most of the variation in the wellbore surveying. These changes are time dependent and can be properly monitored and corrected, however, as the distance of the rig site increases from the monitoring site these corrections are less valuable and will not be able to reduce the amount of error associated with the survey calculations (T.L.Hansen, 2012).

The major problem in these auroral zones is the distance between the rig site and an onshore variometer station, because monitoring of the external magnetic field from any offshore location is an extremely expensive process, so for that reason operators use an onshore variometer station, however, for these high latitudes and offshore locations these stations are not that reliable. To counter this problem, the operators now in the auroral zones place the onshore variometer station at the same geomagnetic location as the rig site, this enables them to reduce some of the uncertainty associated with the survey (I.Edvardsen T. M., 2012).

Models & Errors in Wellbore Position

2.1 Walstorm Model

This model is introduced in 1969 by Walstorm et al. It is a random error propagation model; however, because of the inaccuracies in predicting accurate wellbore position it soon got rejected. The errors in this model compensate each other due to the randomized nature. This model does not take into account the major directional drilling error such as magnetic declination, drill pipe stretch due to temperature, bending stress etc. as all these error terms have some significant systematic components. For that reason, the Ellipses of Uncertainty (EOU) calculated by this method is extremely small and is normally underestimated because of the randomized nature of the error sources.

2.2 Wolff de Wardt Error Model

This model is developed by Shell KSEPL. It is a systematic error propagation model that is used in directional drilling. Due to its systematic nature, the error from one station does not compensate each other as they do in random error model. The model compensates for:-

1.	Relative Depth Error	(Drill Pipe and Wireline Inaccuracies)
2.	Misalignment and Inclination Error	(Bending and Poor Centralizations)
3.	Gyrocompass Error	(Gyro Orientation, Gyro Drift, Gimbal Effect)
4.	Magnetic Error	(Drill String Magnetization, Magnetic Declination)

Because of the systematic nature of the error sources, they are arithmetically added between two consecutive survey stations that cause the positional uncertainty calculated from this model to be ten times larger as compared to the Walstorm Model.

2.3 Instrument Performance Model

This model is also known as IPM, which is developed by BP and is now used as an alternative of Wolff de Wardt Model. This model is assumed to be most comprehensive and complete error model of all. It combines random, systematic and bias error propagation theory. It is a mathematical algorithm that is used to compute the survey uncertainty at any point in a well. The size of the errors is the function of axial rotation of the tool.

2.4 ISCWSA

ISCWSA stands for ***Industry Steering Committee on Wellbore Survey Accuracy***. The main purpose of this model is to maintain standards related to wellbore survey accuracy and secondly, to enhance the awareness and understanding related to wellbore survey accuracy issues across petroleum industry (ISCWSA, 2016). This comprise of two basic models they are:-

2.4.1 MWD Error Model

It is the industry standard MWD error model. This model is created by the collaborative work of SPE WPTS and four major companies which includes Baker Hughes, BP, Statoil and Sysdrill LTD. This model is extremely simple to implement. The errors which have the most dominant effect and are common to all systems are dealt in this error model, which includes pipe tally, BHA, reference field. However, environmental errors are quite dominant and need to be corrected for proper wellbore position accuracy.

2.4.2 GYRO Error Model

This error model is important where the magnetic inferences from BHA, near by wells or magnetic storm are of great concern because in that case MWD error model fails to provide any reliable measurements. This model is the standard error model for estimation of wellbore position accuracies using gyro tools. For this model, the environmental errors are not as dominant as they are for MWD tools. The uncertainties developed in position for this error model are depended on sensor configuration and operational modes.

2.5 Types of Errors

Errors are the part of any experiment that is observed. They play an important role in defining the proper positioning of the well. There are generally three types of errors; random, systematic and gross. The propagation of these error types depends upon the model that is used. The nature of these errors in comparison to one another is totally different. It is of great importance that the nature of these errors should be understood properly in order to implement the right method for their elimination from the survey data. The three most general errors types that are associated with directional survey are discussed below:-

2.5.1 Random Error

These types of errors are random in nature and are extremely difficult to predict. They normally occur when large number of parameters interferes with the experimental results. To reduce the impact of this type of error, it is extremely important to take the large number of observations and then averaging out the result. Also, if the propagation mode is random than the square root of sum of squares are considered for each set of errors. They may also occur because of the instrument use to take the survey since these instruments are strongly affected by the surrounding (Ajetunobi, 2012).

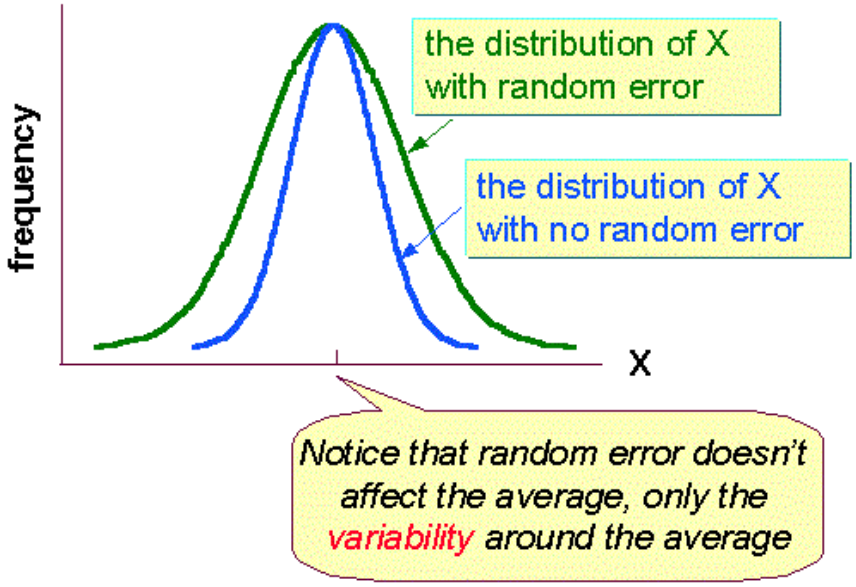

Figure 3 Random Error (M.K.Trochim, 2006)

2.5.2 Systematic Error

These are considered to be consistent and repeatable errors; they are generated by those factors which systematically affect the measurements. In comparison to random errors, these errors are consistent in nature, they can either be positive or negative, and because of this attribute they are recognized to be biased in measurements (M.K.Trochim, 2006).

However, in directional drilling survey there are some errors which can behave in either way, they can be systematic from one station to another or they can change their nature and can convert into random when moving from current to next station. A common example is sagging in MWD tool that is located in drill collar. This can vary in nature from on station to another and are extremely difficult to handle. On the other hand, there are some errors that

are consistent throughout the surveying. Some common examples are errors associated with geodetic reference network, declination, dip angle and TMF. (Ajetunobi, 2012).

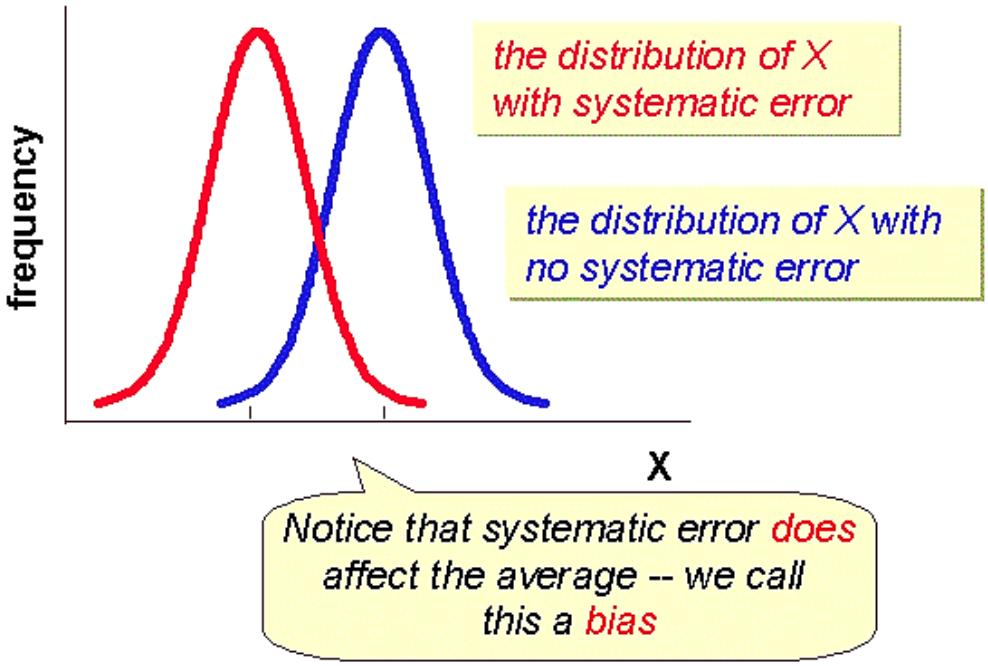

Figure 4 Systematic Error (M.K.Trochim, 2006)

2.5.3 Gross Error

These errors are also known as ***'blunders'***. They occur due to the carelessness, miscommunication and lack of proper judgments from the surveyor and can be in any size or nature which ultimately leads to large discrepancies in measurements. Some common gross error examples in directional survey include:-

1. Use of wrong surface coordinates
2. Improper tally of drill pipe
3. Use of wrong weighting functions

2.6 Directional Survey Errors

With an increase in oil demand, directional drilling is becoming more and more profound technology in order to reach to those oil structures that were difficult to intercept a decade ago. However, for the proper interception at the desire location directional survey needs to be free from all types of error sources. Elimination of errors reduces the size of ellipses of

uncertainty and helps the driller to intercept at the area of interest. Some of the errors that reduces the reliability of directional surveying includes:-

2.6.1 Magnetic Interferences from Drill String

It is considered to be one of the major contributors in azimuth uncertainty especially in Barents Sea and is most commonly linked with MWD tool. MWD tool normally comprises of magnetometer and accelerometers. The interferences from the bit and other magnetic components in Drill String (DS) affect the tool functionality to a great extent, so to model this error source it is common to consider the three orthogonal components acting along each magnetometer axes. Out of three, one is axial component that is acting along the hole and has the dominant effect on azimuth and wellbore position, while the other two are acting in cross axial and in transverse plane and has minimum impact because of toolface dependent nature (I.Edvardsen E. B., 2013).

Equation 1 represents the azimuth error ΔA in the magnetic azimuth A_m which occur due to magnetic interference in axial direction Δb

$$\Delta A = \frac{-\sin I \sin A_m}{B \cos \theta} \Delta b_z \qquad \textbf{Equation 1}$$

B is the magnetic field intensity for the particular location, θ is the dip angle. Together $B\cos\theta$ makes the horizontal component of the Earth's magnetic field and azimuth uncertainty strongly depends upon this component. At high latitude, especially in Barents and North Sea the horizontal component of the Earth's magnetic field is quite small for that reason; the uncertainty associated with azimuth ΔA is large enough to create problems in wellbore positioning. To combat this effect, it is important to increase the size of non-magnetic spacing between the magnetic components in the BHA and the MWD tool sensor.

Another thing that is of great concern is the inclination, as it changes in the well and goes to 90° the well becomes horizontal and as it moves greater than 90° degree the well starts to moves upwards, in that case the physical distance between the bit and MWD sensor decreases and magnetic interference becomes more dominant which ultimately increases the positional uncertainty in the well.

2.6.2 BHA Sag

It is considered to be as the major source of error in inclination measurement. It is defined as the misalignment of MWD accelerometer sensor under the action of gravity and borehole curvature (Macresy, 2006). **Figure 5** shows how the weight of the tool pushes it downward under the action of gravity and causes an offset of the sensor.

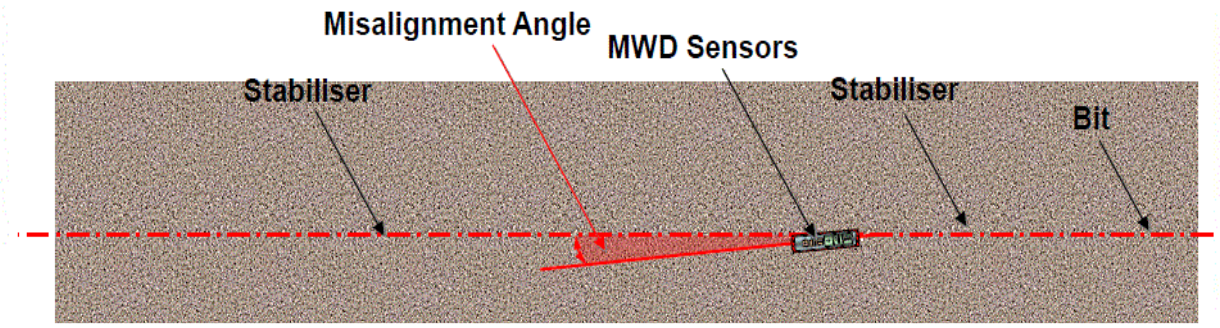

Figure 5 SAG (Misalignment Error) (Bergstrom, 2010)

BHA Sag is directly linked with TVD error term. There are some factors that affect its modeling, which includes the Wellbore and BHA geometry, operating parameters which comprises of mud weight, Weight on Bit (WOB), Bottom-Hole Pressure (BHP) etc. If Sag Correction is applied to any field data it is often assumed that both the hole and the stabilizer are in-gauge. This correction is normally considered systematic in nature and it is modeled as a vertical plane having a gravity component that is perpendicular to the wellbore (H.S.Williamson, 2000).

2.6.3 Measured Depth Error

Improper depth measurements may affect the position of the well. Depth errors in Wireline occur because of thermal expansion of cables and under pressure changes. It is important that these factors should be modeled properly; any residual errors after the proper correction should then be included in the uncertainty model (Andrew G. Brooks, 1996). Unlike other error terms this error should be treated in a completely different way. If there is any uncertainty observed in the measured data then the entire wellbore should be re-measured again starting from the datum. Uncertainty is neither tied nor correlated with the old measurements.

2.6.4 Gyro Drift and Gimbal Effect

Gyroscopic tools are used when there are strong interferences observed because of magnetic storm, magnetic interferences from the nearby well or due to magnetic materials present inside Earth surface. These materials have the tendency to adhere to the tool surface to creating any hindrance to sensor measurements, because in that case MWD tools are not reliable as they experiences some distortion which can affect the positioning of the well. However, there are two major problem associated with these tools that are *gyro drift* and *gimbal effect*.

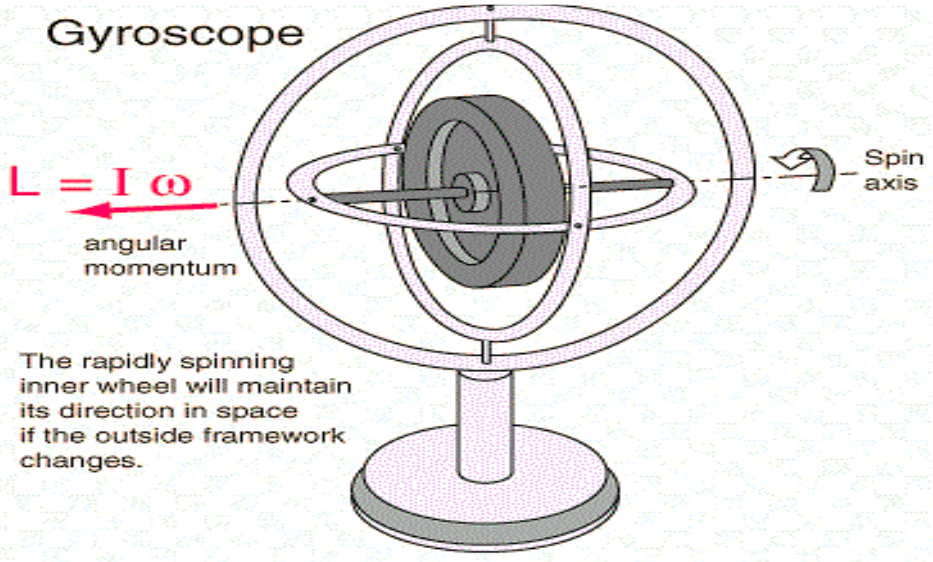

Figure 6 Gimbal effect in Gyro

Due to Earth's inertia, borehole orientation, severe dogleg gyro tools may experience drifting up to 10's of degree (C.J.M.Wolff, 1981). Another problem associated with gyro is the gimbal[3] effect as show in **Figure 6**. At low inclination gyro is properly gimbaled, however, as the inclination increases then the performance of that gimbal construction starts to decrease and there are chances that gyro may flip over. In reality those well having inclination greater than 70° degree will face this flipping problem from gyro and the performance of the tool starts to deteriorate (C.J.M.Wolff, 1981).

[3] Is the ability of an object to rotate about a single axis

2.6.5 Magnetic Declination

Magnetic declination is the angle between the magnetic North and the true North. When using the magnetic tool, uncertainty in magnetic declination can be a major source of error in positioning of the well. Factors that affect the magnetic declination includes location of the well side, magnetic crustal anomalies at that location, altitude, solar magnetic activity and many more. However, crustal anomalies play a vital role in changing declination in comparison with other factors. It is dependent upon the deposition of magnetic material, lava, topographic structures etc.

Errors in declination can be reduced significantly by using a technique called In-Field Referencing (IFR) (Andrew G. Brooks, 1996). This method determines field strength (B), declinations and dip angle for the area of interest for the purpose of providing a more accurate reference to work with. By providing these accurate parameters the lateral uncertainty can be reduced to a great extent.

2.6.6 Geomagnetic Field

Apart from the magnetic interferences from the DS there are also some random magnetic uncertainties that can cause error to the computed azimuth. This is extremely common in the Barents Sea as it is situated in the middle of auroral zone. The total Earth's magnetic field comprises of main field, the crustal field, external disturbance field and local magnetic field.

$$B_T = B_m + B_c + B_d + B_{LMF} \qquad \textbf{Equation 2}$$

Where;

$$\mathbf{B_m = Main\ field}$$
$$\mathbf{B_C = Crustal\ field}$$
$$\mathbf{B_d = Disturbance\ Field}$$
$$\mathbf{B_{LMF} = Local\ Magnetic\ Field\ (DS)}$$

Equation 2 shows the components that make the total magnetic field. The total magnetic field comprises of 95% of the main field and remaining 5% are the rest of the parameters. B_{LMF} occur due to DSI is discussed in **section 2.6.1.** The crustal anomalies are generated as a result of igneous and magnetized rocks that are deposited very close to the Earth's surface. It is extremely important to minimize these anomalies for the purpose of reduction in azimuth

error. For the Barents Sea, the disturbance field creates drastic uncertainty in azimuth measurements especially in MWD tool as compared to other components (Leida C. Monterrosa, 2017).

2.6.7 Temperature and Stresses

Temperature gradient is the change in temperature w.r.t. depth. As drilling starts an increase in temperature is observed by the sensing tool. This increase in temperature can cause a change in length for the pipe and can also cause the change in stresses on the equipment used downhole. However, later one is not that significant, since prior running the tools temperature related stresses are observed and are calibrated under the operating range, but change in length can cause error related to proper position of the well. The change in length can cause the depth measured from wireline and the depth measured from MWD tools to be different. Change in length can also occur because of thermal expansion and the pulling weight from BHA. WOB also increases with depth which is responsible for an elongation in the pipe by pulling it downwards. It is extremely crucial to monitor the WOB and assess its impact on drill collar for the purpose of finding its impact on MWD tool performance.

2.6.8 Cross-Axial Magnetic Interferences

These interferences result from the component that acts perpendicular to z-axis. Most common interference is the hot-spot. During manufacturing of the tool, events such as welding and storing of BHA components create these hot-spots unintentionally. Even while storing they are transferred from magnetic material into non-magnetic material when they are kept in contact for a longer period of time, because in that case some of the magnetism is transferred to the non-magnetic components. This is temporary in nature and needs to be removed by periodically demagnetizing the components.

Sometimes, magnetic interference identical to hot spots are developed because of the use of complex materials such as blades in BHA. Other common examples of cross-axial interferences include nearby well having casing inside them, magnetic fish in any hole section that is abandoned. These interferences are strongly dependent upon the strength of the magnetic poles and its distance from the MWD sensor. If the distance is within 10 m then they have the dominant effect on azimuth uncertainty. To reduce the impact of cross-axial interference it is important to move MWD senor away by increasing NMDC size (Roar Sognnes, 1996).

Error Analysis

As oil industry continues to grow new technologies are develop in order to intercept those shallow formations that are not possible a decade ago. However, interception at the desire location without colliding with the nearby wells needs some analysis of the positional uncertainty and removal of errors associated with the survey measurements. The error terms as discussed in ***Models & Errors in Wellbore Position*** in **Section 2.6** needs some proper assessments so that survey measurement shows the accurate position of the well with minimum uncertainty.

3.1 Short Collar Method

Axial Magnetic Interference as discussed in **section 2.6.1** is the major contributor in azimuth errors. This error is more pronounced when the well is moving in east or west direction. MWD tools comprises of magnetometers and accelerometers. Accelerometers are used to calculated the inclination, whereas, azimuth is calculated by the combination of both. However, because of magnetic interferences magnetometer are highly affected which causes erroneous in azimuth. Magnetic interferences have very little effect on inclinations, so errors in inclinations are extremely small as compare to azimuth.

To remove the error in azimuth a method is introduced naming *"**SHORT COLLAR METHOD**"*. This method does not use the component B_z because it is assumed that this component is the most effected component from the magnetic interference out of all. By in-cooperating this method it was observed that the azimuth errors associated with the survey measurements is reduced by the factor of ten as compare to Standard Method. One major advantage of this method over Standard Method is the use of shorter non-magnetic drill string components without degrading the accuracy of the survey (C.A. Cheatham, 1992).

3.2 Multi-Station Analysis Technique

Multi-Station Analysis (MSA) is a method used to counteract magnetic interferences from DS in directional survey. This method is used to reduce the azimuth uncertainty that is developed as a result of magnetic interferences from DS and ensures that azimuth measurement become more reliable that ultimately helps in accurate wellbore position. However, one the major problem associated with this method is if a well is moving in east/west direction and if for instance, its inclination is greater than 55° degree then MSA method will not allow any correction of axial DSI to take place because at this inclination

BGS Global Geomagnetic Model (BGGS) is having a relatively high degree of inaccuracy, which causes the error of MSA to be larger than Drill String Interferences. In order to minimize this problem it is extremely important to have a proper magnetic reference selection so that both DSI and MSA errors are reduced (Bulychenkov, 2013).

Interferences from DS are generated from two components, one from actively magnetized components another are permeable components that have the characteristic to get magnetized. It is extremely crucial to insulate the MWD sensor as much as possible from these components because these components have the tendency to effect the survey measurement to a great extent. To select the proper length of non-magnetic spacing in BHA, the driller should have information related to well orientation, geomagnetic location and BHA size (Lima, 2004). MSA uses the main field and MWD surveys from each BHA run to optimize the problem, however, if the main field comprises of error and is not properly modeled then MSA is not reliable.

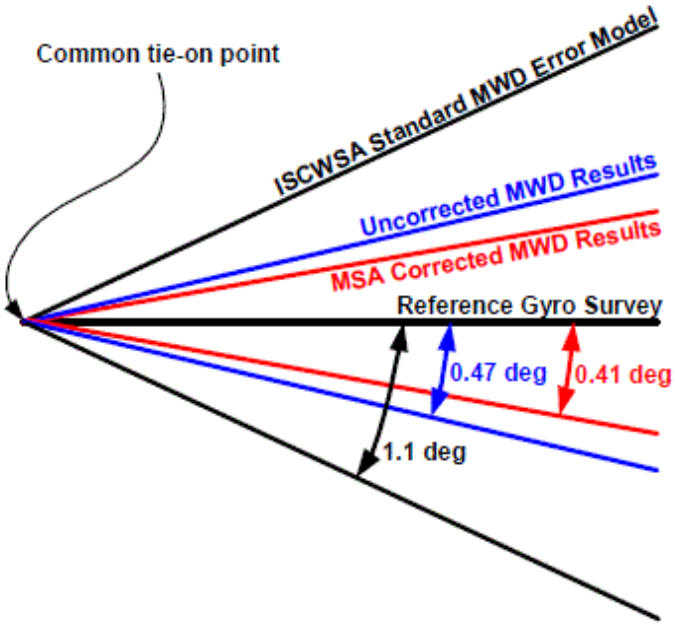

Figure 7 Improvement in Azimuth after MSA (Lima, 2004)

Figure 7 demonstrates an improvement in azimuth uncertainty before and after MSA correction. It is expected that MSA will show significant improvement in wellbore positioning if sensors are properly isolated and main reference field is free from errors.

3.3 Gravity Error Test

Figure 8 shows MWD tools comprises of accelerometers that is having three axes perpendicular to each other

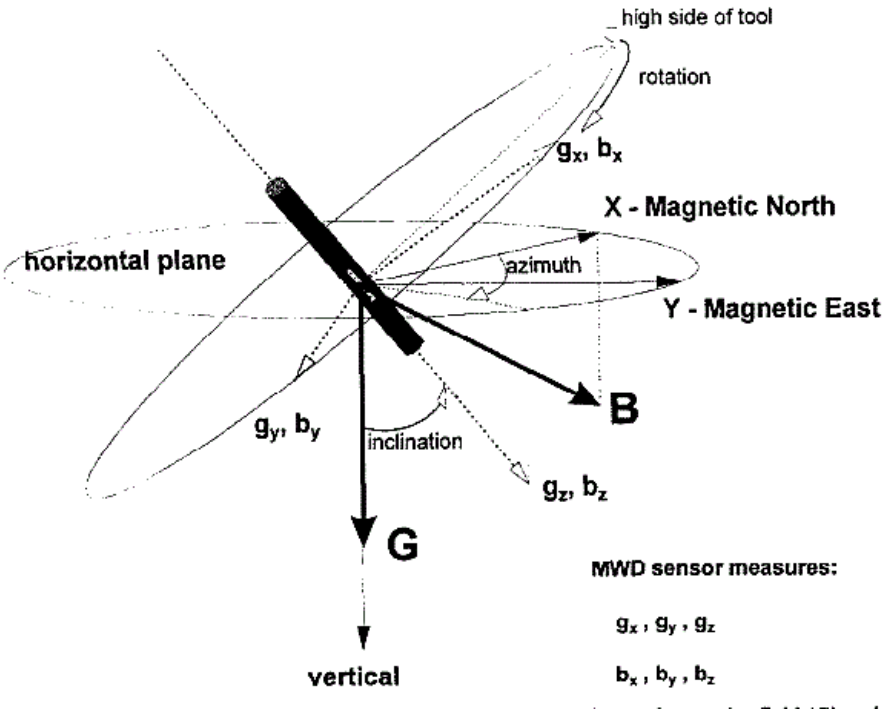

Figure 8 Accelerometer in MWD and its Components (Roar Sognnes, 1996)

The total gravity component is obtained by combining the information from all three axes as shown in **Equation 3**. Any error present in accelerometers will influence its components which ultimately affects inclinations. So, it is of utmost concern to verify the performance of accelerometers at each survey station by considering the errors in knowledge related to local gravity (Ekseth, et al., 2010).

$$G = \sqrt{G_x^2 + G_y^2 + G_z^2} \qquad \textbf{Equation 3}$$

3.4 In-Run and Out-Run Misalignment Test

This test is applicable where misalignment errors are of great concern and is suitable only for those surveys in which toolface changes gradually. If the toolface is constant, then this is not

an ideal option. For this test, it is important to have both in-run and out-run survey for the well path. It is important that before running this test data from both run should be free from all gross accelerometers errors which can be done by applying quality control test such as gravity error test or multi-station test as discussion in **Section 3.2** and **3.3.** This test makes use of the inclination difference test, so it vital to have the in-run and out-run measurement at the same depth run for quality control measurements, for this purpose a depth correlation is established to ensure the method applicability (Ekseth, et al., 2010).

3.5 Demagnetizing Factor Method (Aklestad, 2015)

BHA interference is considered to be major source of error for MWD. In order to eliminate the effect of this error source, it is recommended to maintain a desirable distance between MWD sensors and those magnetic components that are responsible for the interferences; this could be done by incorporating the proper length of non-magnetic components between sensors and magnetic materials in BHA.

It is extremely vital to model the magnetism of each BHA components so as to get an idea of the components responsible for the highest magnetic interference.

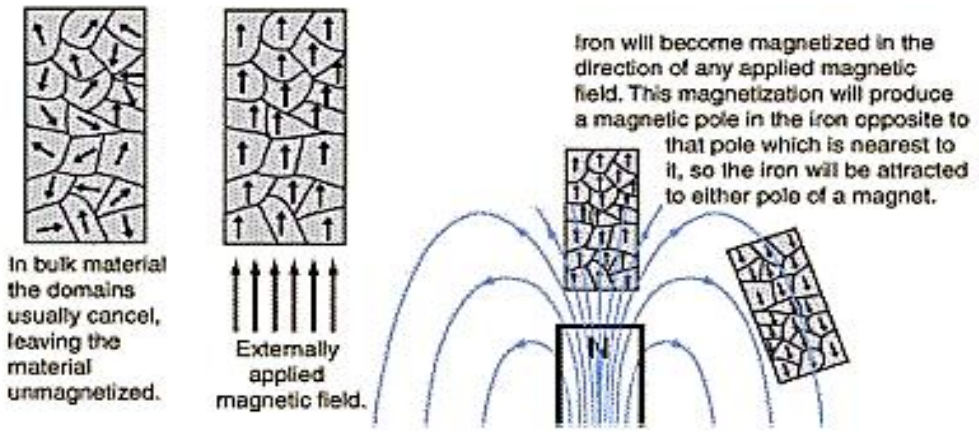

Figure 9 Effect of Magnetic field on Magnetic Material (Aklestad, 2015)

Figure 9 shows the effect of placing a magnetic material in a magnetic field. It shows that the magnetic field inside the material aligned with the external magnetic field, forming an opposite magnetic polarity poles on either ends. These poles are responsible for decreasing the overall magnetization inside an object.

The amount of magnetization is a strong function of the applied field strength, material magnetic permeability and length to diameter ratio for spheroid. The magnetic field inside spheroid is given by **Equation** 4

$$B_{in} = \mu_o \left(\frac{H_{ad}}{N}\right) + \mu_o \left(\frac{N-1}{N}\right) H_{in} \qquad \textbf{Equation 4}$$

Where,

$$\boldsymbol{H_{ad} = applied\ magnetic\ field}$$

$$\mu_o = \boldsymbol{magnetic\ permeability\ of\ free\ space}$$

$$\boldsymbol{N = Demagnetizing\ Factor}$$

$$N = \left(\frac{1}{m^2-1}\right)\left[\frac{m}{2\sqrt{m^2-1}} Ln\left(\frac{m+\sqrt{m^2-1}}{m-\sqrt{m^2-1}}\right) - 1\right] \qquad \textbf{Equation 5}$$

Equation 5 shows the formula for demagnetizing factor, where $\boldsymbol{'m'}$ is the ratio between the semi major axis and semi minor axis which can be obtained by creating the covariance matrix and then determining the Eigen values in which larger value correspond to the semi major axis and smaller values indicates the semi minor axis. For ellipses, the charge density at its center is normally zero. The positive charges are focused on one side, whereas, the negative charges are focused on another.

$$Q = \frac{\mu_o(\mu_{max} - \mu_{min})H_{ad}\,A}{\left(1 + N(\mu_{max} - 1)\right)\left(1 + N(\mu_{min} - 1)\right)} \qquad \textbf{Equation 6}$$

Where,

$$\boldsymbol{A = cross\ section\ area\ of\ ellipse\ m^2}$$

$$\mu_{max=} = \boldsymbol{Maxmium\ Permeability\ of\ BHA\ component\ Wb.m/A}$$

$$\mu_{min} = \boldsymbol{Minimum\ Permeability\ of\ BHA\ component\ Wb.m/A}$$

Equation 6 is used to calculate the magnetic pole strength for BHA or any other component. This equation indicates the amount of magnetization that is left after the external applied field is zero.

Normally, BHA is made up of carbon-steel and it has the tendency to get readily demagnetized as soon as applied magnetic field is removed, however, there is still some

magnetization present that is due to stresses induced during drilling and also because of temperature that increases down-hole which is discussed in **Section 2.6.7.** Once all the information is determine it is easy to get an idea that which component is responsible for causing the major fluctuation in MWD sensor. In this way a proper selection of NMDC or any other materials can be made which reduces this effect. There are couples of advantages for this method, firstly, there is no limitation for BHA size and secondly, it can be used for any location as it is incorporating field strength for any location (Aklestad, 2015).

3.6 Inclination Difference Test

Inclination measured during survey comprises of sag and misalignment errors. To remove these error terms, an inclination-difference tests is performed which is based on two different overlapping surveys. These errors terms are not directly tested but are looked as a combined effect that affects the inclination accuracy. The test does not specifically detect the error source. It just indicates that out of the two surveys that are been compared one have something suspicious.

It is extremely vital to have a depth correlation between the two surveys because this will help in getting the proper inclination difference between the two surveys, which is then useful in eliminating the error terms associated with inclination. Due to the systematic nature of the inclination error there are often cases that these error terms might slip away without getting noticed. It is highly recommended that a proper quality control test is run in order to detect these error sources. (Ekseth, et al., 2010)

3.7 Azimuth Difference Test

In terms of mathematical formulation this test is similar to test discussed above. It is highly recommended that if there is any significant change in BHA then a three station azimuth difference test should be performed, which is a useful test against any errors related to BHA magnetization. It is again important to depth correlate between two surveys before making any further calculations.

$$\text{True Azimuth} = \text{Magnetic Azimuth} + \text{declination} \qquad \textbf{Equation 7}$$

As seen from **Equation** 7**,** true azimuth is strongly dependent upon declination, any error associated with declination cause an error in true azimuth. However, this method does not determine the error in declination directly; it just indicates that something is wrong with

the calculated azimuth in any of the two surveys that are involved. To quantify the value, it is important to perform different types of quality control test that identify the real cause of error too (Ekseth, et al., 2010).

3.8 Measured Depth

Errors associated with depth measurement commonly occur because of drill pipe measurements, thermal expansion of drill pipe, compression of drill string under mud pressure and many more. There is another important issue that is as equally responsible for error in depth measurements as the factor mention previously that is rounding off MWD depth reading to the nearest meter or foot. This error can also cause problems while comparing two survey measurements. To reduce these depth related errors, it is important to properly estimate the vertical depth of Oil-Water Contact (OWC) or properly establish the formation top. One of the major drawbacks for this error source is it cannot be removed by repeated measurements of running in hole, because the length of drill pipe is not measured again and again while running them for next survey (Rune Sele, 2000).

3.9 Noise Induced by Vibration

During drilling another major source of error in measurement that could distort MWD tool sensor measurements is noise. Inclination from NBI and ATI is calculated having bit on bottom while drilling is performed. During drilling bit bouncing creates axial vibrations especially in vertical section and then quickly dampens out as drilling is moved to horizontal section, but still there will be some acceleration as a result of bit bouncing. These accelerations are then sensed by z-axis accelerometer which is the most vital component for measuring inclination in horizontal section. This component is assumed to biased as it always moves in the same direction every time. The amplitude of the vibration is dependent upon the type of bit used and the strength of the rock (Rune Sele, 2000).

3.10 In-Field Referencing (IFR)

This method is used for measuring the geomagnetic field at or near the drilling rig site. Magnetic tools locate the direction of wellbore by using the direction of geomagnetic field at that particular location. However, when using this survey method both the magnetic variations and errors associated with the local magnetic field are ignored.

It is commonly observed that the uncertainties associated with the magnetic tools such as MWD are considerably greater than gyro tool due to error in declination and magnetic interferences from nearby well. In order to reduce these error terms, it is important to measure the local geomagnetic field on regular intervals, for that purpose IFR has the capability to improve the accuracy of the magnetic surveys (D.J.Kerridge, 1995).

The geomagnetic field, as discussed in **Section 2.6.6,** comprise of three principle sources and is dependent upon total field strength (F), dip angle (I) and Declination (D). Geomagnetic Field is regularly measured at the observatory station.

IFR is preferred option for the land rig site especially where any interference from the rig, nearby well or manmade are negligible. For offshore locations, this technique is extremely hard to implement. In the past, this method comprised of some difficulties that are associated with data transmission, sensor calibrations, power supply and transportation.

For North and Barents Sea, the cost of using this method is a great concern since one unit is necessary for one particular drill site. However, one major problem that proves to be vital especially for the Barents Sea is the closest onshore geomagnetic station which is approximately 400 km away.

Figure 10 shows the closet variometer station in Barents Sea, from where this IFR technique can be implemented.

A latest IFR method was introduced that eliminates the need of magnetometer at the drilling rig site. This method comprises of making ‘spot’ and ‘snap shot’ measurements of magnetic field close to the drilling site. These measurements are made in order to establish a baseline between the drilling rig-site magnetometers and remote magnetometers several kilometers away. This method is based on conducting an interpolation from one location to another. By using this interpolation technique, errors such as crustal anomalies, external disturbances are removed from the magnetic geomagnetic field.

However, there are some errors which are difficult to remove in this method and there quantification is dependent upon the latitude of the drill site. For higher latitude, these errors are small as compare to medium latitude. This method is a cost saving option as it reduces the number of gyro runs and errors linked with sensors measurements. (D.J.Kerridge, 1995).

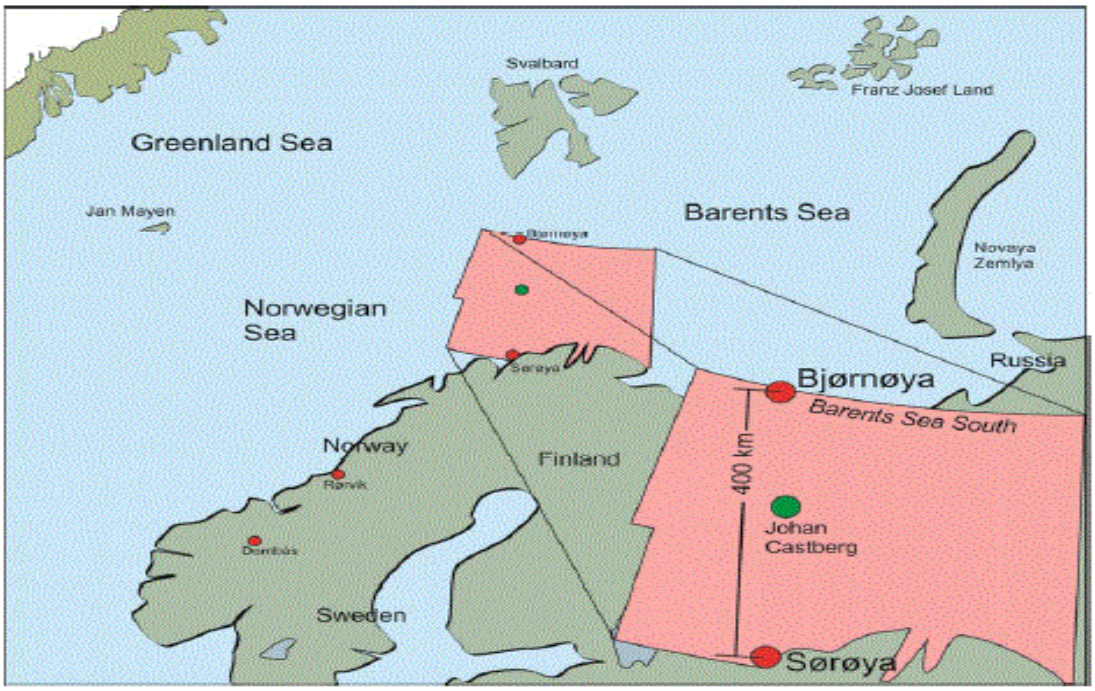

Figure 10 Closest Variometer Station to Barents Sea (I.Edvardsen E. B., 2013)

Positional Uncertainty Analysis and Probability

4.1 Introduction

Analysis of positional uncertainty is an important segment in order to converge at the target. Uncertainties lie in every measurement that are been made during the survey. It is extremely crucial to reduce these uncertainties for the purpose of intersecting at the desire location. Increase in positional uncertainty will reduce the probability of hitting at the target location. The output obtained from the survey tools are inclination, azimuth and measured depth (Andrew Buchanan, 2013), however, these all are measured quantities which comprises of different error sources can offset the well location up to a certain degree. The location of the well is defined by the Ellipse of Uncertainty (EOU). To reduce the dimensions of EOU, ISCWSA as discussed in **Section 2.4** introduces some models related to MWD and Gyro which effectively helps in decreasing the size of uncertainties

4.2 Ellipses of Uncertainty

It is basically defined as the volume of uncertainty in wellbore position at any specific depth.

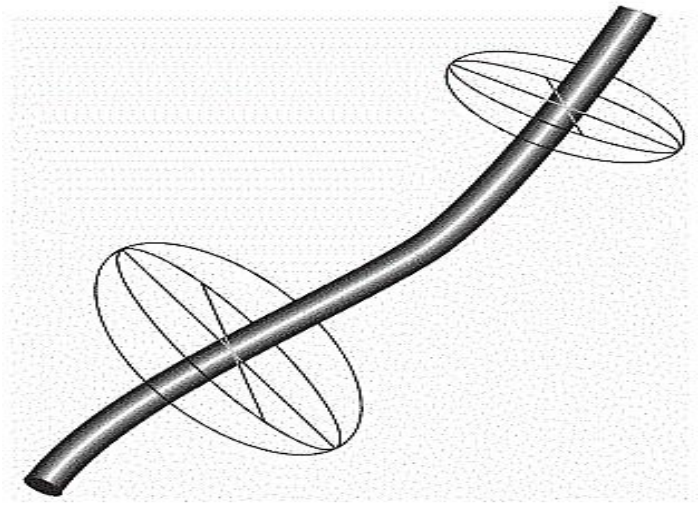

Figure 11 Ellipses of Uncertainty (B. Poedjono, 2007)

Figure 11 represents the ellipse having certain volume and a given statistical confidence level. Selection of proper tool error model helps in minimizing the uncertainty associated with the measurements, thereby ensuring the proper optimization of the driller target.

Analysis of uncertainty not only helps in reducing the cost, but also helps in providing the safe environment for effective and sustainable drilling. The axes of the ellipses are normally

related to the errors linked with the measurements. As the depth increases, the size of EOU also start to increase at each survey station as uncertainties accumulates at each survey stations. Errors, that are responsible for the uncertainty, propagate because of tool used for surveying and the environment in which they are used. The Measured Depth (MD) uncertainty occurs due to thermal expansion and error in length measurements, while errors in azimuth and inclinations occur because of tool offset, magnetic interferences from DS and nearby well.

4.3 Steps Involved in Calculations of EOU

The steps used in self-made model for calculating the EOU dimensions are discussed in this section below:

I. Availability of the survey data that comprises of MD, Inclinations, Azimuths, Northing, Easting, Tool face and Dogleg. This can be obtained directly from the COMPASS^{TM} Report. It is extremely easy to determine ΔN and ΔE at each survey station from the report.

II. The data that is obtained is the measured value. In order to convert it into True value errors needs to be evaluated and should be incorporated accordingly. **Equation 8** shows how to convert measured value into true measurements. The choice of addition and subtraction of the errors depends upon the position of the sensors.

$$\text{True Measurements} = \text{Measured Value} +/- \text{Errors} \qquad \textbf{Equation 8}$$

III. Errors are associated with every measurement. These are responsible for the variation in position of the well and can create drastic uncertainty in well placement. If they are not handled properly they can become a source for decreasing the probability of striking at the desired location. The error source which are responsible from uncertainty are discussed in **Section 2.6**

IV. If the errors propagate systematically at each survey station then they are arithmetically added to the measured value, however, if the propagation mode is random then square root of sum of squares is used.

V. At each survey station the effect of error from the previous stations are also incorporated. New inclinations and azimuths are determined which have the combined effect from different error sources

VI. Based on the Step (V), new Delta N, Delta E and Delta V are obtained using the Minimum Curvature equations listed below in **Equation 9**

$$\emptyset = \cos^{-1}(\cos\alpha_1 \cos\alpha_2 + \sin\alpha_2 \sin\alpha_2 \cos(\beta_2 - \beta_1)$$

$$F = \frac{2}{\emptyset}\left(\frac{180}{\Pi}\right)\tan\left(\frac{\emptyset}{2}\right)$$

Equation 9

$$N = \left(\frac{FL}{2}\right)(\sin\alpha_1 \cos\beta_1 + \sin\alpha_2 \cos\beta_2)$$

$$\Delta E = \left(\frac{FL}{2}\right)(\sin\alpha_1 \sin\beta_1 + \sin\alpha_2 \sin\beta_2)$$

VII. Once the new coordinates are obtained, the Mean value is then determined using the relation in **Equation 10**

$$\bar{\mu} = \frac{\Delta N_1 + \Delta N_2 + \Delta N_3 + \Delta N_4 + \ldots\ldots\ldots\ldots}{\text{Number of Measurements}}$$

Equation 10

The same relation is applied for ΔE coordinates

VIII. The next step involves the determination of the standard deviation for each survey station using the mean ($\bar{\mu}$) obtain from the above equation.

$$\sigma = \sqrt{\frac{\sum_{i=1}^{N}(X_i - \bar{\mu})}{N}}$$

Equation 11

IX. The next part is to determine the Variance for both Delta N and Delta E using the standard deviation in Step (VIII).

$$\text{Variance} = \sigma^2$$

Equation 12

For EOU it is extremely important to determine the relationship between Delta N and Delta E. This relation is established based on Covariance between the two set of data, by using

Equation 13

$$\mathrm{COV} = \mathrm{E}(\mathrm{X} - \mathrm{E}(\mathrm{X}))\mathrm{E}(\mathrm{Y} - \mathrm{E}(\mathrm{Y}))$$

$$\mathrm{COV} = \mathrm{E}(\Delta\mathrm{N} - \overline{\Delta\mathrm{N}})\mathrm{E}(\Delta\mathrm{E} - \overline{\Delta E}) \qquad \textbf{Equation 13}$$

Where;

E(X) and E(Y) are defined as the Expected Value for Delta N and Delta E. In this study model they are considered as the Mean.

X. A 2x2 Covariance Matrix is produced using Delta N and Delta E. The diagonal value consists of variances of Delta N and Delta E, whereas, the offset from diagonal comprises of covariance. **Equation 14** represents the matrix structure that is used in this study.

$$\begin{pmatrix} \sigma_{\mathrm{N}}^2 & \mathrm{Cov}(\Delta\mathrm{N}, \Delta\mathrm{E}) \\ \mathrm{Cov}(\Delta\mathrm{N}, \Delta\mathrm{E}) & \sigma_{\mathrm{E}}^2 \end{pmatrix} \qquad \textbf{Equation 14}$$

XI. Relationship indicated in **Equation 15** was used to compute the Uncertainty Ellipses dimensions where λ denotes the Eigen values and I as a identity matrix.

$$\mathrm{A} - \lambda\mathrm{I} = 0$$

$$\begin{pmatrix} \sigma_{\mathrm{N}}^2 & \mathrm{Cov}(\Delta\mathrm{N}, \Delta\mathrm{E}) \\ \mathrm{Cov}(\Delta\mathrm{N}, \Delta\mathrm{E}) & \sigma_{\mathrm{E}}^2 \end{pmatrix} - \lambda \begin{pmatrix} 1 & 0 \\ 0 & 1 \end{pmatrix} = 0 \qquad \textbf{Equation 15}$$

XII. Step XII will provide with a quadratic equation in the form of **Equation 16**

$$\lambda^2 - \big(\mathrm{Var}(\Delta\mathrm{N}) + \mathrm{Var}(\Delta\mathrm{E})\big)\lambda - \mathrm{Cov}^2(\Delta\mathrm{N}, \Delta\mathrm{E}) + \mathrm{Var}(\Delta\mathrm{N})\mathrm{Var}(\Delta\mathrm{E}) = 0 \qquad \textbf{Equation 16}$$

Where,

a = 1

b = $-\big(\mathrm{Var}(\Delta\mathrm{N}) + \mathrm{Var}(\Delta\mathrm{E})\big)$

c = $-\,\mathrm{Cov}^2(\Delta\mathrm{N}, \Delta\mathrm{E}) + \mathrm{Var}(\Delta\mathrm{N})\mathrm{Var}(\Delta\mathrm{E})$

Using the Quadratic formula $\frac{-\mathrm{b} \pm \sqrt{\mathrm{b}^2 - 4\mathrm{ac}}}{2\mathrm{a}}$ and solving the above equation two Eigen values λ_1 and λ_2 will be obtained where the largest will correspond to the Semi Major Axis value

XIII. A scale factor of 2.4477 is used to create the 95% confidence level ellipse

XIV. To determine the largest axis of the ellipse following formula is implemented

$$\text{Semi Major Axis} = \frac{1}{\sqrt{\text{Largest Eigen Value}} * (\text{SF})}$$

XV. The uncertainty is added to each survey station and at the final survey station uncertainty is the sum of all stations.

XVI. **Equation** 17 denotes the formula implemented to obtain the uncertainty at any particular station

$$\text{Uncertainty at station}_i = \sum_{i=2}^{N} \text{Uncertainty at station}_{i-1} + \text{Uncertainty at station}_i$$

Equation 17

4.4 Probability of Hitting (J.Bang, 2017)

Collision between the wellbore can lead to serious economic and environmental damage. Therefore, it is extremely important to analyze the probability of collision during the well planning and drilling phase. On the other hand, in this study it is important to directly hit the Targeted well since it is based on controlling unwanted flow of oil and gas from the Relief well. However, the method used in section of probability calculation provides an optimistic result as it is effective only for straight wellbore section. It is of utmost concern to properly quantify the probability since it helps in altering the drilling plan to make it as precise as possible before drilling commence.

Analysis of the probability requires the quantification of position uncertainty between the two wells. The position uncertainty is available for all data points at different survey stations. Calculations of position uncertainty are explained in **Section 4.3**. However, apart from the position uncertainty there are also other factors that can influence the direct hitting

probability which includes center to center distance between the two well, radius of ellipses for both wells and standard deviation of center to center distance. The following are the steps involved in calculation of probability for the direct hitting between two well:-

I. Determine the center to center distance between the two wells which in this case is denoted by D_{cc}.

II. From the analysis done in **Section 4.3** the size of semi major axis can be determined. This analysis is done for both the Relief Well and the Targeted Well. These axes are then converted into Radii by using the expressions indicated below

$$\mathrm{R_R} = \frac{\text{Semi Major Axis of Relief Well}}{2} \;\&\; \mathrm{R_T} = \frac{\text{Semi Major Axis of Target Well}}{2}$$

III. Before the estimation of the probability, it is important to select the desired location for the intersection. According to normal industry standards the intersection probability for that location should be approximately equal to 0.5% especially in the Relief Well case

IV. It is commonly assumed that the survey data is normally distributed for that reason Gaussian Normal Distribution is feasible as the erroneous nature and the distribution of the survey data becomes clearer. For normal probability distribution **Equation 18** is implemented.

$$\mathrm{P(x)} = \frac{1}{\sigma\sqrt{2\Pi}} * \mathrm{e}^{\left(\frac{\mathrm{x}-\bar{\mu}}{2\sigma^2}\right)} \qquad \textbf{Equation 18}$$

V. The error function that is associated with the Gaussian Normal Distribution is calculated using the **Equation** 19 indicated below.

$$\mathrm{erf}(x) = \frac{1}{\sqrt{2\Pi}} \int_0^x e^{\frac{-y^2}{2}}\, dy \qquad \textbf{Equation 19}$$

VI. Using this erf $function$ provided in **Equation** 19**,** the probability of hitting direct into Targeted Well is calculated using **Equation 20** below. The equation is more suitable for the straight section well, as it provides an optimistic result for more curvature wellbore.

$$P_{DH} = \frac{1}{2}\left(\mathrm{erf}\left(\frac{D_{cc}+R_R+R_T}{\sqrt{2}\sigma_{cc}}\right) - \mathrm{erf}\left(\frac{D_{cc}-R_R-R_T}{\sqrt{2}\sigma_{cc}}\right)\right) \qquad \textbf{Equation 20}$$

VII. The contribution of individual error source in the total hitting probability is also estimated by simply interchanging the R_R and R_T obtained from total with R_R and R_T for individual ellipse generated from each error source. However, other parameters are kept constant.

RESULTS & DISCUSSION

5.1 Introduction

The main focus in this work is to try and reflect the working principle of Landmark COMPASS^{TM} software in a self-made model and then match the two different data series. This work is the continuation of the semester project, where a Relief Well is planned to intersect the Targeted Well to control the unwanted flow of oil and gas up to the surface. However, a detail error analyses along with some special cases are discussed in this work. The geographical coordinates for the Relief Well is $73°19'N$ & $24°15'E$ and map coordinates $8{,}139{,}213\ mN$ & $411{,}989\ mE$. On the other hand, the Targeted Well is considered to be 700 m away from the Relief Well having map coordinates $8{,}139{,}913\ mN\ and\ 411{,}989\ mE$. Both the wells are designated in the North direction having small changes in East coordinates

5.2 Relief Well

Figure 12 represents the North and East coordinates of the Relief Well with respect to Measured Depth (MD). The well is decided to give an inclination from 510 mMD, however, the maximum change in azimuth for the entire well path is considered to be 4° degrees. Consequently, the well is more dominant towards the North side rather than on the East.

The trajectory of the well path also affects the dominance of the different error sources. Impacts from some of the error sources have more considerable effect when the well path is north dominated. The maximum dogleg for this well is $10.8°\ degrees/30\ m$. And the total Measured Depth (MD) is 1400 mMD. The well is decided to collide into the Targeted Well at the depth of around 690 mMD to prevent the unwanted flow of oil and gas up to the surface.

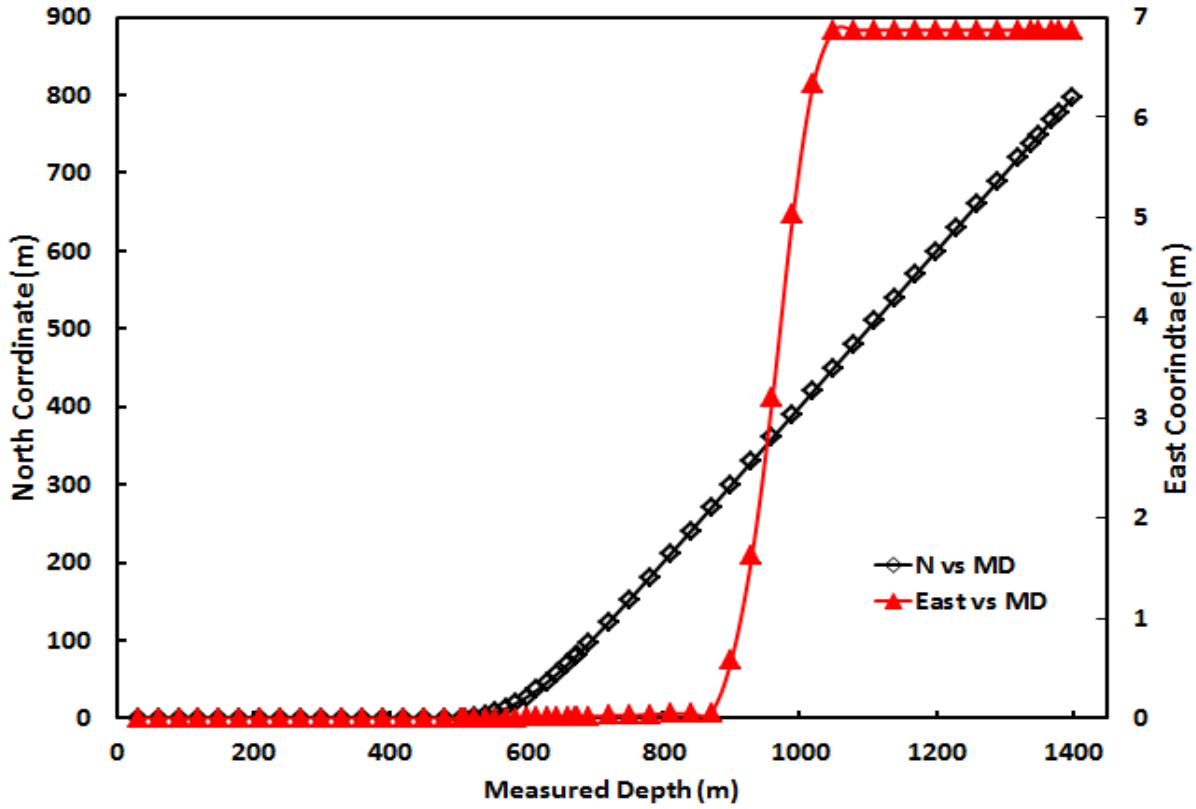

Figure 12 Relief Well Trajectory in North and East Coordinate System

5.3 Error Analysis from COMPASS™

During this study, the impacts of each error sources are separately analyzed and based on the results the Semi Major Axis of the ellipses are calculated. The total ellipse generated by COMPASS™ at each survey station is the square root of the sum of squares of each error source. **Table 4** in **Appendix A** shows the ellipse size developed as a result of each error source at each survey station.

The impact of each error term in simply obtained by removing all the error terms except the one that is been analyzed from the tool IPM files and then generate a separate "Error Ellipses Report" for each term. From the analysis, it is noticed that declination error is the most dominant factor that contributes heavily on the ellipse size. The dominance of a particular error term is dependent upon the direction of the well path. Some error sources have considerable impact if the well trajectory is more towards East, while some have more impact if the well is moving towards North, which is the case in this study.

The total Semi Major Axis of the Ellipse at the final station is 19.69 m at 1400 mMD. The same procedure is applied for the Targeted Well. However, for the Targeted Well the ellipse

size is consider till the depth of 690 mMD where the Relief Well is planned to intersect. At that depth of interest, the ellipse semi major axis generated by COMPASS^{TM} is approximately 2.38 m.

Figure 13 and **Figure 14** represent the contribution of each error terms in the total size of semi major axis. The figures indicates the sensor errors which includes accelerometer biased, accelerometer scale factor, magnetometer biased and magnetometer scale factor have little contribution to the uncertainty ellipse dimension, because these terms are dependent on $\sin(Az_m)$ and in this case both the wells are oriented towards North having small change in azimuth, so this factor is close to zero with ultimately reduces the overall impact of these sensors terms.

On the other hand, error terms that includes Declination (DEC) and DIP Angle contributes heavily in ellipse dimension, having uncertainty around 17.86 m and 6.37 m at the final station. Both of these terms are a strong function of Total Magnetic Field (TMF), which gives the idea that the major uncertainty lie in this parameter that is true in the case especially of Barents Sea as this factor is extremely difficult to evaluate

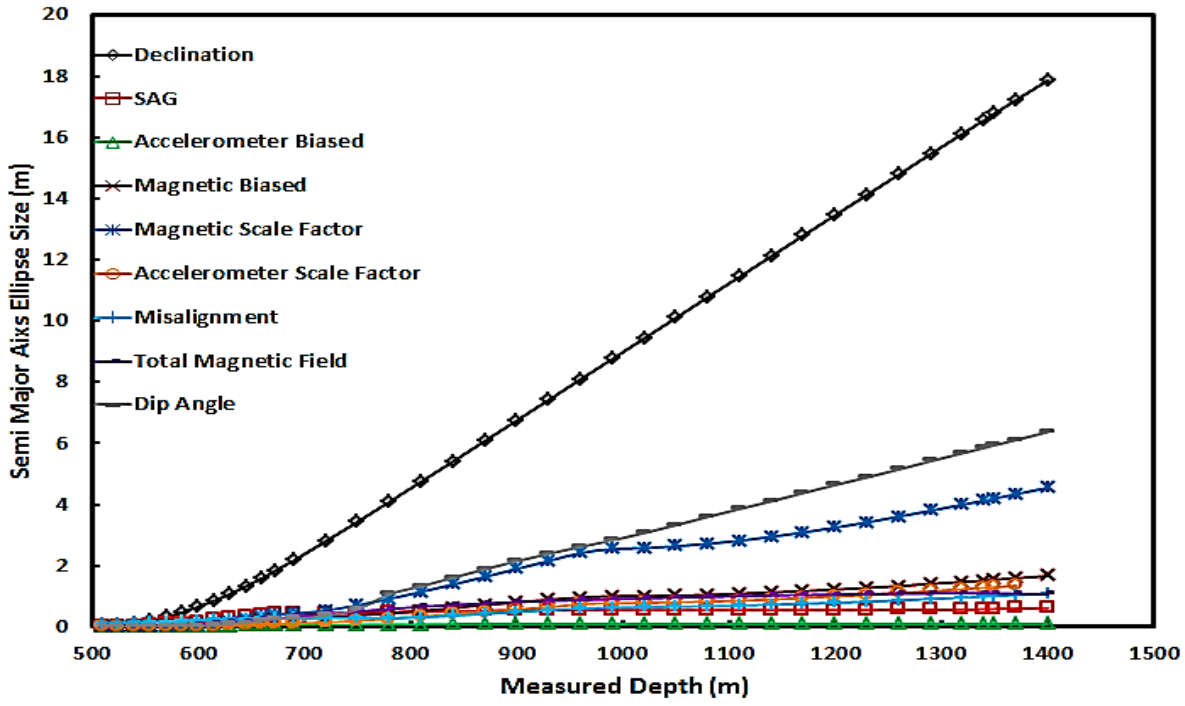

Figure 13 Relief Well 1 Semi Major Axis Size for each Error Terms

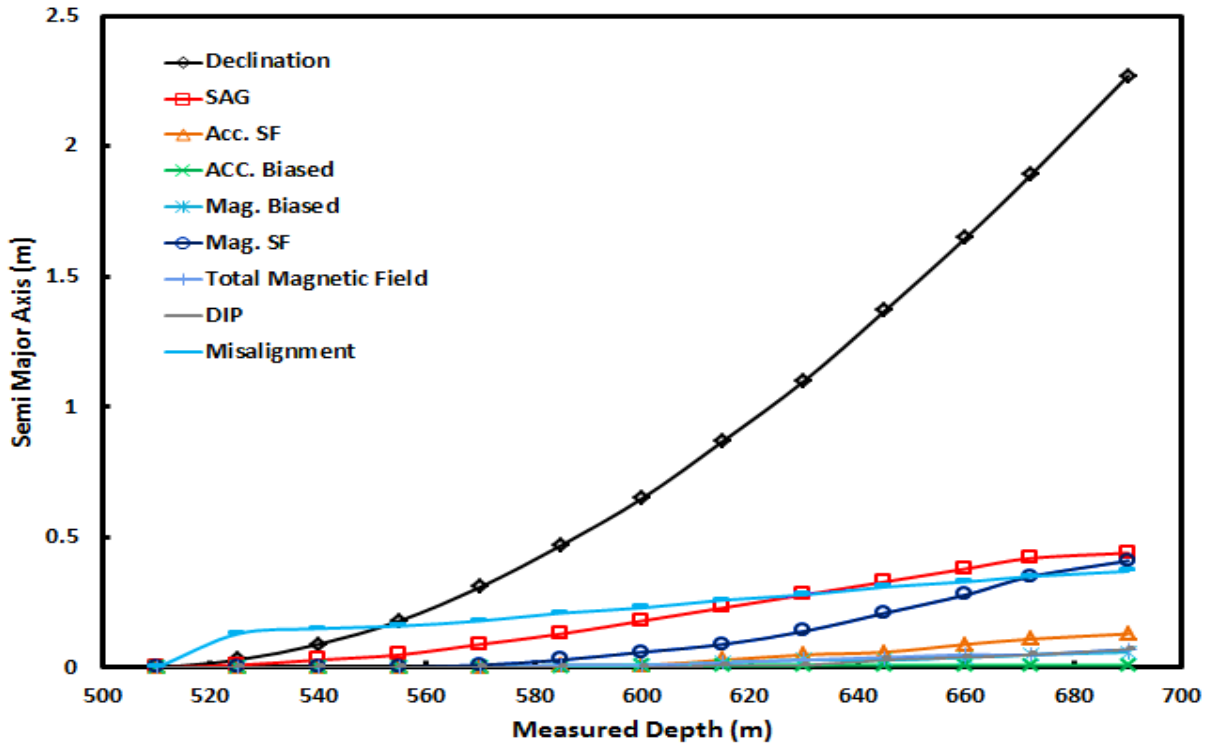

Figure 14 Target Well Semi Major Axis Size from each Error Terms

5.4 Probability of Hitting from COMPASS™

Section 4.4 describes the procedure for calculating the Probability of Hitting/ Collision between two well. The same procedure is implemented for calculating the probability of hitting the Targeted Well from the Relief Well. The total probability of hitting obtain from COMPASS™ is 0.0399, which represents 1 proper intersection in every 25 attempts.

Figure 15, indicates the contribution of each error term in the total probability of 0.0399. These probabilities are dependent upon the ellipse radii, center to center distance and its standard deviation of the distance.

Table 1 below indicates the probability contribution of each error term in total probability at the last survey station of 1400 mMD. By considering, the square root of the sum of square, the total probability at each survey station can be obtained.

Table 1 Relief Well Last Station Probability for each Error Term

mMD	DEC	AB	ASF	MB	MSF	TMF	MIS	DIP	SAG
1400	0.036	1.9E-4	0.0027	0.003	0.0086	0.0019	2.9E-3	0.010	0.0024

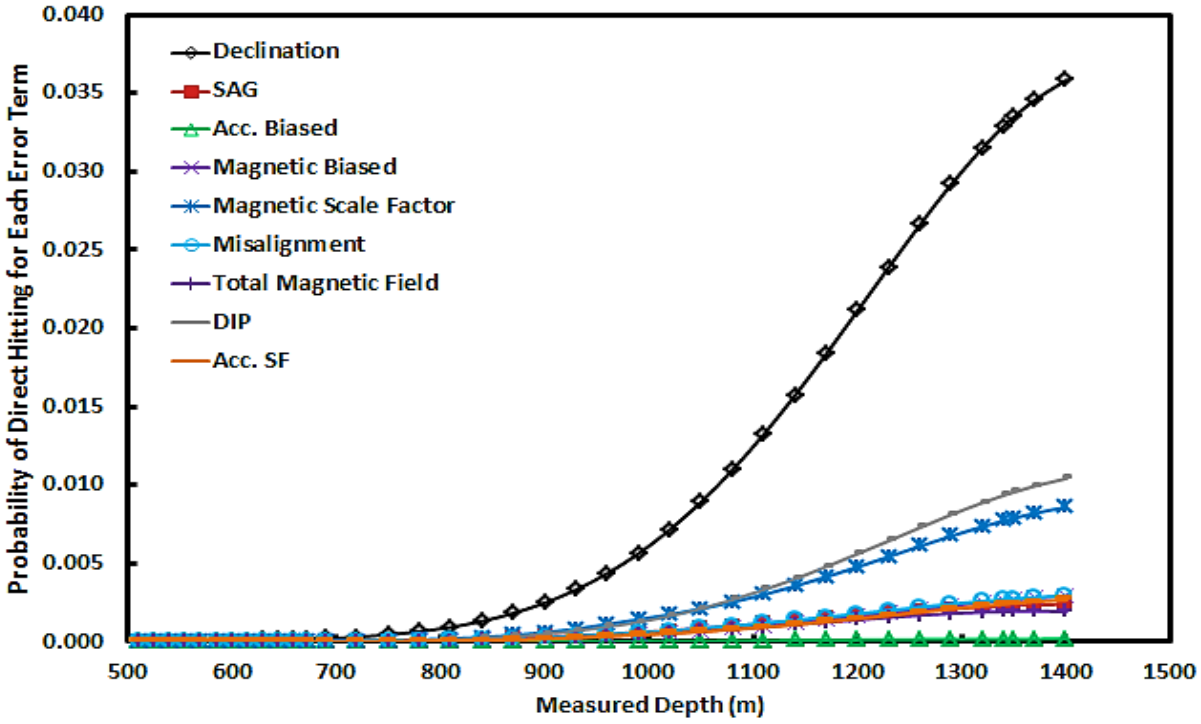

Figure 15 Contribution of each Error Term in Total Probability for the Relief Well

5.5 Model and Performance

The ultimate aim behind this study is to develop a model that not only analyze the error sources associated with directional survey in far north, but also try and reduce the uncertainty ellipse dimension.

The model evolved by incorporating equations given in **Table 8** in **APPENDIX B.** However, for the analysis purpose an exemplar BHA shown in **Figure 37** is used to determine the DSI. Before starting the analysis, some useful parameters are determined separately that helps in the further investigation. These parameters are discussed below.

5.5.1 BHA Interferences

The method used in this analysis is ***Demagnetization Factor*** that is discussed in **Section 3.5.** Sensors in the exemplar BHA are placed at 25.65 m away from the bit. Priority should be given to that phenomenon that creates any interference and are responsible for reducing the working capabilities of sensors.

The BHA in this study is divided into three main regions. Region 1 is allotted the area from bit to the stabilizer with the total magnetic length of 12.35 m. This region is 13.30 m away from D&I sensors. Out of all, this region has the most considerable impact on the sensors performance as bit is made up of carbon steel that is having a high magnetic permeability and profound magnetic characteristics. This is region is considered to be the main segment of study, as its impact can seriously changes the sensors performance and results in the high level of uncertainty.

Region 2 comprises of stabilizer and UBHO, both having magnetic capabilities that deteriorates the performance of sensors. This region is however, 3 m in length and is the closest of all the other regions, on the other hand, this area does not show any interferences as both the lower and upper end of the region are having same magnitude but different polarity.

Region 3 comprises of crossover and collars with a total magnetic length of 74.7 m. However, the interferences experienced from this region are relatively small, as this region is 35.9 m away from the sensors. **Table 2** indicates the magnitude of the interferences that occurs in the BHA.

Table 2 BHA Interferences

REGIONS	DISTANCE (m)	INTERFERENCES (nT)
Region 1	13.30	140.14
Region 2	3.8	0
Region 3	35.9	8.51E-11

Region 1 is showing a relatively high interference of about 140.14 nT, to reduce this interference from the bit, selection of the appropriate length of Non-Magnetic Drill Collar (NMDC) is of utmost concern. Increasing the size of NMDC between the bit and MWD sensor can significant reduces the impact of the interferences from the bit. In the above BHA example, the size of NMDC is 9.5 m that is responsible for this 140.14 nT of interference. A sensitivity analysis, indicated in **Figure 16** is performed related to the proper selection of NMDC, which shows that as the size of NMDC is increased there is a drastic reduction in interference, since the sensor are moving away from the potential source. **Table 3** shows the variable size of NMDC and the resultant bit interferences

Table 3 Length of NMDC verses Interferences	
Length (m) NMDC	**Interference from Bit (nT)**
9.5	140.14
10	128.46
20	33.91
30	13.76
40	6.92
50	3.97
60	2.48

It is also observed that the Z component of the Magnetometer Biased (MB) is the most affect component out of all and is highly influenced from the bit interference. This parameters not only is depended upon the Total Magnetic Field (TMF), but is also affected by bit interference.

Figure 38 in **APPENDIX B** shows the impact of bit interference on this component. It is monitored that as the size of NMDC decreases, the error associated with this components starts to decrease and moves towards zero. In the analysis, the size of NMDC is 9.5 m that shows a high degree of fluctuations in this parameter; however, if the size of NMDC is increase to 20 and then to 40 it is observed that the error term starts to reduce significantly and moves towards the zero. This is possible because the physical distance between the MWD tool sensors and the bit is getting larger, which enables the sensor to perform with high degree of accuracy as compare with the 9.5 m NMDC where the distortion from bit magnetism is relatively higher and sensor performance is lower.

However, the cost of increasing the size of NMDC should be taken into consideration, as increasing the size needs some additional equipment that ultimately affects the overall cost of BHA.

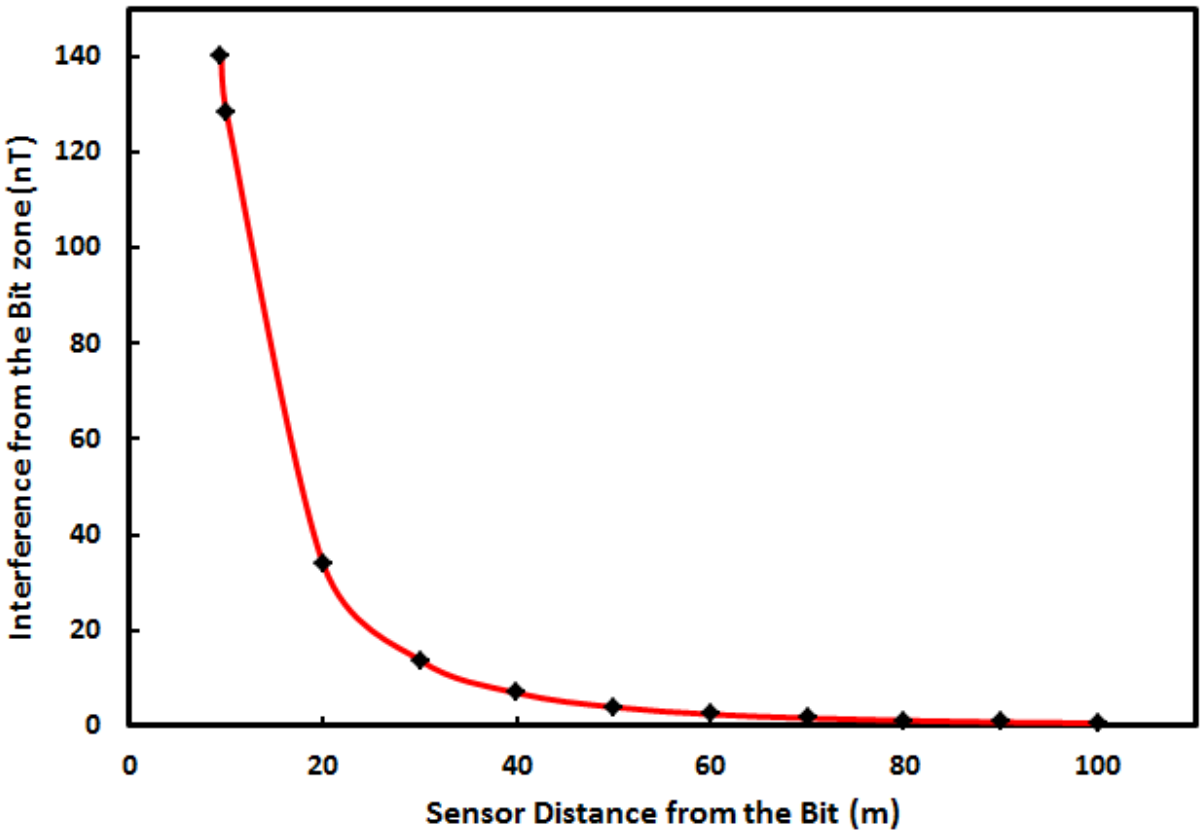

Figure 16 NMDC Sensitivity Analyses

5.5.2 Permanent Magnetism

During the designing of the model the permanent magnetism for the selected area is also evaluated. The area of interest is situated in Barents Sea having $73°19'N$ & $24°15'E$ coordinates. At these coordinates, the total magnetic field observed is around 54,368.96 nT, having horizontal and vertical components to be 9,213.5 nT and 53,582.6 nT.

Using these parameters the permanent magnetism of the BHA is calculated. The normal trend indicates a very consistent pattern for each B_x, B_y and B_z. However, in this case there are quite a large number fluctuations in B_x and B_y components. This could be because of the stresses that are induced as a result of temperature and inclination change at this shallow depth, or it could be because of magnetic materials that could adhere on the surface of the drill pipe while drilling. However, a proper investigation study of the geology is required for further analysis which is not the part of this work.

5.5.3 Temperature Quality Control Check

The ultimate aim of this analysis is to have a quality control check of whether the tool will work in the given operating range or not. Normally, MWD tools are calibrated to work in a temperature range of about $10°C\ to\ 175°C$. To prove this assumption, first the formation temperature is evaluated by using a geothermal gradient of $0.04\ ^\circ{}^{C}/_{m}$ and sea temperature of $6°C$ for the area of interest. By using **Equation 21** formation temperature is determine at each TVD.

$$\text{Formation Temperature} = (\text{TVD} - \text{Water Depth}) * \text{Geothermal Gradient} + \text{Sea Temperature}$$

Equation 21

Figure 17 shows an operating range for the MWD tool along with the formation temperatures at different TVDs. It is quite visible that MWD tool will operate in its working range. This phenomenon will not cause any additional stresses on the MWD sensors while drilling.

It is normal industry practice, to have a check of formation temperature before the start of any drilling activity by using temperature logs, as it will help in defining the operating range of the tool and other equipment's which will ultimately assist in lowering the unwanted stresses and problems. Since, the well in this analysis is at extremely shallow depth, so any change in temperature will not affect the working performance of MWD tool.

Normally, mud from the surface is circulated at the temperature of around 4°C, which is considered to be quite cool in the riser region, but gain some heat while moving in subsurface, however, in this case the well is located at the shallow depth of 650 mTVD, and since the mud is circulated in a close loop it will not get heated up and will not cause any increase in temperature. On the contrary, this analysis is vital for HPHT wells, as an increase in temperature will cause the BHA components to get elongated, which results in high level of stresses.

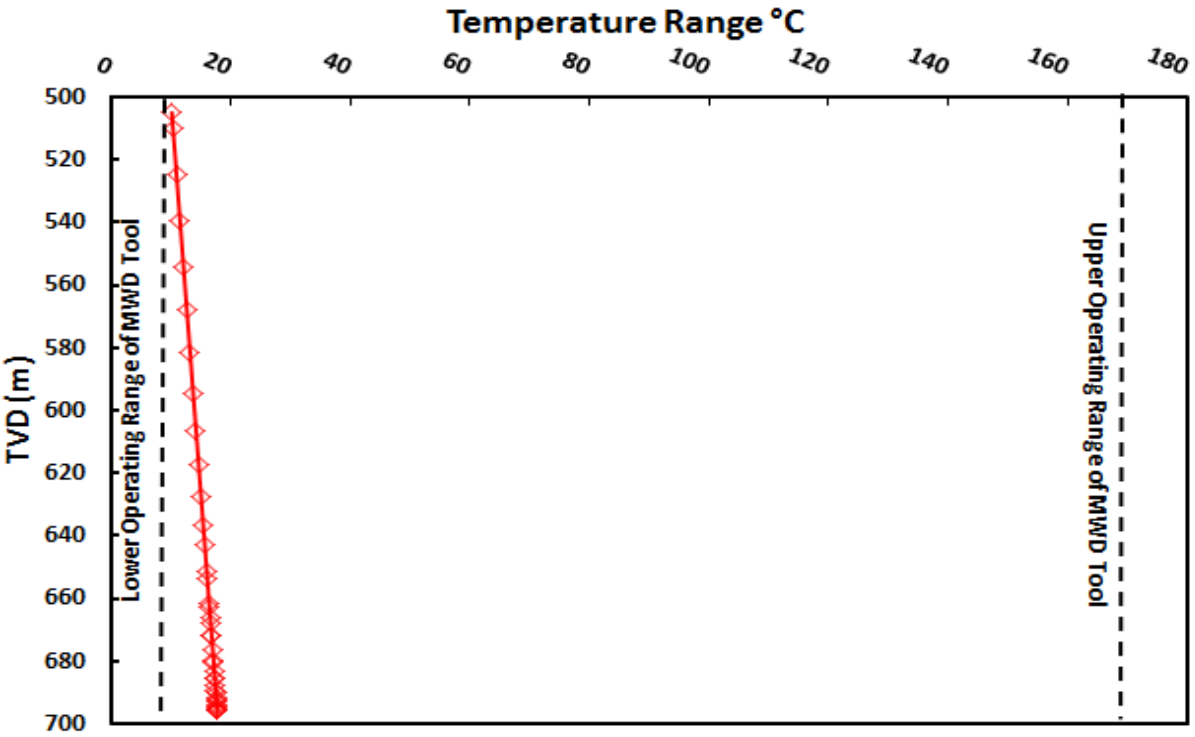

Figure 17 Formation Temperature and MWD Operating Range

The second quantification analysis that is performed is to have a check on the exact change in length for each BHA components under these temperature conditions. This will help in determining the stresses that each component will experience while drilling, as change in length will cause a change in strain and that will directly affects the stresses. It is of utmost concern; to ensure that equipment does not crosses its elastic limit as this will damage them which ultimately increase the drilling cost. For the analysis purpose BHA is considered to be made up of carbon steel, having expansion of coefficient of $0.0000117\ {}^{m^{\circ}C}/_{m}$. The total length of the BHA at the start is $274.45\ m$, however, at the end there is a slight change in length of $0.05448\ m$. **Figure 18** shows the change in length of each BHA components and **Equation 22** shows how the change in length is determine.

$$\text{Change in length } (\Delta L) = \alpha * L * \Delta T \qquad \textbf{Equation 22}$$

Where;

$$\alpha = Expansion\ of\ coefficient$$
$$L = Original\ Length$$
$$\Delta T = Change\ in\ Temperature$$

This change in length is not significant because of the shallow depth of the field. However, it should be of a great concern, if the field is at high depth of around 5000 m where the elongation of BHA can significantly reduce the performance of MWD sensors.

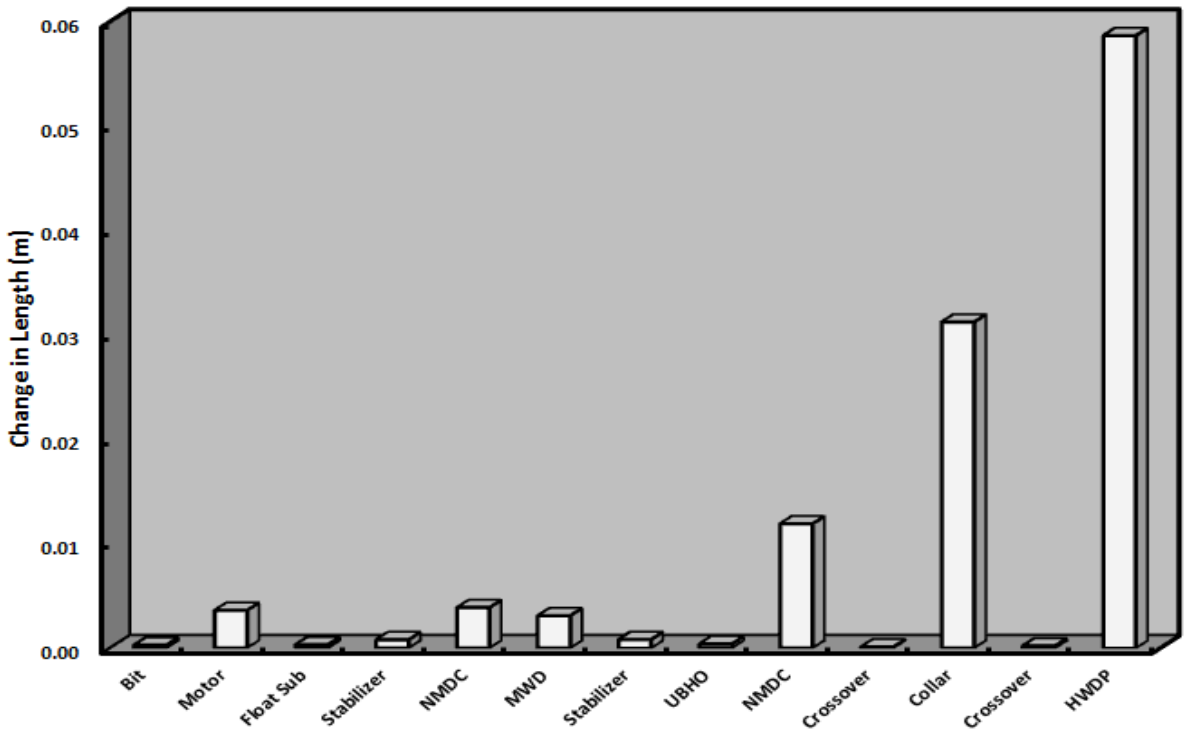

Figure 18 BHA Components change in Length

5.5.4 Sensor Errors

MWD tool comprises of magnetometer and accelerometer that are used to determine the azimuth and inclinations during drilling operation. However, there are some errors sources that are responsible for the variation in output which could lead to a high level of uncertainty during drilling phase. It is extremely important, to implement a proper correction method to reduce the uncertainty and to collide at the desire location.

During this study, the scale factor and biased errors are examined as they both are responsible for the uncertainty in azimuth and inclination calculation. Magnetometer performances only affect the azimuth and can cause a high degree of uncertainty, whereas accelerometer can affect both inclinations and azimuths.

5.5.4.1 Magnetometers Biased and Scale Factor Error

In the study a total of 38 survey stations are evaluated and the effect of both scale factor and biased error terms are observed on magnetometer performance. **Figure 19,** shows the effect of both errors and there magnitude. It is quite discernible that both the error terms are increasing linearly with respect to the depth. However, biased error has more dominant effect and is almost twice in value as compared with the scale factor error because it is strong depended upon the TMF component, which is assumed to be the most uncertain parameter out of all. On the other hand scale factor error terms are mostly the function of sin A_m, and since the well in this study is more North dominated so this factor is small, hence scale factor error is less than half against biased error.

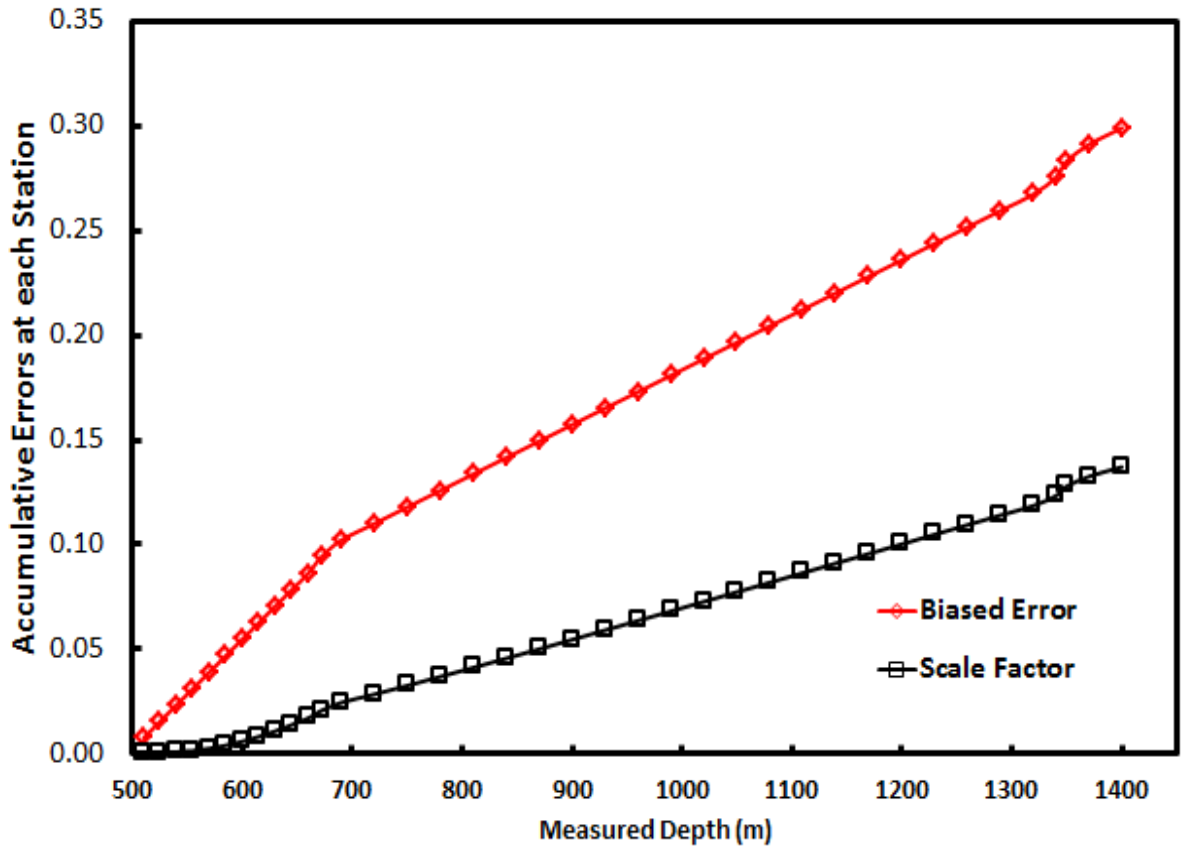

Figure 19 Magnetometer Biased and Scale Factor Error

It is rule of thumb that 1° of fluctuation in angle can creates approximately 17.45 m of uncertainty in either direction (Jamieson, 2017). As in this case, the accumulative error at the last survey station of 1400 mMD from scale factor is approximately 0.137° degree, which causes an uncertainty roughly about 6.6 m. On the other hand, biased term causes an error of

0.3° degree in azimuth which leads to 9.1 m of uncertainty at the final depth. The weighting function for scale factor is considered to be 0.0016, while for biased it is assumed to be 70 nT. Errors at each station are summed in the previous station error in order to determine the cumulative effect.

For Magnetometer Biased there are a total of two XY components and one Z component. This Z-component is highly affected by bit interference. **Section 5.5.1** comprises of an effective solution for reducing the impact of bit interference on this component. On the other hand, for Scale Factor there are three XY terms and one Z terms (equations can be seen in **APPENDIX B**). At each survey station, all of the components are determined separately and finally there square root of sum of square is evaluated.

Equation 23 is implemented to determine error at each survey depth.

$$\text{Survey station}_i = \sqrt{(\text{MBXY1}^2) + (\text{MBXY2}^2) + (\text{MBZ}^2)}$$

$$\text{where } i = 1, \dots, N$$

$$\text{Survey station}_i = \sqrt{(\text{MSF1}^2) + (\text{MSF2}^2) + (\text{MSF3}^2) + (\text{MSFZ}^2)} \qquad \textbf{Equation 23}$$

$$\text{where } i = 1, \dots, N$$

$$\text{Error at station}_i = \text{Error at station}_i + \text{Error at station}_{i-1}$$

$$\text{where } i = 2, \dots, N$$

5.5.4.2 Accelerometer Biased and Scale Factor Error

The same analysis is performed for accelerometer. Using the equations mentioned in **Table 8** in **APPENDIX B** the accumulative effect of both biased and scale factor error for accelerometer are evaluated. It is noticeable that the biased error term is again responsible for the high degree of inaccuracy as compared with the scale factor term because, accelerometer biased error term is highly depended upon the total gravity component, and since the well in the study is situated in the Barents Sea this parameter comprises of a high degree of uncertainty. To determine this component effectively there is no nearby variometer station available, as they all are situated approximately 400 km away.

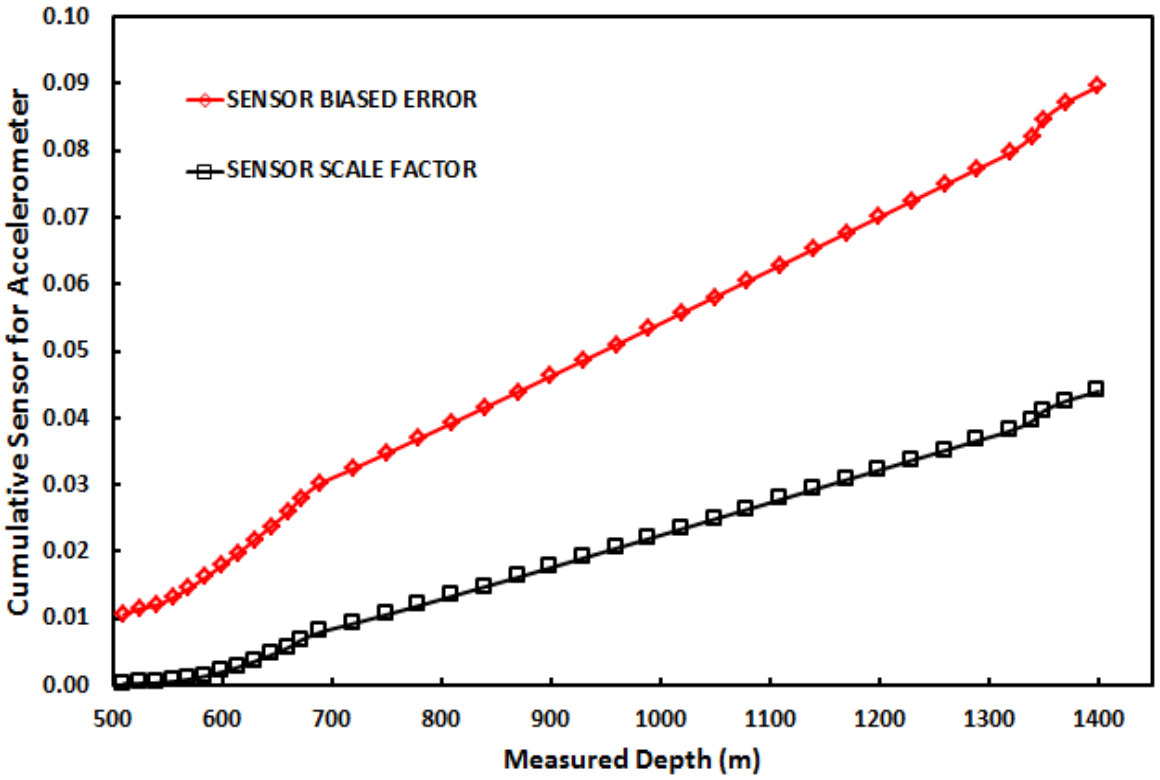

Figure 20 Accelerometer Biased and Scale Factor Error

Figure 20 represents the cumulative effect for both biased and scale factor error in azimuth. The weighting function values that are used in this case are $0.004ms^{-2}$ *and* 0.0005 for biased and scale factor error. It is observed that the error associated in azimuth are small in magnitude for both terms, hence, the contribution in EOU are small as compared with the other terms. The equation below represents the method applied while calculating the error and there resultant sum at each survey station.

$$\text{Survey station}_i = \sqrt{(\text{ABXY1}^2) + (\text{ABXY2}^2) + (\text{ABZ}^2)}$$

$$\text{where i} = 1, \ldots, \text{N}$$

$$\text{Survey station}_i = \sqrt{(\text{ASF1}^2) + (\text{ASF2}^2) + (\text{ASF3}^2) + (\text{ASFZ}^2)}$$

$$\text{where i} = 1, \ldots, \text{N}$$

$$\text{Error at station}_i = \text{Error at station}_i + \text{Error at station}_{i-1}$$

$$\text{where i} = 2, \ldots, \text{N}$$

Equation 24

5.5.5 Misalignment Error

It is defined as an offset of the survey tool with respect to borehole axis, in this way the sensors are offset by some degrees. However, this error results in small change in inclination and azimuth at each survey station, but it could be significant to miss the target. The weighting error functions used are $w_{12}\ and\ w_{34}$. This error comprises of four XY components and can propagate either systematically or random. To determine the four error terms equations in **APPENDIX B** are implemented. **Equation 25** till **Equation 29** below indicates the complete process which is applied to incorporate the effect of misalignment error and to determine the change in azimuth and inclination. **Equation 27** can also be implemented for the azimuth calculation as well.

$$\text{Inclination Error}_i = \sqrt{(\text{MIS1}^2)_i + (\text{MIS2}^2)_i + (\text{MIS3}^2)_i + (\text{MIS4}^2)_i} \quad \textbf{Equation 25}$$

$$\text{where i} = 1, \dots, \text{Nstations}$$

$$\text{Error at station}_i = \text{Error at station}_i + \text{Error at station}_{i-1} \quad \textbf{Equation 26}$$

$$\text{where i} = 2, \dots\dots, \text{N}$$

$$\text{New Inclination} = \text{Old Inclination} + \text{Error at station}_i \quad \textbf{Equation 27}$$

$$\text{Azimuth Error}_i = \sqrt{(\text{MIS1}^2)_i + (\text{MIS2}^2)_i + (\text{MIS3}^2)_i + (\text{MIS4}^2)_i} \quad \textbf{Equation 28}$$

$$\text{where i} = 1, \dots, \text{Nstations}$$

$$\text{Error at station}_i = \text{Error at station}_i + \text{Error at station}_{i-1} \text{where i} = 2, \dots\dots, \text{N} \quad \textbf{Equation 29}$$

It is appreciable that for the entire wellbore section both the errors associated with inclinations and azimuth are equivalent to each other, as both are linearly increasing with indistinguishable difference exist between the two. A change in $2.35°\ and\ 2.28°$ degrees is observed in azimuth and inclination at the last survey station which is shown in **Figure 21.** Since the studied field is at this shallow depth, this change is significant to miss the intersection location within the Targeted Well, as it causes the positional uncertainty to be high. To compensate this effect, the misalignment correction method should be applied on the entire survey

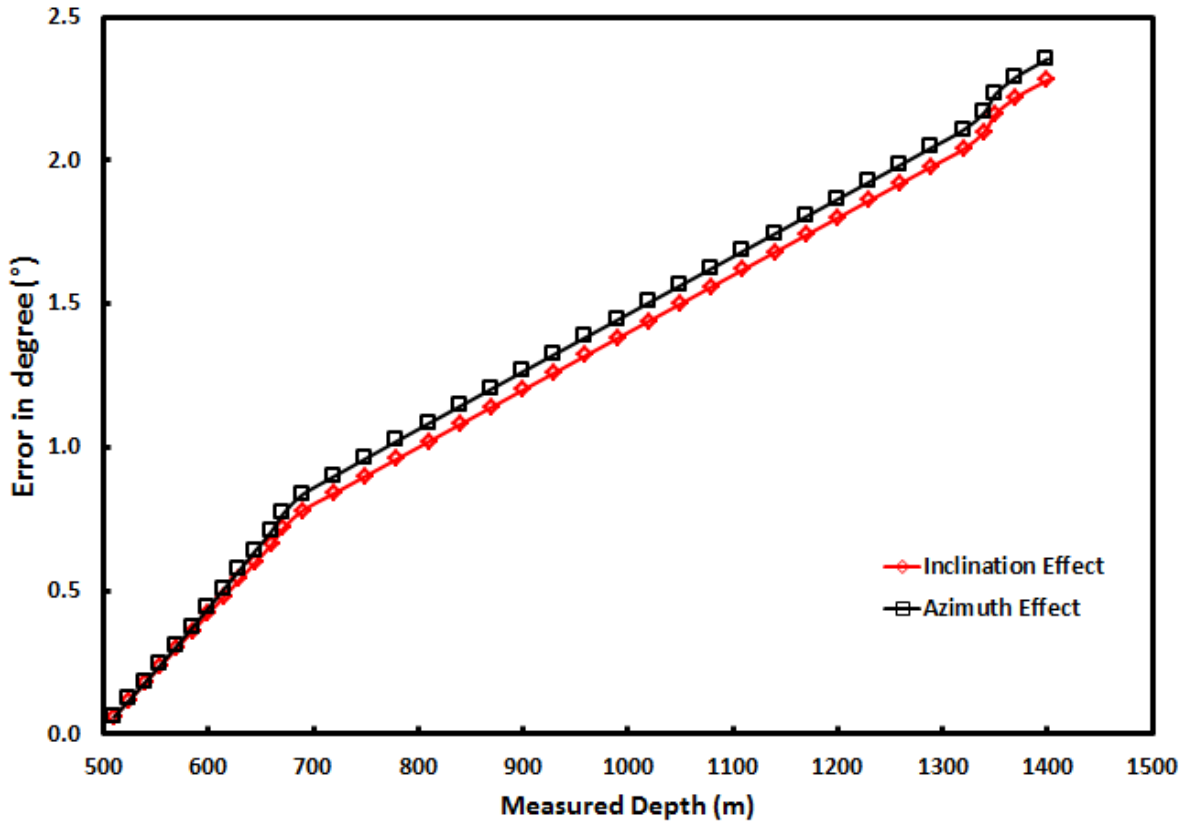

Figure 21 Deflection in Azimuth and Inclination due to Misalignment Error

5.5.6 Calculation Related to the Contribution of each Error Term in EOU

During analysis, the model is used to find out the contribution of each error term in the total EOU. The method used is described below:-

i. A total of nine error terms are analyzed, which comprises of Accelerometer Biased and Scale Factor, Magnetometer Biased and Scale Factor, Dip angle, Total Magnetic Field, Declination, SAG and Misalignment errors.

ii. For each terms mentioned above, the error associated with azimuth and inclination are investigated using the equations in **Table 8** in **APPENDIX B.**

iii. A total of 38 survey stations are analyzed for each error term. And for each station a new inclinations and azimuths are determined, which is then incorporated in Minimum Curvature Method to find out new Northing (Delta N) and Easting (Delta E).

iv. For each error term separately, steps mentioned in S**ection 4.3 (VII onwards)** are applied and EOU is calculated at each survey station.

Figure 22, shows the result of analysis in which Declination, Dip angle and Magnetic Biased causes the most uncertainty out of all error terms, this is because all these factors are depended upon Total Magnetic Field (TMF) which is the most uncertain parameter in auroral zone where are field is situated. To find the total uncertainty at each station square root of sum of squares are taken at each depth. The model provides a total ellipse semi major axis of 19.02 m at 1400 mMD. To further reduce this uncertainty, the number of survey stations should be increased or the tool should be modified with proper error terms and weighting error function

Figure 23 represents the EOU for the Targeted well. The well is only considered till the depth of 690 mMD, as this depth is planned to be the intersection point. Till this depth, the total uncertainty determined is 2.81 m. Once these uncertainty ellipses are determined, comparison of the model result with COMPASS^{TM} is then conducted to evaluate the model accuracy. The comparison study includes Separation factor, Hitting Probability, Center to Center Distance and EOU contrast.

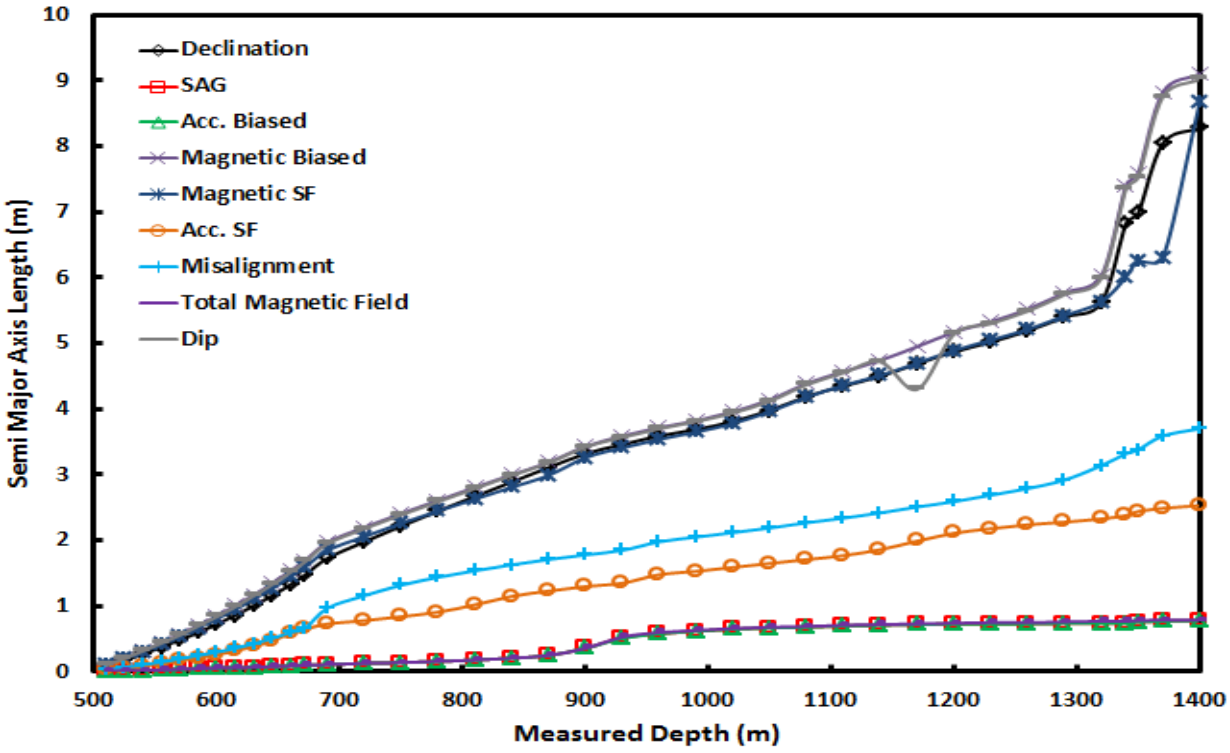

Figure 22 Model EOU for each Error Term

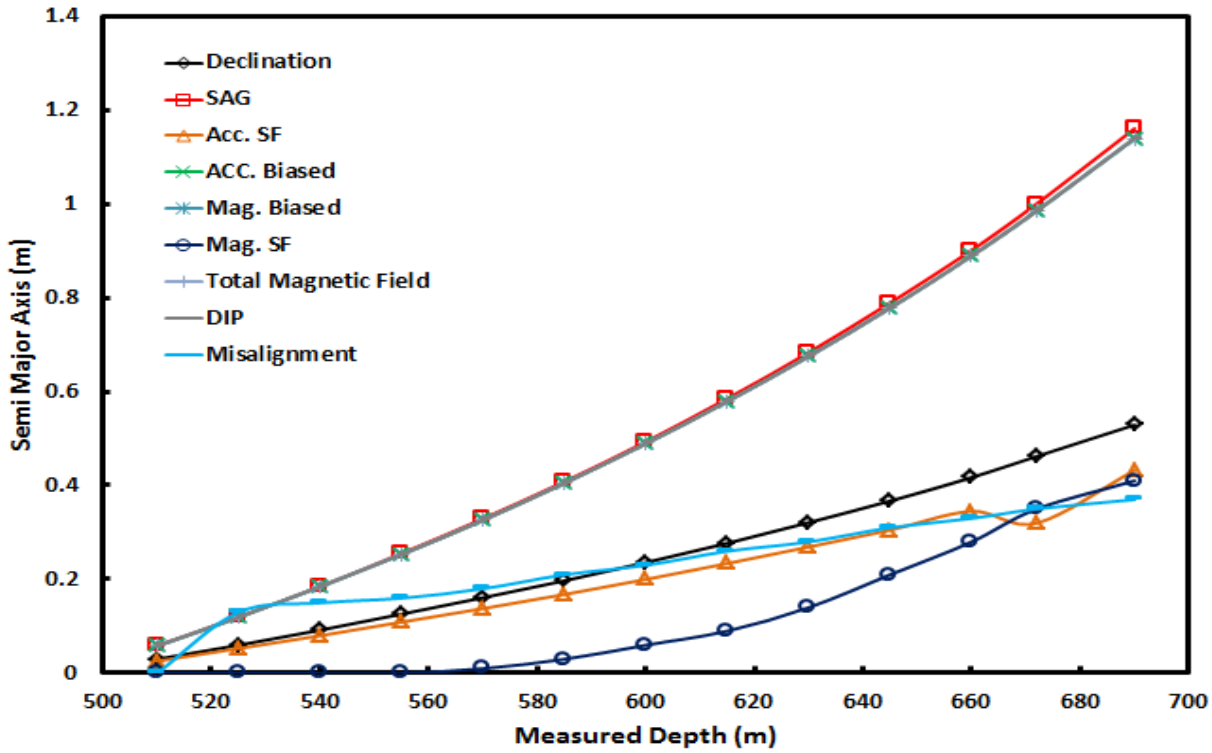

Figure 23 Target Well EOU from Model

5.6 Comparison between MODEL and COMPASS™ Results

During this work, the main idea along with different error models is to replicate the working principle of Landmark Compass™ and then compare the results generated by the model with that of Compass™.

5.6.1 Center-Center Distance

The surface map coordinates that are assigned to the Relief Well are $8{,}139{,}213\ mN\ and\ 411{,}989\ mE$. On the other hand, for the Target Well they are $8{,}139{,}913\ mN\ and\ 411{,}989\ mE$. From the coordinates, it is visible that a distance of 700 m is kept between the two locations in the North direction, while the East coordinate is same for both. To calculate the center to center distance, first the Northing and Easting for both well are determined at each Measured Depth (MD). Next, these coordinates are added to the surface map coordinates in order to convert them to the bottom-hole location. For the Relief Well, the point of interest is at 1400 mMD, while for Target Well it is 690 mMD. Once, the map coordinates for both the well are retrieved, the next step is to calculate the distance between the two well using the distance formulae as indicated by **Eq. 30**

$$\text{Distance} = \sqrt{(\text{Map North}_{\text{Relief}} - \text{Map North}_{\text{Target}})^2 + (\text{Map East}_{\text{Relief}} - \text{MapEast}_{\text{Target}})^2} \quad \textbf{Eq. 30}$$

The above formula is applicable till the depth of 690 mMD since this MD is considered to be the intersection point for the Target well. Below this depth, the distance is found by keeping $\text{Map North}_{\text{Target}}$ *and* $\text{Map East}_{\text{Target}}$ constant while changing the Relief Well coordinates. The idea behind the assumption is as the Relief Well has to hit the Target Well so it should move closer to it hence; its coordinates will keep on changing at each MD, while keeping the Targeted Well location is stationary.

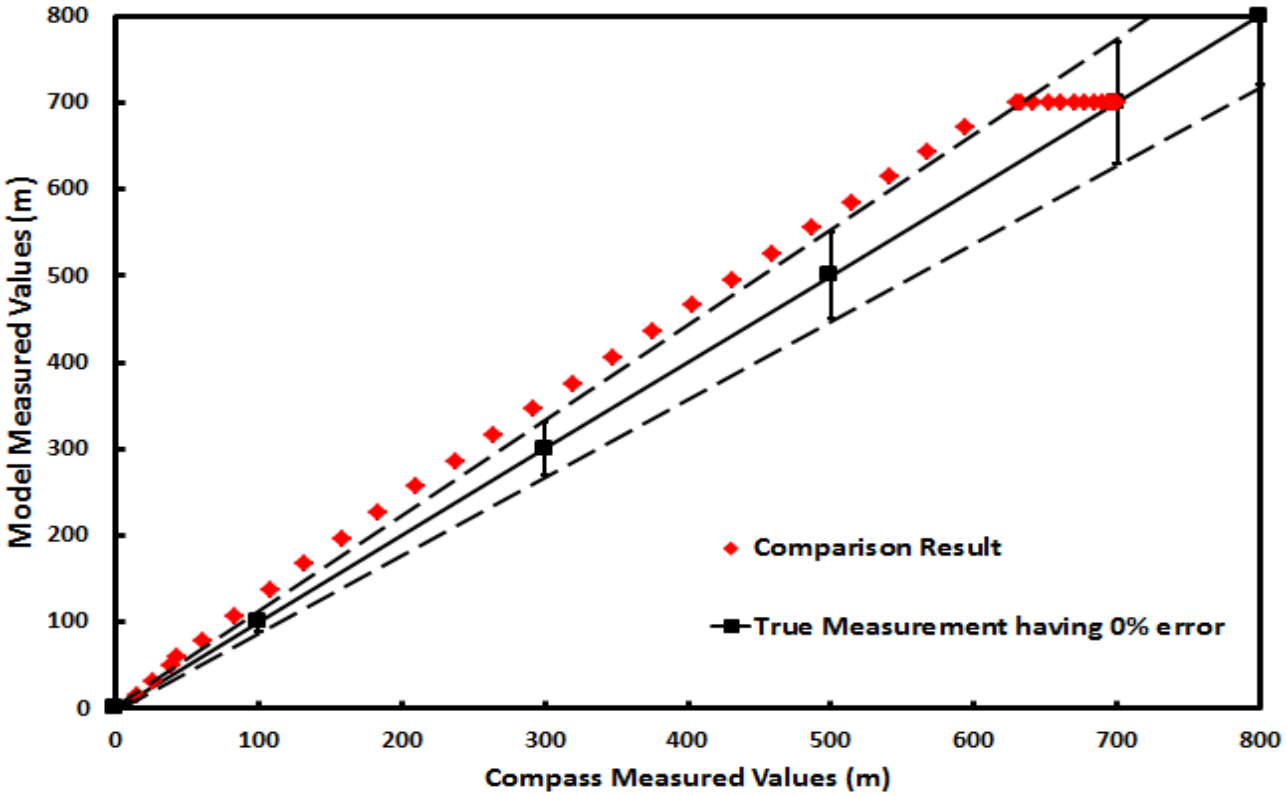

Figure 24 Comparison of Center to Center Distance Between Two Models

Figure 24 represents the difference in measurements between COMPASS^{TM} and the self-made model. The small vertical black line indicates the error bar having 10% deviation. And the dotted line represents the complete region for 10% of deviation. It is quite visible that the center to center distance that is calculated from the two models is very close to this 10% deviation line, which provide with the information that the measurements obtain from the model comprises of 10% of inaccuracies. However, at the intersection point, that is the main

concern for this study the measured value is very close to the true measurement, which is indicated by the dark black line of 0% deviation.

Figure 39 in **APPENDIX B** comprises of the plot that represents the center to center distance obtained from both models. It is observed that divergence between the two cases starts from the stations where the well is given an inclination. This indicates that there are some inaccuracies exist between the two models in terms of errors propagation modes.

5.6.2 Separation Factor Plot

In this phase, the Separation Factor for both cases is evaluated. For this analysis, distances between the ellipses are obtained using the relationship shown in **Equation 31**

$$\text{Ellipse Distance} = \text{Center to Center Distance}_{\text{both well}} - \text{Ellipse Radii}_{\text{Relief}} - \text{Ellipse Radii}_{\text{Target}} \quad \textbf{Equation 31}$$

Next step is to obtained the Separation Factor measurements; this is retrieved by using the relationship shown in **Equation** 32

$$\text{Separation Factor} = \frac{\text{Ellipse Distance}}{\text{Radii}_{\text{Target}} + \text{Radii}_{\text{Relief}}} \quad \textbf{Equation 32}$$

Till the depth of 690 mMD the $Radii_{Target}$ *and* $Radii_{Relief}$ wells both are changing, however, below this depth the parameter $\text{Radii}_{\text{Target}}$ well is again kept constant as stated previously, since the Relief well is approaching towards the Target Well in the North direction.

Figure 25 represents the comparison analysis related to the Separation Factor between the two cases. The black line represents the 0% deviation from true measurement, dotted black for 10% deviation, while dotted blue and red represents 20 and 30% deviation. It is quite discernible that the model measurements approaches towards the true measurements having 0% deviation which are retrieve from COMPASS^{TM} as the separation decreases. When both the wells are far apart from each other the model underestimates the Separation Factor values and the inaccuracies exits between the two models is greater than 30%, however, at the final depth of interest the Separation factor obtain from the model is approximately 0.35 while from COMPASSTM it is 0.32. **Figure 40** in **APPENDIX B** represents the Separation Factor Plot for both cases. As the separation factor value is less than 1 at the depth of 1400

mMD, it can be deduced that ellipses for both wells are overlapping each other and the wells are now in range of colliding one another.

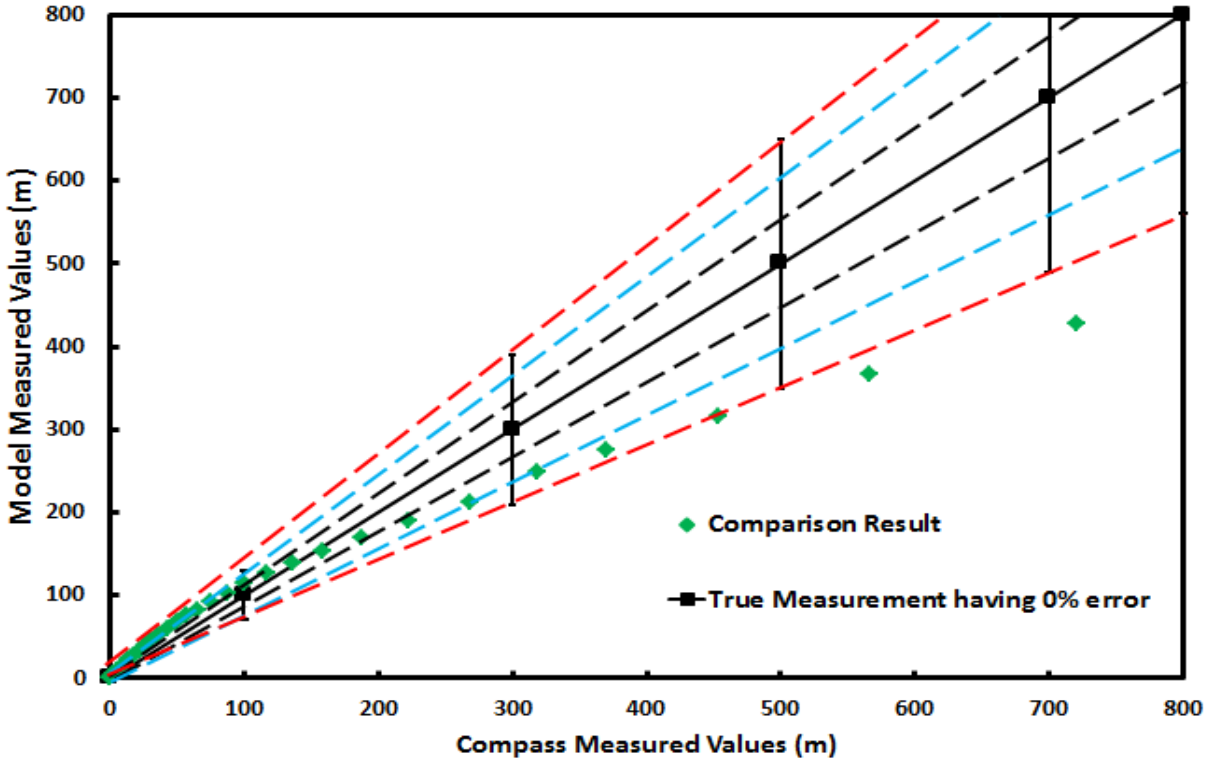

Figure 25 Separation Factor Plot Comparison between Two Data Series

5.6.3 Probability of Collision

Intersection at the desire point is of utmost concern in order to prevent the unnecessary flow of oil and gas up to the surface. For this analysis, probability of collision between the two wells needs some consideration to avoid any causeless sidetracks and an increase in drilling cost. **Section 4.4** deals with the complete method for calculating the probability of hitting at the desire location. **Equation 33** is used to calculate the number of attempts needed to intersect at the location of interest.

$$\text{Number of Attempts} = \frac{1}{\text{Probability of Collision}} \qquad \textbf{Equation 33}$$

Figure 26 represents the deviation between the two set of data series. The bold black line illustrates the 0% deviation between the two set of data. As the point starts to move away from the 0% deviation line, error percentage is increased by a factor of 10% which is shown by different dotted lines. The data series shows that the observed measurements from the model moves towards the 0% deviation lines indicates a strong collaboration between the two

data series as it moves towards the desired intersection. Both data series provides 25 numbers of attempts to hit the Targeted well. However, a large uncertainty is observed when the wells are far apart from each other. This deviation occurs as a result of variation in EOU between the two data series. **Figure 41** in **APPENDIX B** shows the comparison of result between COMPASS™ and from Model.

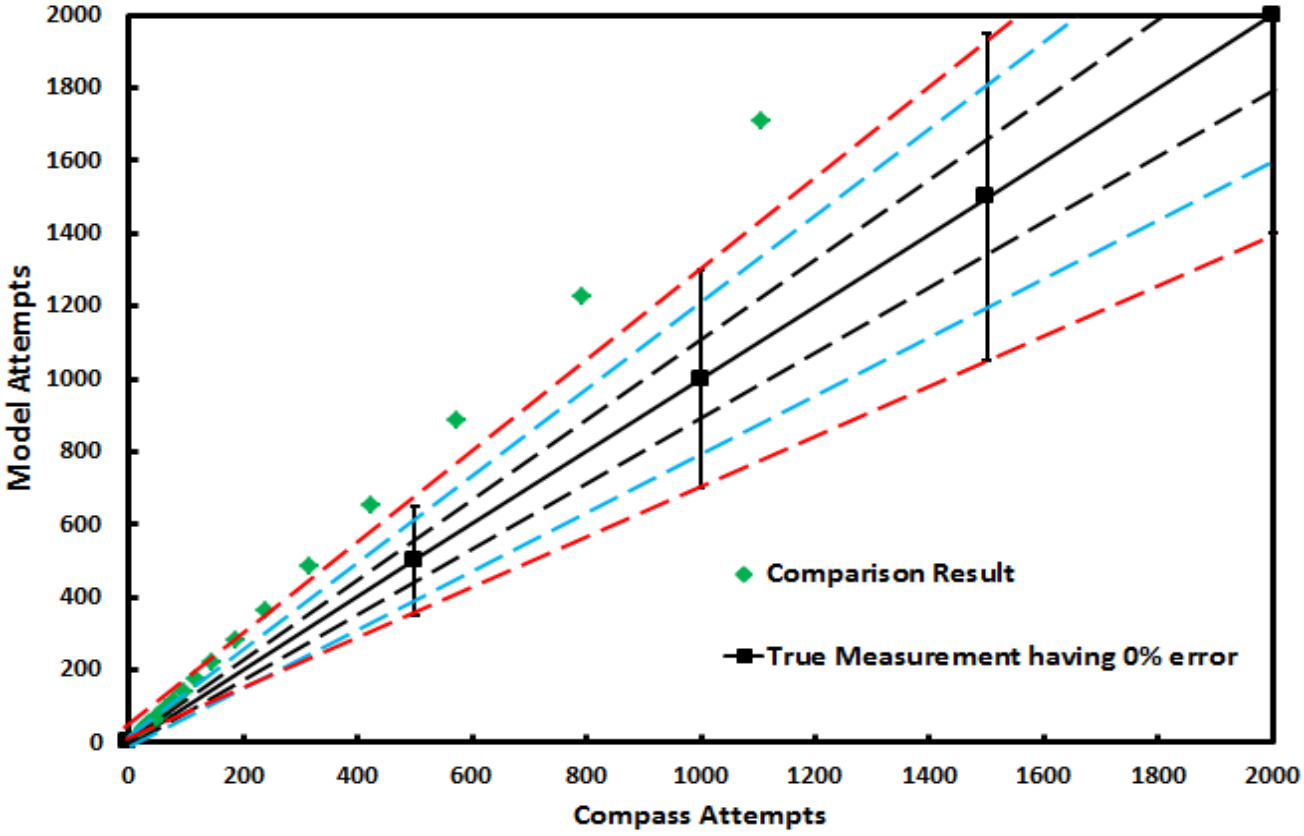

Figure 26 Probability of Collision Comparison between Two Data Series

5.6.4 Ellipse of Uncertainty Comparison

Section 4.3 deals with the complete method to calculate the EOU for a given well trajectory. **Figure 27** represents a scattered distribution plot for EOU between the two data series. The figure shows a maximum deviation of around 30% between the two sets of data. This inconsistency between the two set of data occurs because of different number of survey stations in both series, and secondly due to the selection of diverse propagation of error sources from one station to another. However, at the point of intersection which is of major concern, the EOU obtained from the model is 19.02 m while from COMPASS™ it is 19.69 m. This variation between the two data series is less than 5% and is indicated by red dot on the plot.

Another important factor than can contribute up to a certain fraction is rounding off error which can also create uncertainty between the two measurements. In the model, all the calculations are been made using two decimal places, while for COMPASS™ they are different. **Figure 42** and **Figure 43** in **APPENDIX B** show the result of semi major axis for two data series having 38 and 26 numbers of survey stations respectively.

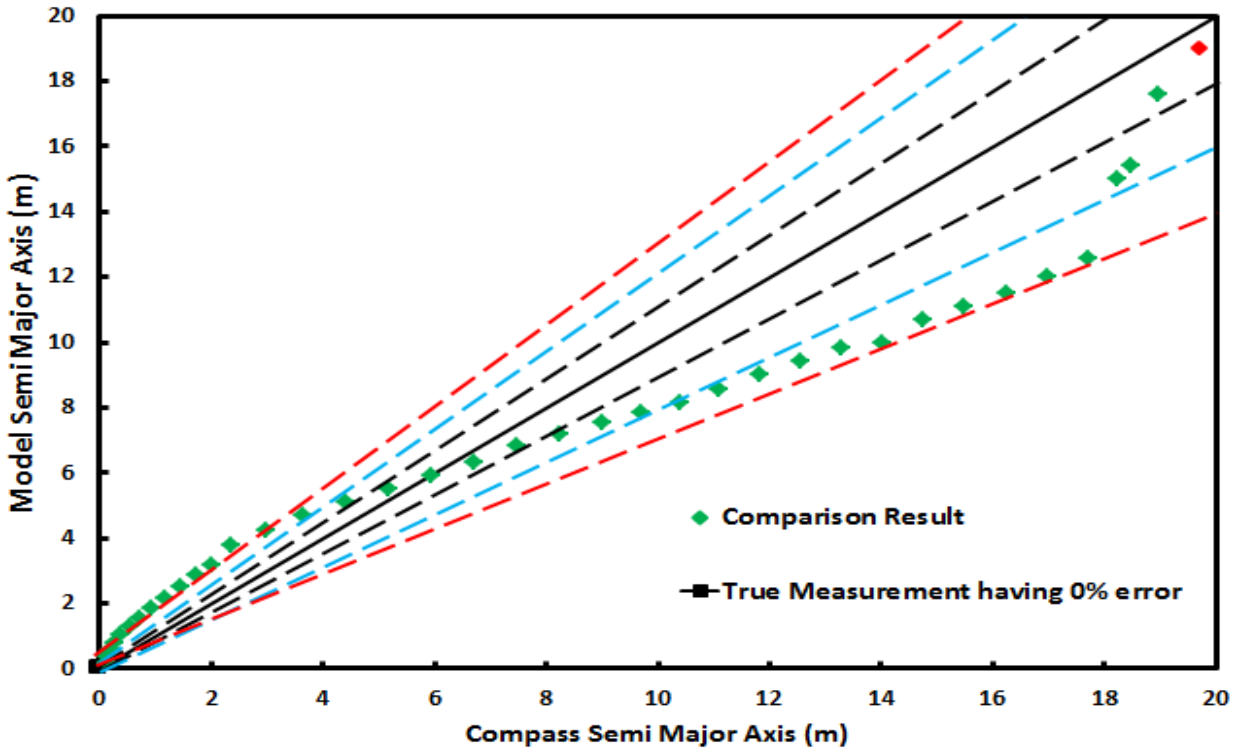

Figure 27 EOU Comparison Analysis

5.7 Effect of Changing KOP

An investigation study is performed to find the impact of changing the KOP on uncertainty ellipse. In the previous examples, the KOP is considered to be at 505 mMD. In this analysis a new survey is established, in which the KOP is shifted to 645 mMD to investigate the variation in EOU. For the new directional survey, all the remaining other parameters are kept constant, since the idea is to monitor the EOU behavior with respect to KOP. However, they all start from the new KOP of 645 mMD.

Following plots indicated the changes that are observed while the changes in inclination and the shift is being made.

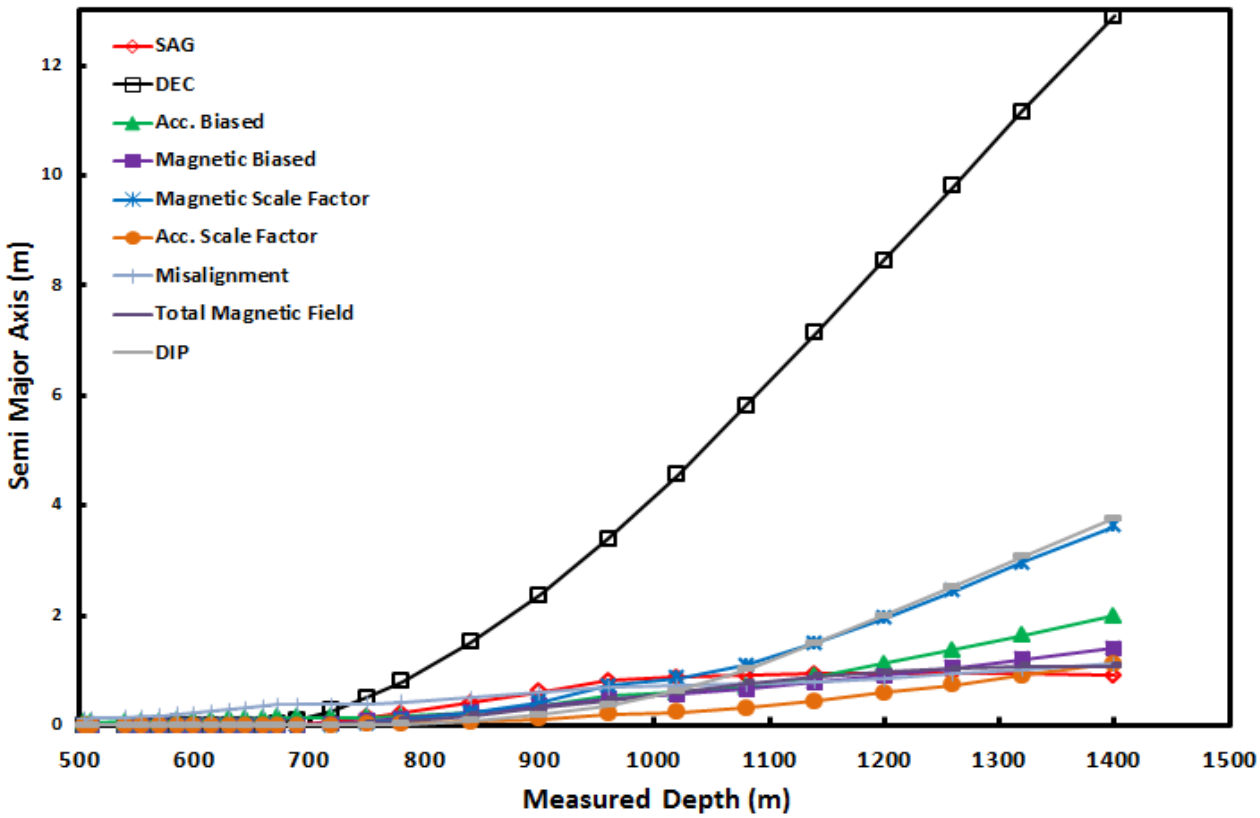

Figure 28 COMPASS™ Semi Major Axis Data at the KOP of 645 mMD

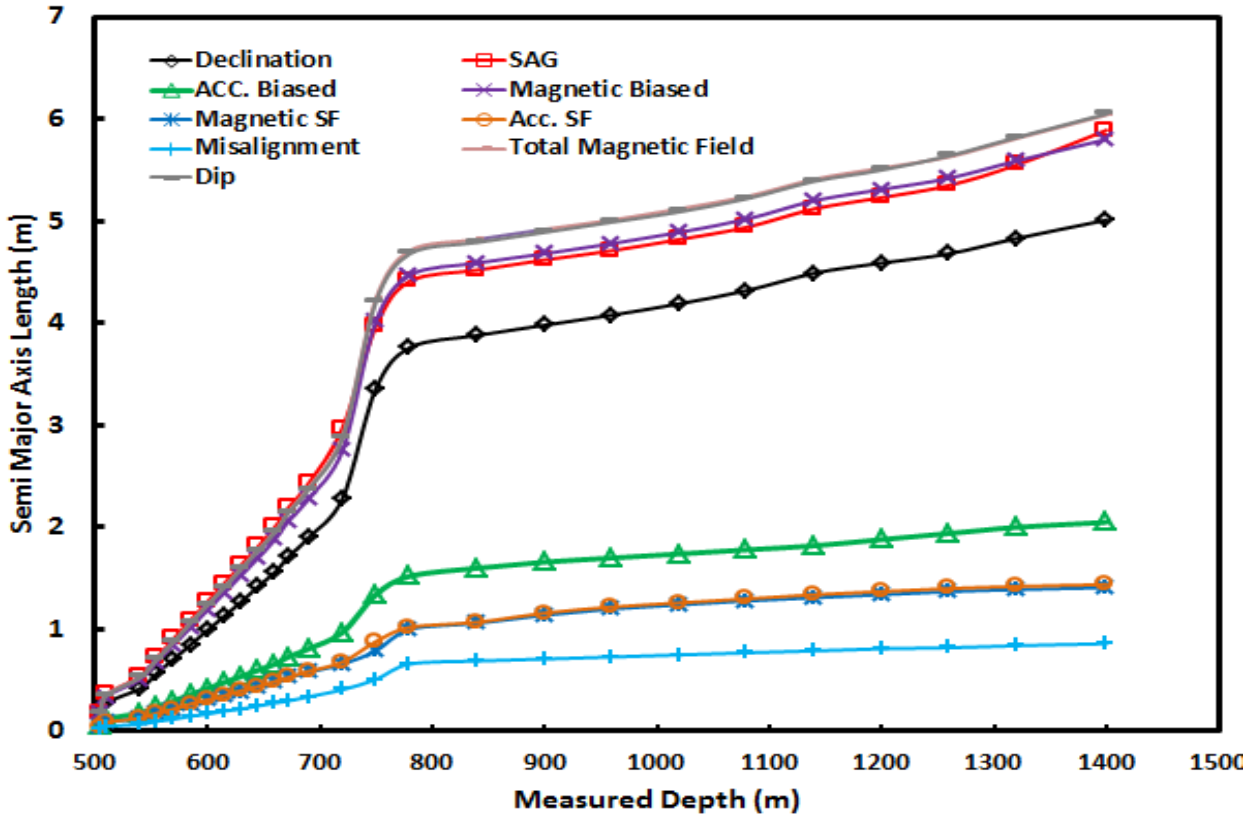

Figure 29 Model Semi Major Axis Data at the KOP of 645 mMD

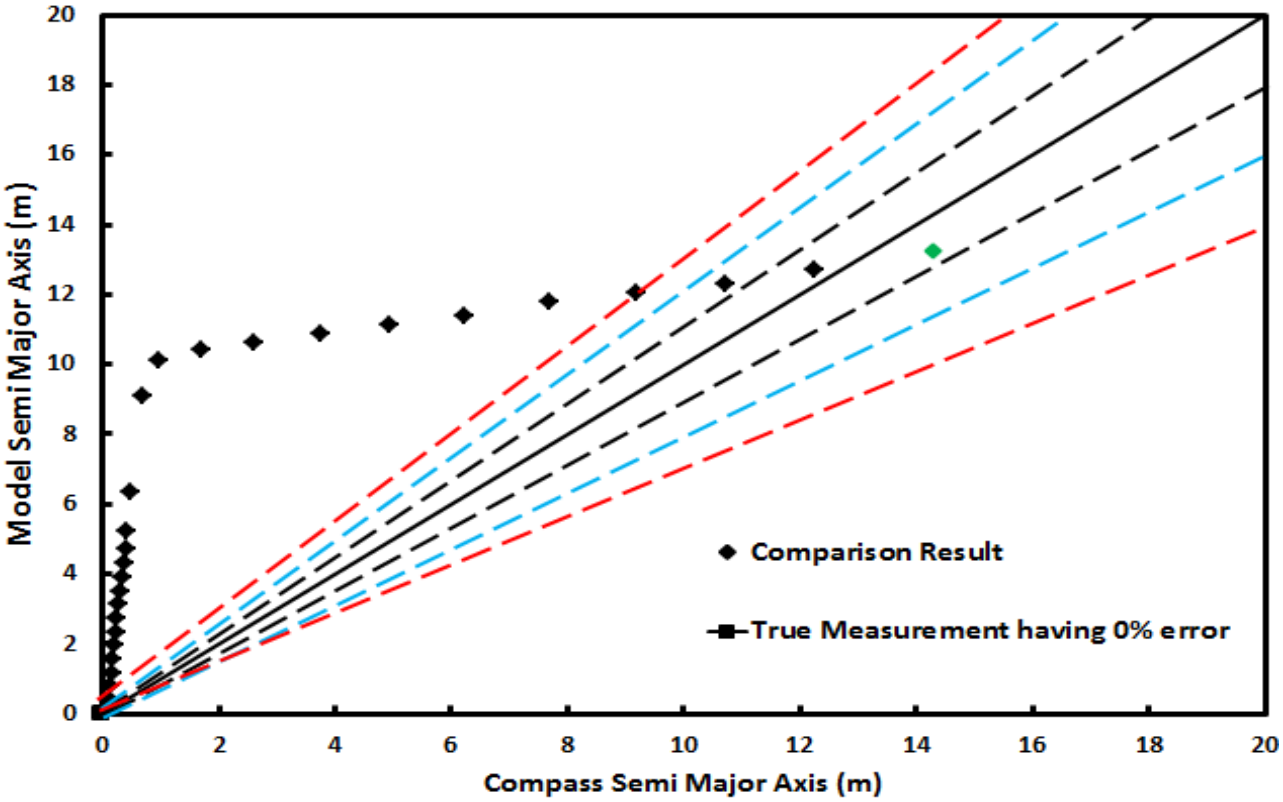

Figure 30 Error Analysis between two Data Series (COMPASS™ and Model) at 645 mMD

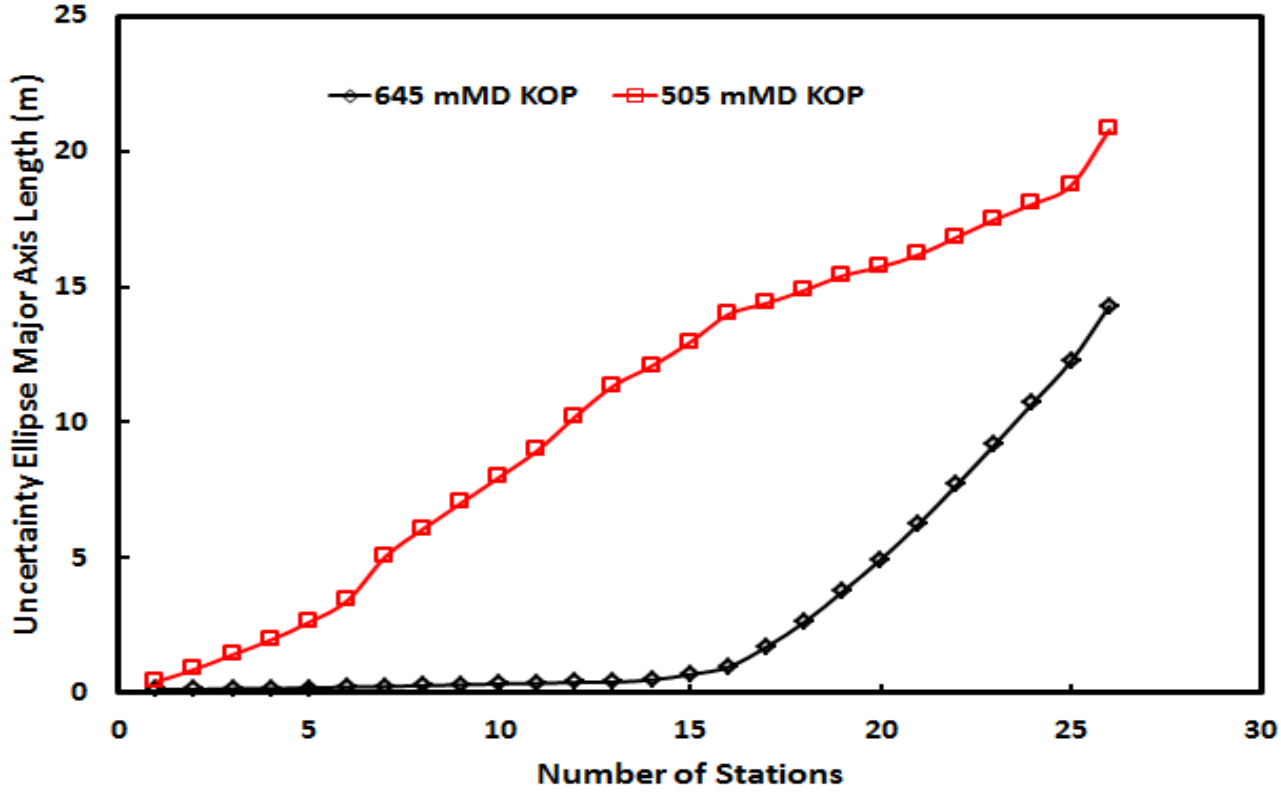

Figure 31 Change in EOU between two cases

Figure 28 and **Figure 29** represent the contribution of individual error sources in the total uncertainty ellipses. It is quite observable that for COMPASS^{TM} the declination error term plays the most influential role to the ellipses of uncertainty, having a contribution of 13 m. However, for the model, uncertainty is generated by equal contribution from four different major error sources which includes SAG, Magnetic Biased, Dip Angle and Declination. Apart from SAG, all three remaining factors are strongly influenced by the total magnetic field (TMF). It is concluded that the major uncertainty lies in TMF component that needs to be check in order to make the model as comparative as COMPASS^{TM}.

Figure 30, on the other hand, shows the error analysis between the two data series. Both series shows a drastic deviation of greater than 30% as indicated by red dotted line till the depth of 1140 mMD, however, the model approaches towards the COMPASS^{TM} measurement at the final depth of 1400 mMD, where the deviation is considered to be less than 10% as indicated by black dotted line. The final semi major axis generated by COMPASS^{TM} is 14.3 m, while for model it was 13.3 m.

Figure 31, shows the comparison of two cases where KOP is changed. For this analysis purpose, the total numbers of survey stations are kept constant. A drastic difference in uncertainty is observed between the two set of data series. However, while changing the KOP it is important to check the dogleg for the entire well path, ensuring that it is under the desire limit. In the case, when the KOP is at 505 mMD the maximum dogleg observed is $12°degree/30\ m$, on the contrary, when it is moved to the depth of 645 mMD it increased to $13°degree/30\ m$. This tracking on dogleg is crucial when the well enters in casing setting phase, since in this phase higher dogleg creates more stresses and apply more bending on casing pipe.

5.8 Effect of Changing the Number of Survey Stations

A second observation study is made related to change in number of station. Same procedure is implemented as discussed in **Section 4.3.** Each nine error sources are calculated separately and their impact are check on the uncertainty ellipses. In COMPASS^{TM} changes in IPM file of the tool are made to check the contribution from each error term on EOU.

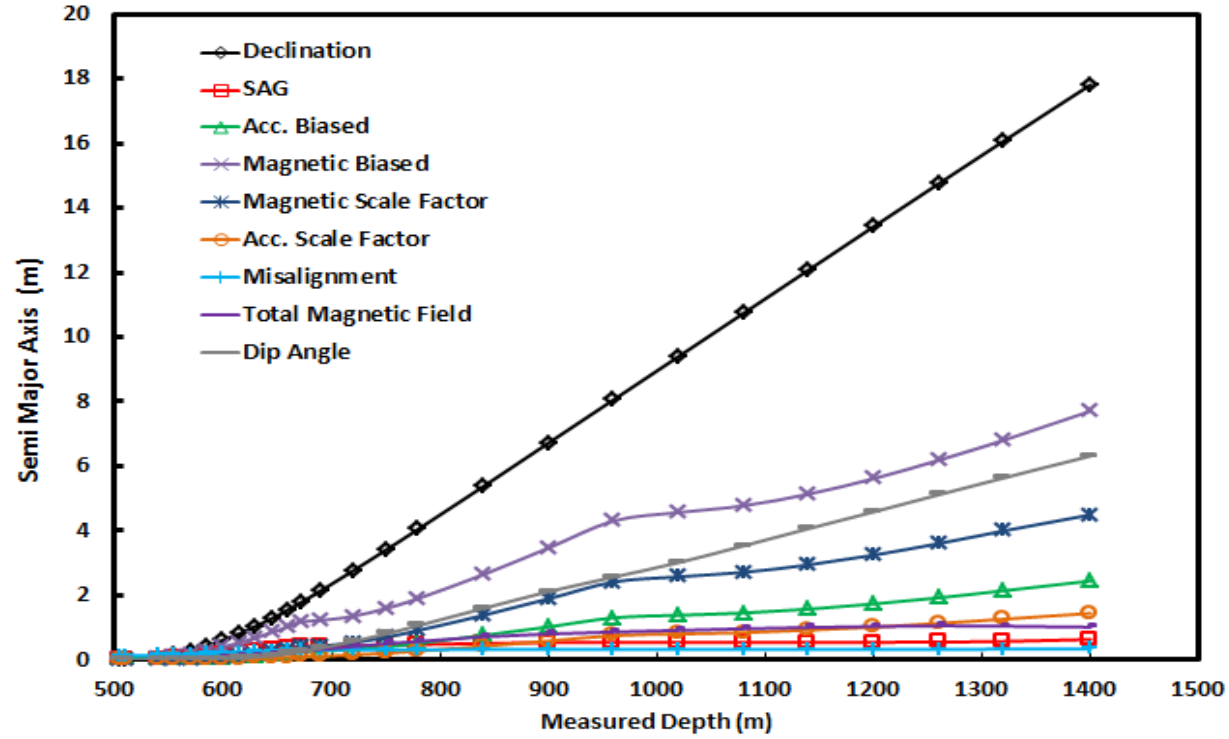

Figure 32 COMPASS Data for Contribution from Each Error Term in EOU

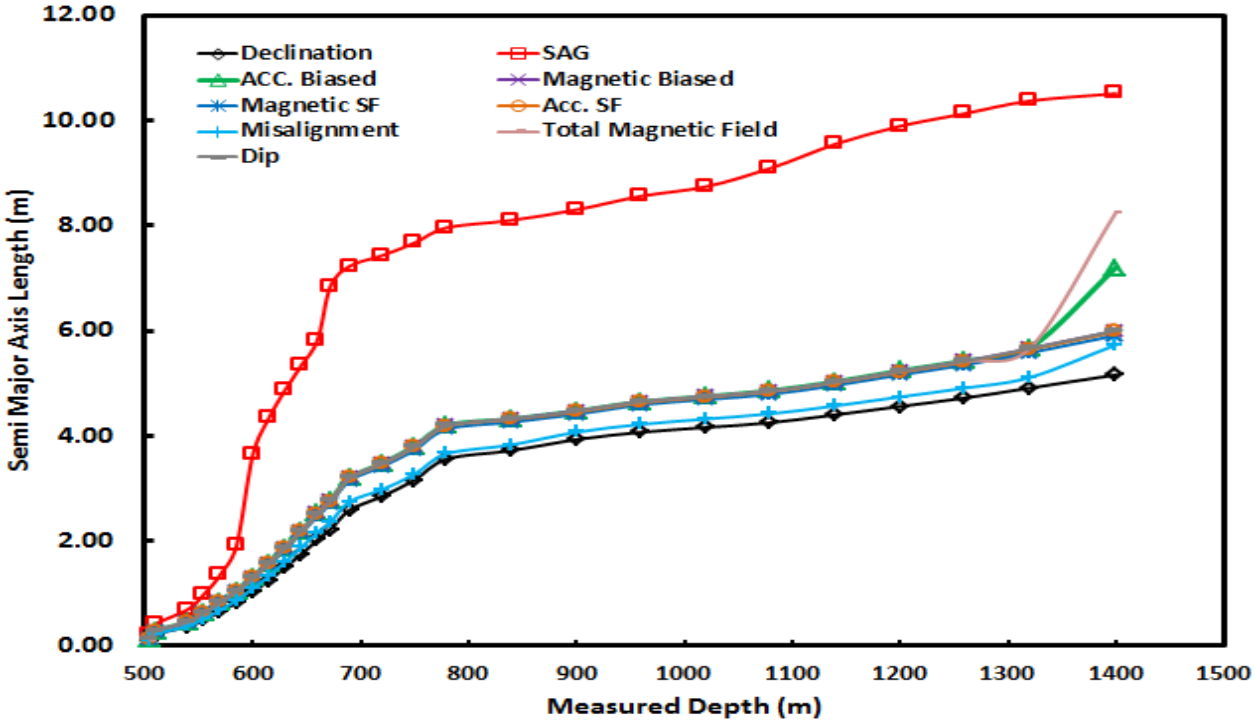

Figure 33 Model Data for Contribution from Each Error Term in EOU at 505 mMD

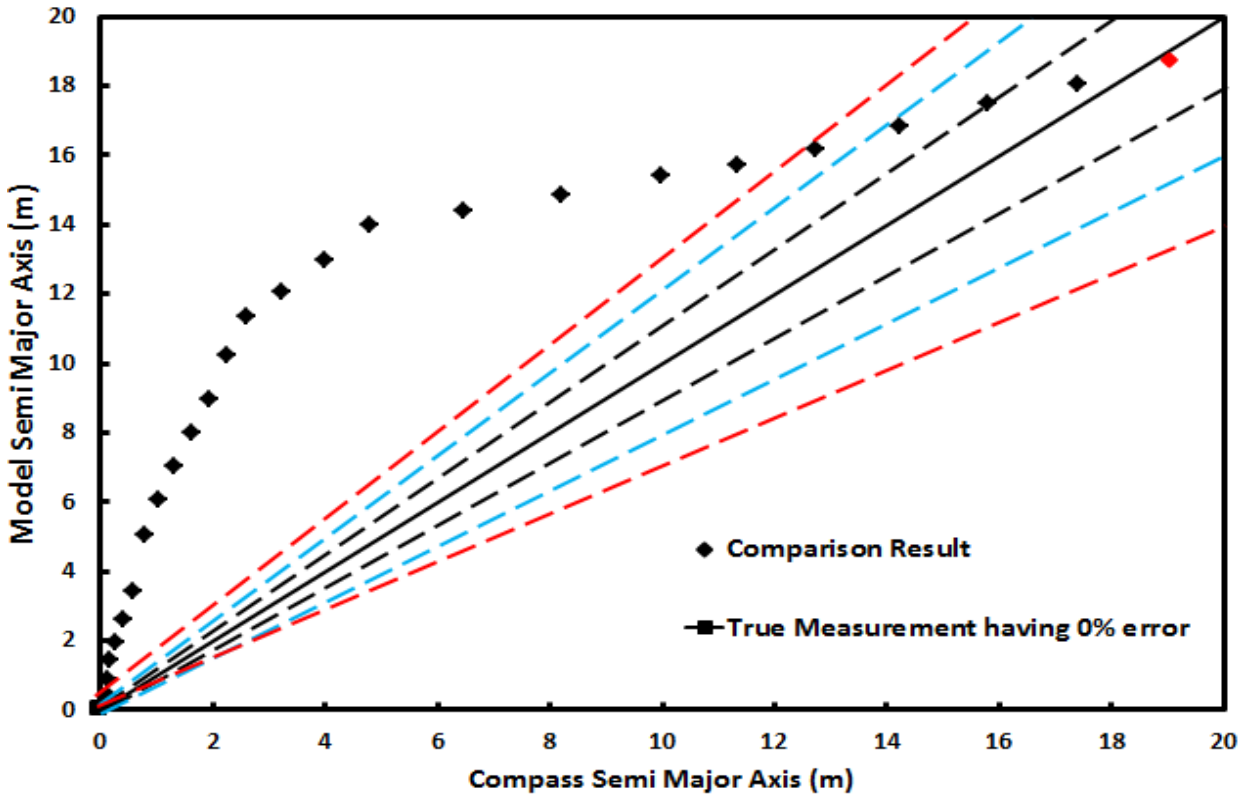

Figure 34 Error Analysis for the Two Data Series

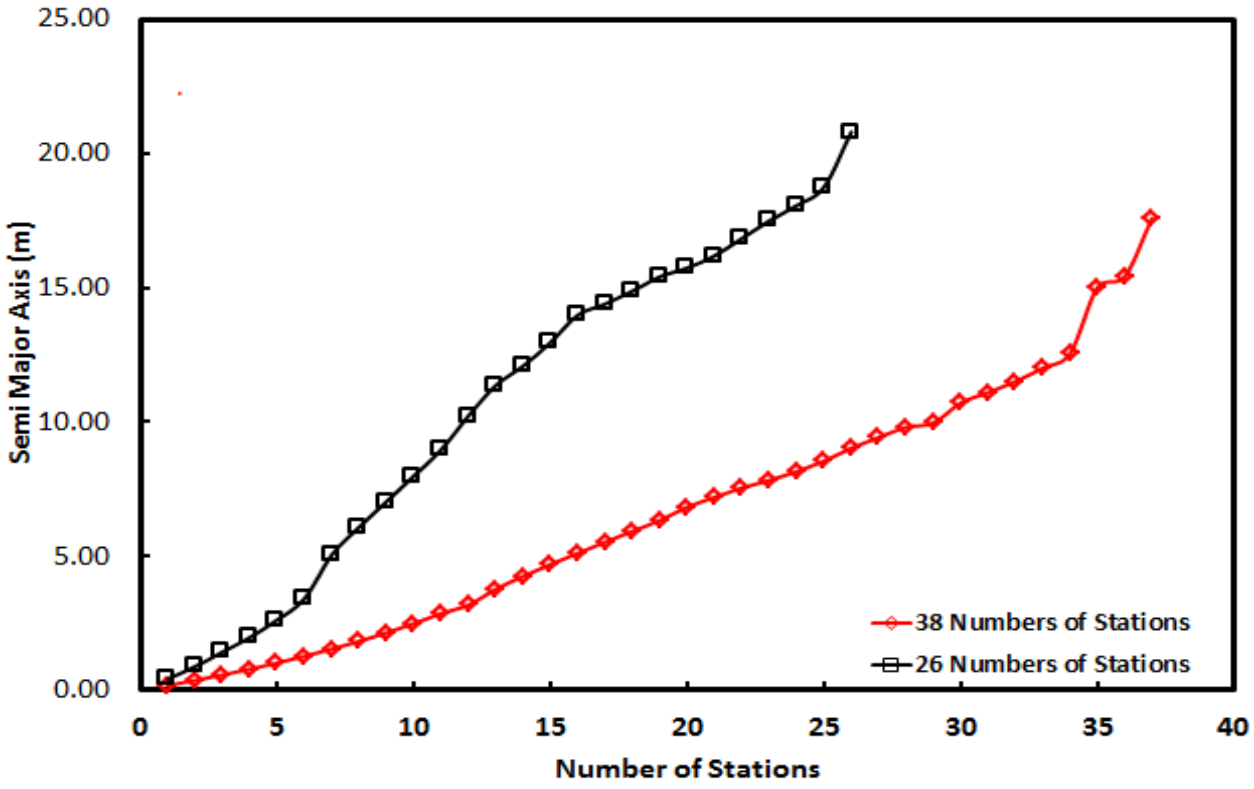

Figure 35 Comparison between Models with same KOP but Different Number of Stations

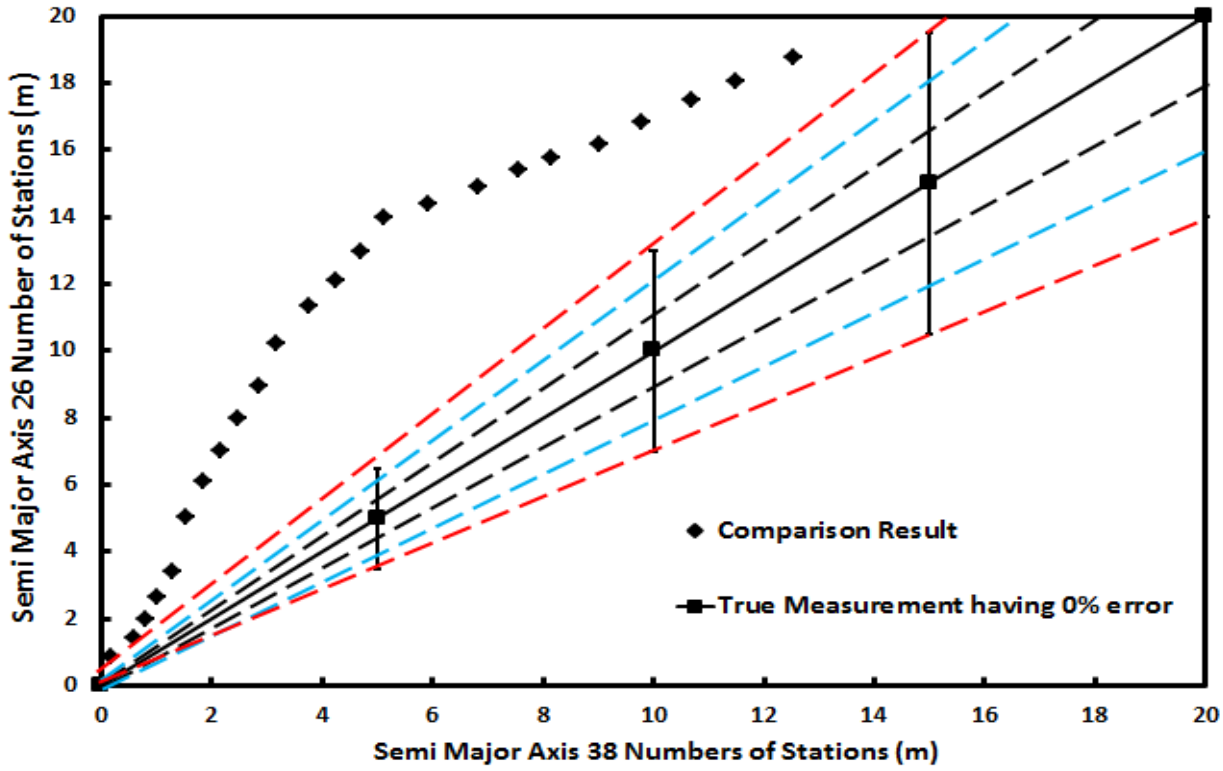

Figure 36 Increase in Error Percentage in EOU After Changing in Numbers of Stations

Figure 32 and **Figure 33** indicate the individual contributions of each error source in the total ellipses of uncertainty from both COMPASS™ and the Model. During this analysis, a separate directional survey is generated that comprises of 26 numbers of stations. As compare with the previous model, there are a total of 12 survey stations less in this model. According to COMPASS™ ,all error source that are a strong function of the magnetic field contributes heavily in the total uncertainty ellipses, which indicates that this factor is again the major uncertainty parameter out of all. However, for the model result, all factors are responsible equally in the contributing to EOU except SAG, which is responsible for the highest contribution in EOU. This might be because of a sudden change in inclinations at such small TVDs.

Figure 34 shows the comparison result between the COMPASS™ and the model. Data that is obtained from COMPASS™ is considered to be the true measurements. Dotted lines indicate the percentage of deviation between the two data series; however, black bold line represents the 0% deviation line. It is observed that, initially both data set are having a large percentage of variation between them, however, it reduce well below 5% at the depth of 1400

mMD. The deviation in the result occurs due to the use of a different ΔMD at the first survey station, as in model analysis is performed directly from the depth of 505 mMD. It also occurs as a result of selecting the different modes of propagation for each individual error terms.

Figure 35 shows a comparison study that is performed between the two data sets gathered from the model, having different survey stations but same KOP at 505 mMD. It is discovered that the survey data having 26 survey stations have higher uncertainty as compared with the survey data having 38 numbers of stations. This increase in uncertainty is because of poor tool performance between stations, which cause an increase in accumulated errors at each survey stations, thereby, decreasing the overall sensitivity of the survey.

An analysis is also performed to determine the change in error percentage when the numbers of stations are scaled down from 38 to 26. **Figure 36** shows an increase in error percentage by the factor of greater than 30% in position uncertainty when the stations are reduced. The uncertainty in the tool performance is expanded, which increase the overall uncertainty at each survey station. A weak correlation exists between the two survey data, which shows that lower the number of stations higher will be the uncertainty ellipse size and more inaccuracies will be created in hitting the target at the desire location

CONCLUSION

The main intention behind this work is to generate a model that analyze different error sources associated with directional survey. The study is based on two different wells that are planned to intersect each other to prevent the unwanted flow of oil and gas. For this reason, the probability of the intersection is also determined between the two wells. Following outcomes are generated after conducting the analysis:-

1) It is concluded that, some of the error sources are having considerable impact on the total uncertainty due to this north dominance trajectory
2) Major uncertainty lie in the Total Magnetic Field (TMF) parameter
3) Bit is considered to be the highest interference region in the entire BHA, that can be reduced by increasing the size of NMDC, which causes the sensors to move away from the bit.
4) The Z-component of the Magnetic Biased is assumed to be the most effected component by bit interference. This impact can again be reduced by increasing the size of NMDC
5) Due to the shallowness of the field, the impact of temperature is considered to be negligible; however, special consideration should be given to HPHT well having the MD of around 5000 m.
6) The model shows a less than 5% deficiency at the depth of interest, however, there are some discrepancies between the two data series, which is developed because of the selection of different propagation modes and the use of the diverse MD at the first station.
7) Factors such as Center to Center distance, Separation Factor and Probability of collision between the two wells obtained from both model shows a relatively low contrast between each other.
8) Error associated with rounding off creates a high degree of discrepancy between the two model
9) It is also observed that, as the number of survey stations are reduce, the EOU will increase because of poor tool performance
10) Changing the KOP will decrease the size of EOU, however, it will result in a high bending stresses on the casing string that needs to be considered during installation

FURTHER WORK

This work involves an intensive study related to Error Modeling and Positional Uncertainty calculation, as it involves the reflection of COMPASS^{TM} and its working principle. However, there are some further tasks that need some more attention in order to generate a more accurate model.

1) During the designing of the model both the Relief Well and the Targeted well are oriented towards the North direction, because of this, errors such as Declination and Dip angle are more dominant and have major contribution in the uncertainty ellipses. However, a new well path can be developed which is regnant in the East direction to see the change in contribution. This study is important as the wells in Barents Sea face more disturbances when they are deviating in East/West direction.
2) Declination, Dip Angle and Sag all error sources are depended upon the TMF of the area of interest. It is important to proper model the TMF especially in Barents Sea where magnetic disturbance and magnetic storms are quite common.
3) The work mainly focuses on MWD and positional uncertainty is calculated using error terms for MWD only, however, the same work can be performed with the help of GYRO to investigate the difference in ellipse dimensions from the two cases, so that the better tool can be used in proper environment.
4) A proper casing design and kill well simulation study can also be performed to tackle the unwanted flow of oil and gas from the Targeted Well.
5) Factors such as Covariance between ΔN and ΔE needs to be estimate accurately to reduce the deficiency between the two models. Also, errors associated with rounding off should be taken into consideration to further reduce the contrast between the two data series
6) While changing the KOP, the effect of bending on the casing string needs to be assessed, so that they can withstand in any harsh environment.
7) Study related to different wellbore equipment should be done when NMDC and KOP is changed. The same study should also be performed for the planning of the Relief Well.
8) The analysis done in this work is mainly focused on 2σ; however, a detailed error analysis should also be performed by considering the effect of 1σ and 3σ.

BIBLIOGRAPHY

(OCIO), N. C. (n.d.). *Earth Magnetosphere*. Retrieved from Space Weather Prediction Center: http://www.swpc.noaa.gov/phenomena/earths-magnetosphere

A.Berchan, B. (2015). *Drilling,Completion,Intervention and P&A-design and operations.* Trondheim: NTNU Department of Petroleum Engineering and Applied Geophysics.

Ajetunobi, M. O. (2012). *Depth Issues in the Oil Patch.* Stavanger: University of Stavanger.

Aklestad, W. P. (2015). Modelling Drillstring Magnetic Interference of Wellbore Surveys USing Demagnetizing Factor. *SPE/IADC Drilling COnference and Exhibition* (pp. 1-14). London: SPE.

Andrew Buchanan, C. A. (2013). Geomagnetic Referencing-The Real-Time Compass for Directional Drillers. *Oilfield Review* , pp. 1-16.

Andrew G. Brooks, H. W. (1996). An Improved Methof for COmputing Wellbore Position Uncertainty and its Application to Collision and Target Intersection Probability Analysis. *SPE European Petroleum Conference* (pp. 1-10). Milan: SPE.

B. Poedjono, G. A. (2007). A Comprehsive Approach to Well-Collision Avoidance. *AADE National Technical Conference and Exhibition* (pp. 1-12). Houston, Texas: AADE.

Benny Poedjone, N. B. (2013). Improved Geomagnetic Referencing in the Artic Environment. *SPE Artic and Extreme Environments* (pp. 1-21). Moscow: SPE.

Bergstrom, N. S. (2010). *Wellbore Survey Quality Considerations.* Houston: Halliburton Sperry Drilling.

Bulychenkov, K. (2013). Improving Multistation Analysis of MWD DIrection Magnetic Surveys. *SPE Artic and Extreme Environments Confrernce & Exhibition* (pp. 1-9). Moscow: SPE.

C.A. Cheatham, S. S. (1992). Effects of Magnetic Interference on Directional Sureys in Horiztontal Wells. *IADC/SPE Drilling Conference* (pp. 101-110). New Orleans: SPE.

C.J.M.Wolff, J. (1981). *Borehole Position Uncertainty Analysis of MEasuring Methods and Derivation of Sysmatic Error Model.* SPE.

D.J.Kerridge, J. R. (1995). Reduction of Wellbore Postional Uncertainty Through Application of a New Geomagnetic In-Field Referencing Technique. *SPE Annual technical Conference & Exhibitions* (pp. 1-16). Dallas: SPE.

Design, S. C. (2009). *Drilling Process*. Retrieved from PETROCASA ENERGY Website: http://petrocasa.com/petrocasa/drilling-processes.php

Edvardsen, I. (2015). *Effects of Geomagnetic Disturbances on Offshore Magnetic Directional Wellbore Positioning in the Northern Auroral Zone.* Tromso: The Research Council of Norway.

Ekseth, R., Torkildsen, T., Brooks, A. G., Weston, J. L., Nyrnes, E., Wilson, H. F., et al. (2010). High-Integrity Wellbore Surveying. In R. Ekseth, T. Torkildsen, A. G. Brooks, J. L. Weston, E. Nyrnes, H. F. Wilson, et al., *SPE Drilling and Completion* (pp. 438-447). Society of Petroleum Engineers.

G.Gutierrez Murillo, G. Z. (2014). Challenges and Success in Horizontal Drilling Shallow 3D Unconventional Turbidite Reservoir, Mexico. *SPE Latin American and Caribbean Petroleum Engineering Conference* (pp. 1-13). Maracaibo: SPE.

H.S.Williamson. (2000). *Accuracy Prediction for Directional MWD.* SPE Drill & Completion.

Hansen, T. L. (2014, April 2). Northern Lights. *The Northern Lights-where,when and what'*. Tromso, Norway: Tromso Geophysical Observatory.

I.Edvardsen, E. B. (2013). *Improving the Accuracy abd Reliability of MWD Magnetic Wellbore Directional Surveying in the Barents Sea.* New Orleans: SPE .

I.Edvardsen, E. U. (2014). Improving the Accuracy and Reliability of MWD/Magnetic Wellbore and Directional Surveying in Barents Sea. *SPE Drilling & Completion* (pp. 1-11). SPE.

I.Edvardsen, T. M. (2012). Improving the Accuracy of Directional Wellbore Surveying in the Norwegian Sea. *SPE Annual Technical Conference and Exhibition* (pp. 1-12). San Antonio,Texas: SPE.

ISCWSA. (2016). *Roadmap To The Future.* International Assoication of Directional Drilling.

J.Bang. (2017). Quantification of Wellbore Collision Probability by Noval Analytic Methods. *SPE/IADC Drilling Conference and Exhibition* (pp. 1-32). Hague: SPE/IADC .

J.Bang, T. (2009). Targeting Challenges in Northern Areas Due to Degradation of Wellbore Positioning Accuracy. *SPE/IADC Drilling Conference and Exhibition* (pp. 1-14). Amsterdam: SPE.

Jamieson, P. A. (2017). *Introduction to Wellbore Positioning* . ISCWSA.

Leida C. Monterrosa, M. F. (2017). MWD Surveying Enhancement Techniques and Survey Management Workflows Applied at a Barents Sea Field for Accurate Wellbore Position. *SPE/IADC Drilling COnference and Exhibition* (pp. 1-22). Hague: SPE.

Lima, C. a. (2004). MWD Survey Accuray Improvements Using Multistation Analysis. *IADC/SPE Asia Pacific Drilling Technology* (pp. 1-7). Kuala Lumpar: SPE.

M.K.Trochim, W. (2006, October 20). *Random Error*. Retrieved from Reserach Methods Knowledge Base: https://www.socialresearchmethods.net/kb/index.php

Macresy, R. a. (2006). Improved BHA Sag Correction and Uncertainty Evaluation Brings Value to Wellbore Placement. *SPE Annual Technical Conference and Exhibition* (pp. 1-11). San Antonio: SPE.

Mantle, K. (2013/2014). The Art of Controlling Wellbore Trajectory. pp. 54-55.

Mcculloch, J. B. (n.d.). The Value of Real Time Geomagnetic Reference Data to the Oil and Gas Industry. In J. B. Mcculloch. Aberdeen: Space Weather.

Neal J.Adams, T. C. (1985). Drilling Engineering A Complete Well Planning Approach. In T. C. Neal J.Adams, *Drilling Engineering A Complete Well Planning Approach* (p. 331). PennWell Books.

Roar Sognnes, B. S. (1996). Improving MWD Survey Accuracy in Deviated Wells by Used of New Triaxial Magnetic Azimuth Correction Method. *SPWLA 37th Annual Symposium*, (pp. 1-14).

Rune Sele, P. E. (2000). Improving Wellbore Position Accuracy of Horizontal Wells by using a Continuous Inclination Measurement from a Near Bit Inclination MWD sensor. *Journal of Canadian Petroleum Technology*, 1-6.

Schlumberger. (2017). *Sidetrack*. Retrieved from Schlumberger Glossary Oilfield: http://www.glossary.oilfield.slb.com/Terms/s/sidetrack.aspx

T.L.Hansen, I. M. (2012). Improving the Accuracy of Directional Wellbore Surveying in the Norwegian Sea. *SPE Annual Technical Conference and Exhibition* (pp. 1-12). San Antonio: SPE.

APPENDIX A

Table 4 Relief Well Semi Major Axis Size From Compass For Each Error Source

MD	SAG	DEC	MB	MSF	AB	ASF	TMF	MIS	DIP
510	0.01	0.04	0.00	0.00	0.00	0.00	0.00	0.11	0.00
525	0.01	0.07	0.01	0.00	0.00	0.00	0.00	0.12	0.00
540	0.03	0.13	0.01	0.00	0.00	0.00	0.00	0.14	0.00
555	0.06	0.21	0.03	0.01	0.01	0.01	0.01	0.16	0.00
570	0.09	0.33	0.05	0.02	0.01	0.01	0.02	0.18	0.00
585	0.13	0.48	0.07	0.05	0.02	0.02	0.04	0.20	0.01
600	0.18	0.66	0.1	0.08	0.03	0.03	0.07	0.22	0.03
615	0.23	0.86	0.13	0.13	0.04	0.04	0.10	0.24	0.05
630	0.28	1.08	0.16	0.18	0.04	0.05	0.14	0.26	0.09
645	0.33	1.33	0.2	0.25	0.05	0.07	0.18	0.27	0.13
600	0.38	1.6	0.24	0.34	0.06	0.09	0.23	0.28	0.20
672	0.42	1.83	0.27	0.41	0.07	0.11	0.27	0.29	0.26
690	0.43	2.18	0.28	0.44	0.07	0.12	0.33	0.29	0.28
720	0.44	2.8	0.32	0.54	0.07	0.15	0.42	0.29	0.37
750	0.46	3.44	0.37	0.71	0.08	0.21	0.51	0.29	0.58
780	0.48	4.09	0.45	0.92	0.08	0.27	0.59	0.229	1.07
810	0.50	4.75	0.53	1.15	0.08	0.34	0.66	0.32	1.33
840	0.52	5.41	0.62	1.39	0..09	0.42	0.72	0.37	1.61
870	0.53	6.08	0.72	1.64	0.09	0.49	0.77	0.43	1.89
900	0.54	6.75	0.81	1.90	0.09	0.57	0.82	0.49	2.15
930	0.55	7.42	0.89	2.16	0.09	0.65	0.85	0.55	2.39
960	0.55	8.09	0.97	2.42	0.09	0.74	0.88	0.61	2.62
990	0.55	8.76	1.01	2.55	0.09	0.78	0.91	0.64	2.83
1020	0.55	9.43	1.01	2.58	0.09	0.79	0.93	0.65	3.07
1050	0.55	10.1	1.03	2.64	0.09	0.81	0.96	0.66	3.33
1080	0.55	10.78	1.05	2.72	0.09	0.83	0.98	0.68	3.60
1110	0.55	11.45	1.09	2.82	0.09	0.86	1.01	0.70	3.86
1140	0.55	12.12	1.13	2.95	0.09	0.90	1.03	0.73	4.11
1170	0.55	12.79	1.17	3.09	0.09	0.95	1.05	0.76	4.38

MD	SAG	DEC	MB	MSF	AB	ASF	TMF	MIS	DIP
1200	0.55	13.46	1.22	3.25	0.09	1.00	1.06	0.79	4.64
1230	0.55	14.12	1.28	3.42	0.09	1.05	1.08	0.83	4.89
1260	0.56	14.79	1.34	3.61	0.09	1.11	1.09	0.87	5.15
1290	0.56	15.46	1.41	3.80	0.09	1.17	1.10	0.92	5.42
1320	0.57	16.12	1.48	4.00	0.09	1.24	1.10	0.96	5.68
1340	0.58	16.56	1.52	4.13	0.09	1.28	1.10	0.99	5.85
1350	0.59	16.78	1.55	4.20	0.09	1.30	1.10	1.01	5.94
1370	0.6	17.21	1.59	4.34	0.09	1.35	1.09	1.04	6.11
1400	0.62	17.86	1.67	4.55	0.1	1.41	1.07	1.09	6.37

Table 5 Targeted Well Semi Major Axis Size From Compass For Each Error Source

MD	DEC	AB	ASF	MB	MSF	TMF	MIS	DIP	SAG
510	0	0.00	0.00	0.00	0.00	0.00	0.00	0.00	0.00
525	0.03	0.00	0.00	0.00	0.00	0.00	0.13	0.00	0.01
540	0.09	0.00	0.00	0.00	0.00	0.00	0.15	0.00	0.03
555	0.18	0.00	0.00	0.00	0.00	0.00	0.16	0.00	0.05
570	0.31	0.00	0.00	0.01	0.01	0.00	0.18	0.00	0.09
585	0.47	0.00	0.01	0.01	0.03	0.01	0.21	0.00	0.13
600	0.65	0.01	0.01	0.02	0.06	0.01	0.23	0.00	0.18
615	0.87	0.01	0.03	0.03	0.09	0.02	0.26	0.01	0.23
630	1.10	0.01	0.05	0.03	0.14	0.03	0.28	0.01	0.28
645	1.37	0.01	0.06	0.04	0.21	0.04	0.31	0.03	0.33
660	1.65	0.01	0.09	0.05	0.28	0.05	0.33	0.04	0.38
672	1.89	0.01	0.11	0.06	0.35	0.05	0.35	0.05	0.42
690	2.27	0.01	0.13	0.08	0.41	0.07	0.37	0.07	0.44

Table 6 Relief Well EOU For Each Error Source

MD	DEC	AB	ASF	MB	MSF	TMF	MIS	DIP	SAG
510	0.02	0.01	0.03	0.10	0.10	0.01	0.03	0.1	0.01
525	0.05	0.02	0.06	0.21	0.20	0.02	0.07	0.21	0.02
540	0.09	0.02	0.09	0.32	0.31	0.020	0.11	0.32	0.02
555	0.14	0.03	0.13	0.44	0.42	0.03	0.15	0.44	0.03
570	0.19	0.04	0.17	0.57	0.54	0.04	0.20	0.56	0.04
585	0.26	0.05	0.21	0.71	0.67	0.05	0.25	0.70	0.05
600	0.35	0.06	0.26	0.85	0.81	0.06	0.30	0.84	0.06
615	0.44	0.06	0.32	1.01	0.95	0.06	0.36	0.99	0.06
630	0.55	0.07	0.39	1.17	1.11	0.07	0.43	1.16	0.07
645	0.69	0.08	0.47	1.35	1.27	0.08	0.51	1.33	0.08
600	0.84	0.9	0.59	1.54	1.45	0.09	0.60	1.52	0.9
672	0.97	0.10	0.65	1.70	1.60	0.10	0.67	1.68	0.10
690	1.26	0.11	0.73	1.97	1.85	0.11	0.97	1.95	0.11
720	1.49	0.13	0.78	2.20	2.06	0.13	1.16	2.18	0.13
750	1.70	0.14	0.84	2.41	2.26	0.14	1.32	2.39	0.14
780	1.90	0.16	0.91	2.61	2.45	0.16	1.44	2.59	0.16
810	2.10	0.18	1.02	2.81	2.63	0.18	1.54	2.79	0.18
840	2.29	0.21	1.15	3.00	2.81	0.21	1.63	2.99	0.21
870	2.50	0.25	1.23	3.19	2.99	0.25	1.71	3.18	0.25
900	2.70	0.36	1.30	3.43	3.26	0.36	1.78	3.42	0.36
930	2.91	0.51	1.35	3.59	3.41	0.53	1.85	3.57	0.51
960	3.12	0.58	1.48	3.72	3.54	0.60	1.98	3.70	0.58
990	3.33	0.62	1.53	3.8	3.65	0.63	2.05	3.81	0.62
1020	3.55	0.65	1.59	3.96	3.78	0.66	2.12	3.94	0.65
1050	3.78	0.67	1.65	4.14	3.96	0.68	2.19	4.12	0.67
1080	4.01	0.68	1.71	4.39	4.18	0.69	2.27	4.37	0.68
1110	4.25	0.70	1.77	4.57	4.36	0.71	2.34	4.55	0.70
1140	4.49	0.71	1.86	4.74	4.51	0.72	2.42	4.72	0.71
1170	4.73	0.72	1.99	4.95	4.70	0.73	2.51	4.90	0.72
1200	4.98	0.73	2.11	5.17	4.89	0.74	2.59	5.14	0.73

MD	SAG	DEC	MB	MSF	AB	ASF	TMF	MIS	DIP
1230	5.24	0.73	2.18	5.33	5.05	0.75	2.69	5.30	0.73
1260	5.50	0.73	2.24	5.52	5.21	0.75	2.79	5.49	0.73
1290	5.76	0.74	2.28	5.77	5.42	0.76	2.92	5.74	0.74
1320	6.04	0.74	2.33	6.03	5.63	0.77	3.14	5.99	0.74
1340	7.85	0.74	2.38	7.40	6.01	0.77	3.32	7.35	0.74
1350	8.07	0.76	2.44	7.59	6.25	0.78	3.38	7.53	0.76
1370	9.71	0.77	2.49	8.82	6.30	0.79	3.59	8.75	0.77
1400	10.03	0.78	2.53	9.10	8.66	0.79	3.70	9.02	0.78

Table 7 Targeted Well EOU For Each Error Source From Model

MD	DEC	AB	ASF	MB	MSF	TMF	MIS	DIP	SAG
510	0.030	0.058	0.026	0.058	0.026	0.058	0.045	0.058	0.059
525	0.060	0.119	0.053	0.119	0.053	0.119	0.093	0.119	0.120
540	0.092	0.184	0.080	0.184	0.080	0.184	0.142	0.184	0.185
555	0.126	0.253	0.109	0.253	0.109	0.253	0.195	0.253	0.255
570	0.161	0.326	0.138	0.326	0.138	0.326	0.251	0.326	0.329
585	0.197	0.405	0.168	0.405	0.168	0.405	0.310	0.405	0.408
600	0.236	0.489	0.200	0.489	0.200	0.489	0.373	0.489	0.493
615	0.277	0.579	0.234	0.579	0.234	0.579	0.441	0.579	0.585
630	0.321	0.675	0.269	0.675	0.269	0.675	0.512	0.675	0.683
645	0.367	0.778	0.305	0.778	0.305	0.778	0.589	0.778	0.789
660	0.417	0.889	0.345	0.889	0.345	0.889	0.670	0.889	0.901
672	0.462	0.985	0.320	0.985	0.320	0.985	0.743	0.985	1.000
690	0.529	1.139	0.432	1.139	0.432	1.139	0.853	1.139	1.160

APPENDIX B

Table 8 Error Model Parameters For MWD (Jamieson, 2017)

ERROR	Value	Inc.	Azimuth
AB 1	0.004ms^{-2}	$\frac{\cos I}{G}$	$\frac{\tan\theta \cos I \sin A_m}{G}$
AB 2	0.004ms^{-2}	0	$\frac{\cot\theta - \tan\theta \cos A_m}{G}$
AB Z	0.004ms^{-2}	$\frac{-\sin I}{G}$	$\frac{\tan\theta \sin I \sin A_m}{G}$
ASF 1	0.0005	$\frac{\sin I \cos I}{\sqrt{2}}$	$\frac{-\tan\theta \sin I \cos I \sin A_m}{\sqrt{2}}$
ASF 2	0.0005	$\frac{\sin I \cos I}{\sqrt{2}}$	$\frac{-\tan\theta \sin I \cos I \sin A_m}{2}$
ASF 3	0.0005	0	$\frac{\tan\theta \sin I \cos A_m - \cos I}{2}$
ASF Z	0.0005	$-\sin I \cos I$	$\tan\theta \sin I \cos I \sin A_m$
MB 1	70nT	0	$\frac{-\cos I \sin A_m}{B \cos\theta}$
MB 2	70nT	0	$\frac{\cos A_m}{B \cos\theta}$
MB Z	70nT	0	$\frac{-\sin I \sin A_m}{B \cos\theta}$
MSF 1	0.0016	0	$\frac{\sin I \sin A_m(\tan\theta \cos I + \sin I \cos A_m)}{\sqrt{2}}$
MSF 2	0.0016	0	$\frac{\sin A_m(\tan\theta \sin I \cos I - \cos I \cos I \cos A_m - \cos A_m)}{2}$
MSF 3	0.0016	0	$\frac{\cos I \cos A_m \cos A_m - \cos I \sin A_m \sin A_m - \tan\theta \sin I \cos A_m}{2}$
MSF Z	0.0016	0	$-(\sin I \cos A_m + \tan\theta \cos I) \sin I \sin A_m$
C. DEC	0.36	0	1
Dec (HC)	5000nT	0	$\frac{1}{B \cos\theta}$
XY MIS 1	0.06°	w_{12}	0
XY MIS 2	0.06°	0	$\frac{-w_{12}}{\sin I}$
XY MIS 3	0.06°	$w_{34} \cos A$	$-w_{34} \sin A \sin I$

APPENDIX B

ERROR	Value	Inc.	Azimuth
XY MIS 4	0.06°	$w_{34} \sin A$	$\frac{w_{34} \cos A}{\sin I}$
SAG	0.2°	$\sin I$	1
DIP	0.2°	0	$\frac{-\sin I \sin A_m (\cos I - \tan\theta \sin I \cos A_m)}{(1 - \sin I \sin I \sin A_m \sin A_m)}$
TMF	130 nT	0	$\frac{-\sin I \sin A_m (\tan\theta \cos I + \sin I \cos A_m)}{B(1 - \sin I \sin I \sin A_m \sin A_m)}$

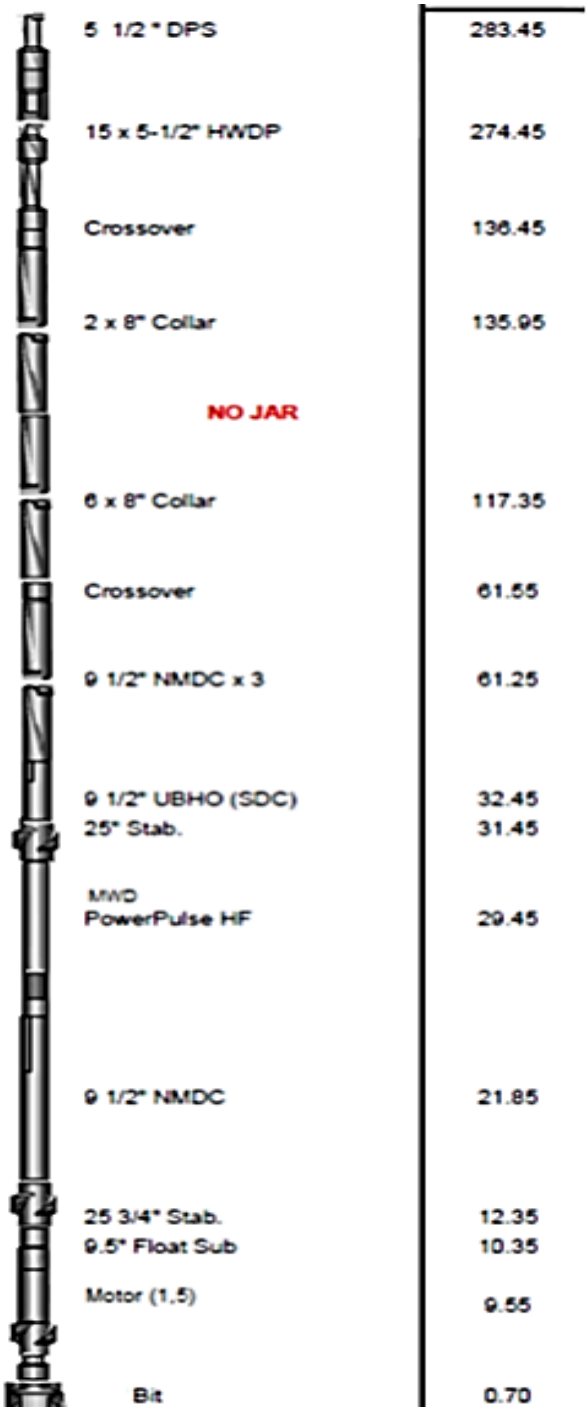

Figure 37 Exemplar BHA (A.Berchan, 2015)

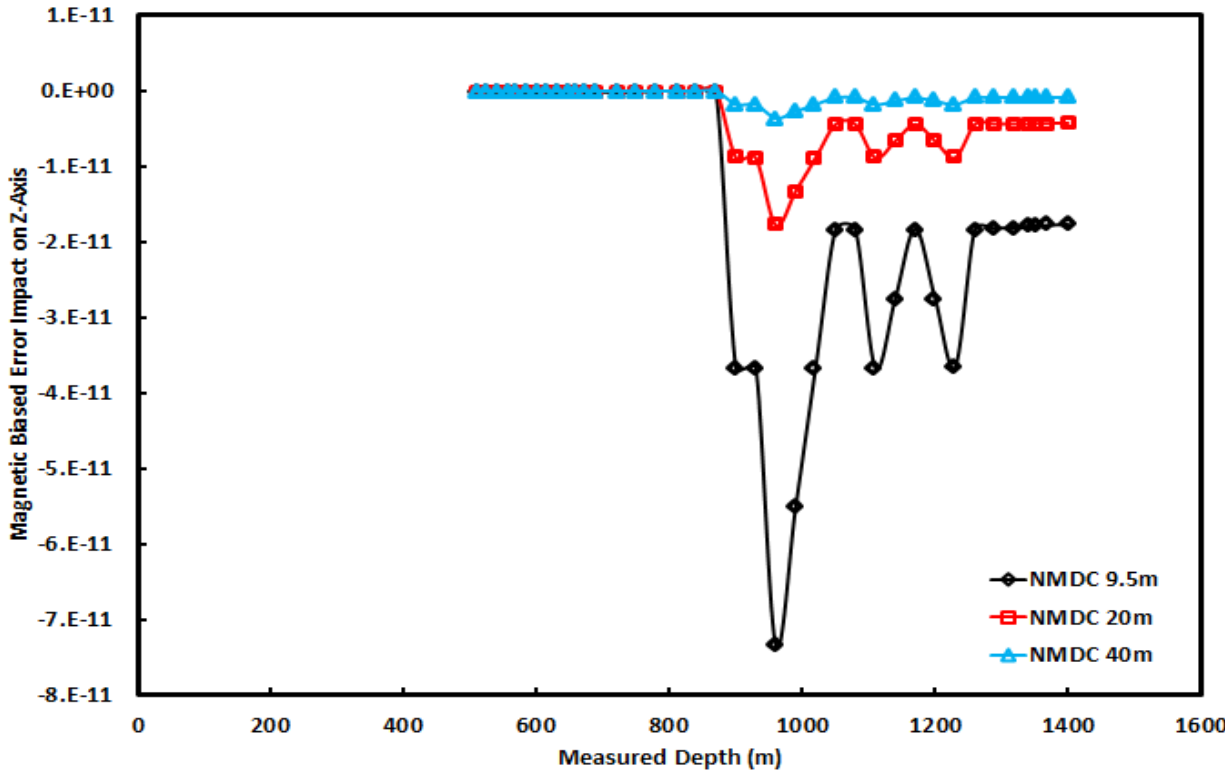

Figure 38 Impact of NMDC on Z-Axis Component of Magnetometer

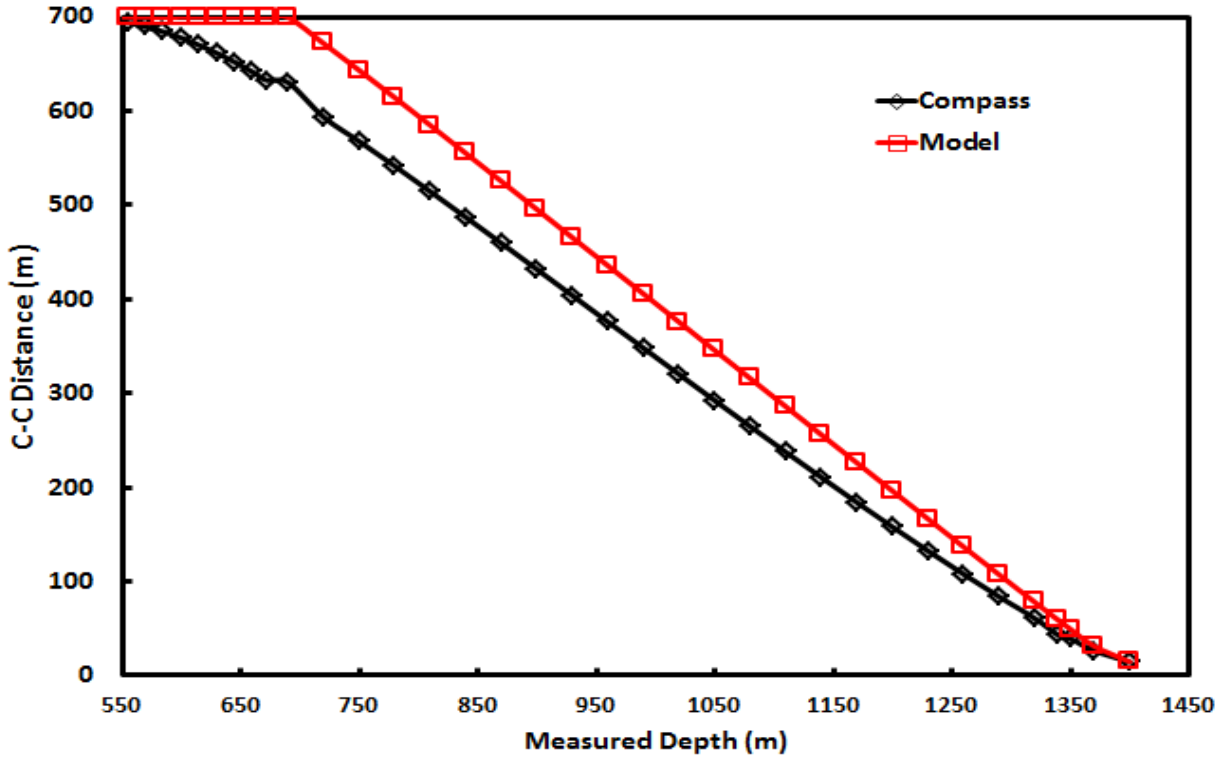

Figure 39 Center to Center Distance from COMPASS and MODEL

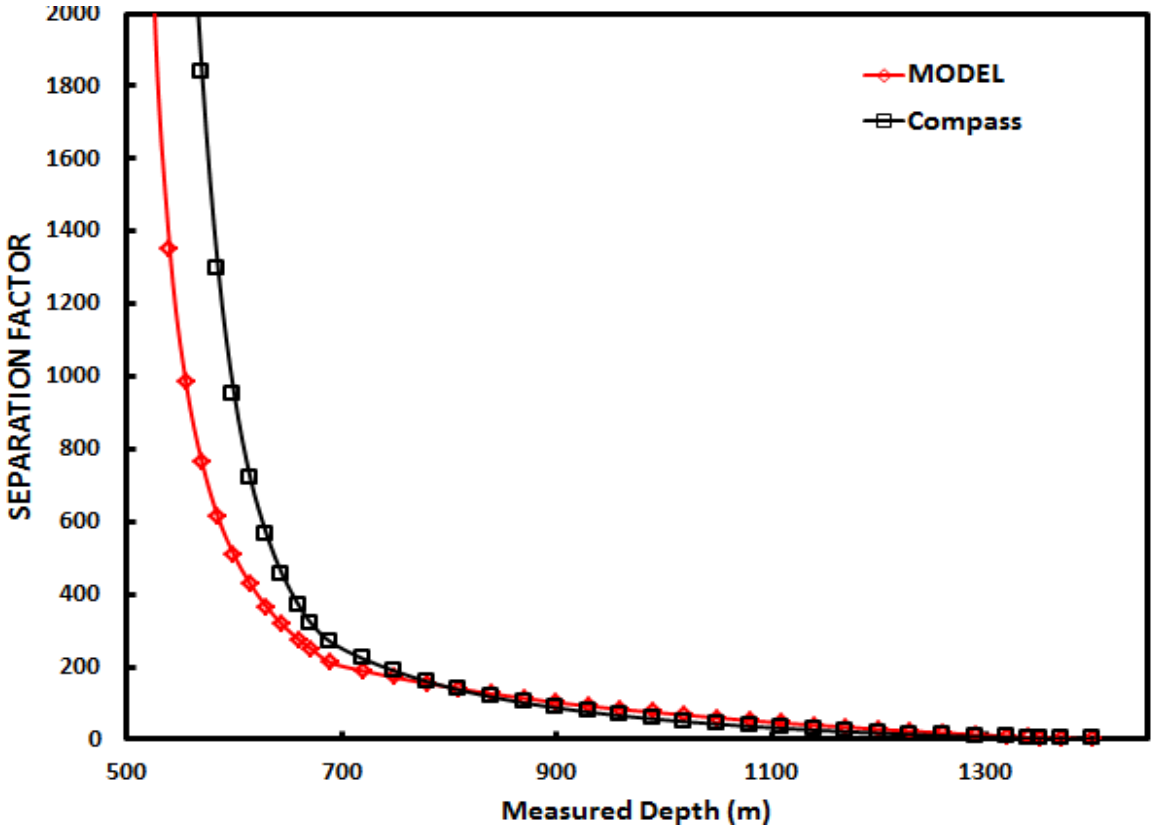

Figure 40 Separation Factor Plot from COMPASS and MODEL

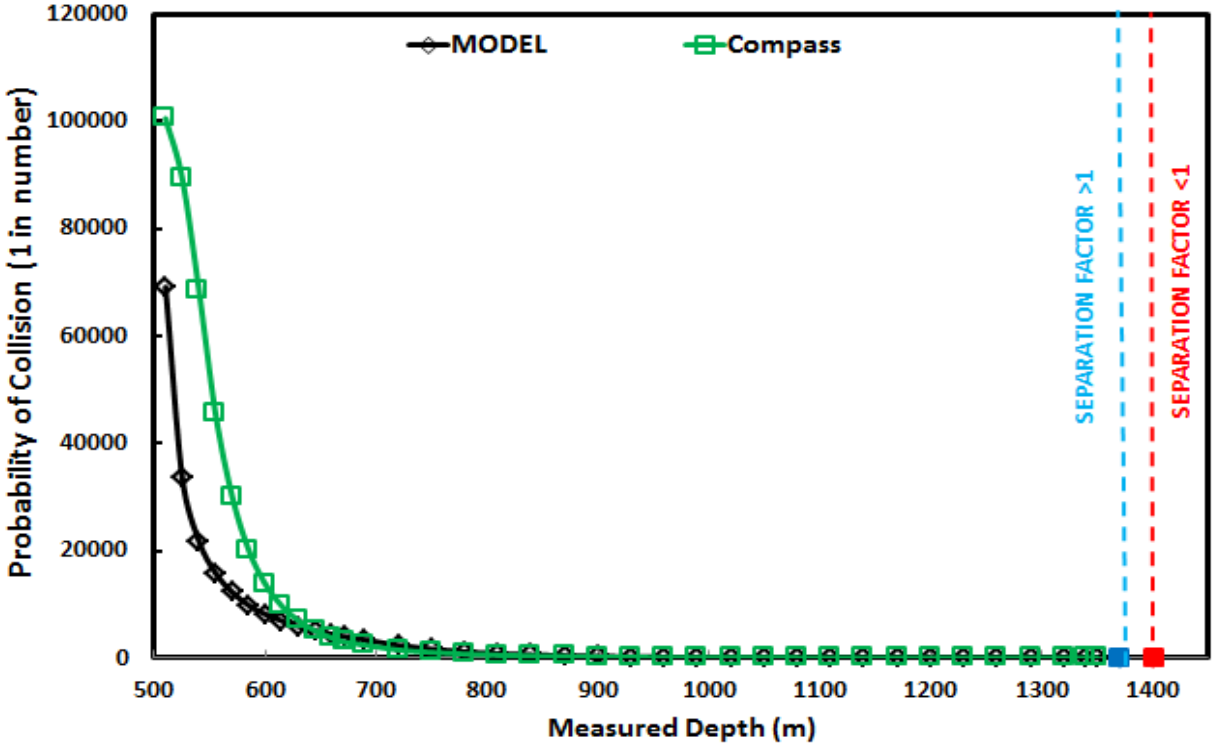

Figure 41 Number of Collision from COMPASS and MODEL

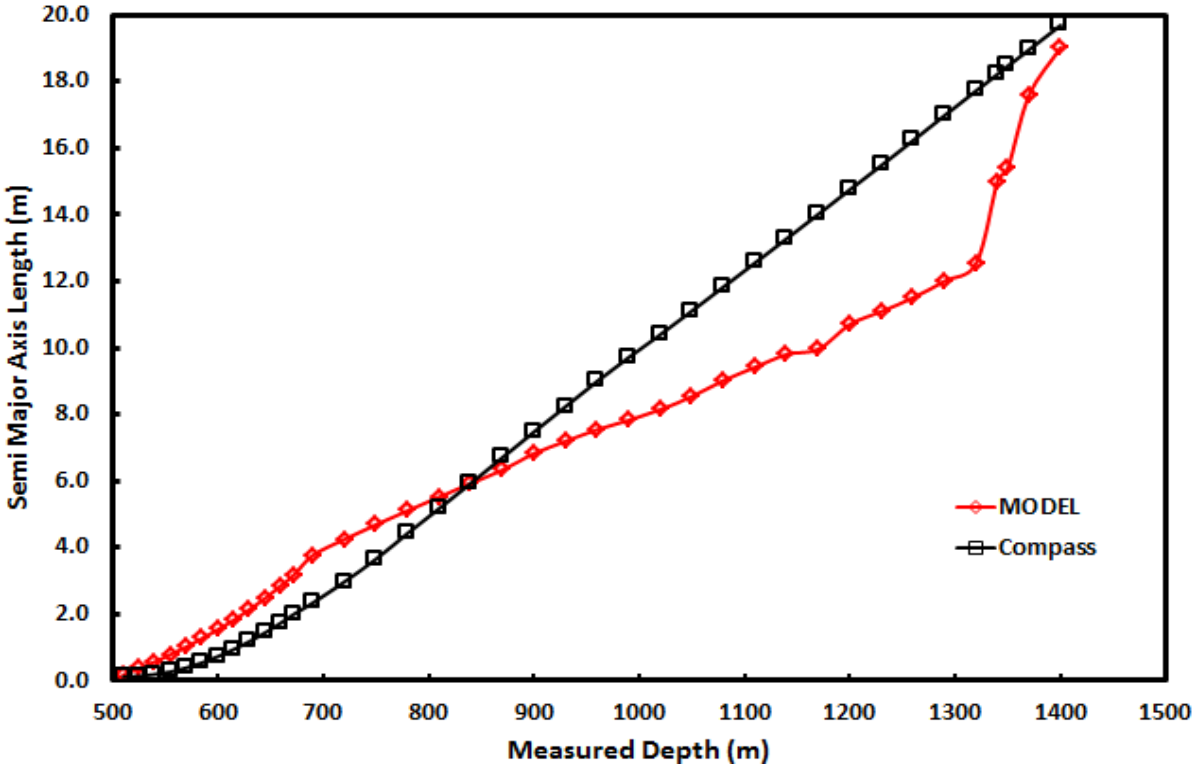

Figure 42 Semi Major Axis from COMPASS and MODEL for 38 Number of Stations

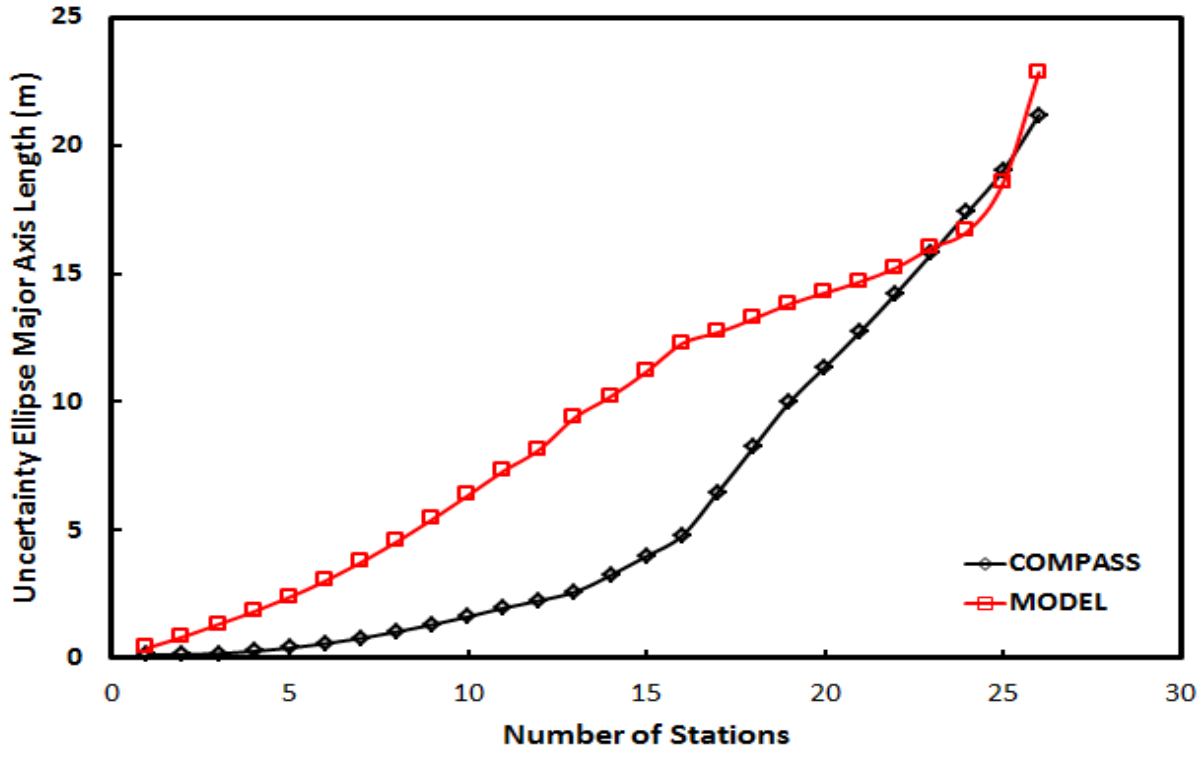

Figure 43 Semi Major Axis from COMPASS and MODEL for 26 Number of Stations